# MEASUREMENT OF THE ELECTRON-INITIATED IMPACT IONIZATION COEFFICIENT OF INDIUM PHOSPHIDE USING InP-GaAsSb-InP DOUBLE HETEROJUNCTION BIPOLAR TRANSISTORS

by

Selena Lam
B.A.Sc., University of British Columbia, 1998

THESIS SUBMITTED IN PARTIAL FULFILLMENT OF
THE REQUIREMENTS FOR THE DEGREE OF
MASTER OF APPLIED SCIENCE

in the School
of
Engineering Science


SIMON FRASER UNIVERSITY
January 2004

# Approval

Name: Selena Lam

Degree: Master of Applied Science

Title of thesis: Measurement of the Electron-Initiated Impact Ionization Coefficient of Indium Phosphide Using InP-GaAsSb-InP Double Heterojunction Bipolar Transistors

Examining Committee:

Chair: Dr. Marek Syrzycki

Dr. Colombo Bolognesi, Senior Supervisor
Professor, School of Engineering Science

Dr. Simon Watkins, Supervisor
Professor, Department of Physics

Dr. Mike Thewalt, Examiner
Professor, Department of Physics

Date Approved: January 15, 2004

# PARTIAL COPYRIGHT LICENCE



**Title of Thesis/Project/Extended Essay:**

Measurement of the Electron-Initiated Impact Ionization Coefficient of Indium Phosphide Using InP-GaAsSb-InP Double Heterojunction Bipolar Transistors

**Author:**

(Signature)

Selena Lam

January 18, 2004
(Date Signed)

# ABSTRACT

InP-GaAsSb-InP double heterojunction bipolar transistors (DHBTs) are used to measure the electron-initiated impact ionization coefficient of InP at room temperature and over a temperature range of 125 K to 380 K. The staggered band lineup of these devices allows injection of a pure electron current of controlled magnitude into a region where the electric field strength is also well-known. The procedure is verified by performing measurements of the InGaAs electron-initiated impact ionization coefficient at room temperature, and a method is developed to select the appropriate range of base-emitter bias or injected emitter current for extracting the impact ionization coefficient. The components of the reverse-bias leakage current are examined and the significance of the surface leakage current is demonstrated for the InP devices. The numerical value of the extracted coefficient varies with device perimeter to area ratio due to the surface leakage current. However, the temperature trend is clear: the electron-initiated impact ionization coefficient of InP decreases by over one order of magnitude between 125 K and 380 K.

# Acknowledgements

I would like to thank Dr. Colombo Bolognesi, my senior supervisor. I have benefited greatly from his expertise and knowledge, and from his dedication in establishing and running the Compound Semiconductor Devices Laboratory.

Thanks are also due to Dr. Simon Watkins, whose group grew the semiconductor layers, and to Martin Dvorak, for his work on device processing. Nourredine, Georg, Dave and others in the CSDL provided invaluable assistance and encouragement. Thank you for making the lab an enjoyable, productive workplace.

I would like to acknowledge financial support from the National Sciences and Engineering Research Council, the B.C. Advanced Systems Institute, Simon Fraser University, and teaching and research assistanceships.

Finally, many thanks are due to my family.

# Table of Contents

# List of Tables

# List of Figures

# Chapter 1
# Introduction

## 1.1 Background

Indium phosphide (InP) is a technologically important semiconductor whose material properties have enabled various applications requiring high performance components. InP-based electronic devices are found in products such as cellular phones, wireless LANs, and direct broadcast satellite receivers. Military applications include high frequency satellite communications, missile seekers, and radar [1]. The electronic devices in these products must meet demanding specifications: high frequency operation, high current gain, low noise, and either high output power or high efficiency operation at low voltages. Both digital and analog circuits are implemented using InP-based transistors. Until recently, InP electronic devices have been perceived as too costly and unreliable for mainstream commercial applications; however, this is changing rapidly and a number of manufacturers have announced InP products: it is generally accepted that telecommunications at 40 GHz and beyond will require InP based components. The rapidly growing field of optoelectronics also relies heavily on InP for transmitters and receivers at wavelengths of 1.5 to 1.6 μm. In fact, InP optoelectronics has largely driven the development of InP technology so far.

The present dissertation focuses on impact ionization effects in InP/GaAsSb/InP double heterojunction bipolar transistors (HBTs). In HBTs, materials with different energy bandgaps are used to form the emitter and base, and sometimes the collector. In a homojunction transistor, the choice of doping levels in the emitter and the base must reflect a tradeoff between gain and high frequency performance. Energy gap differences provide the design freedom to overcome this fundamental limitation [2]. Wide bandgap InP can be used for the emitter of an HBT, while a narrow bandgap material such as

InGaAs or GaAsSb [3] forms the base. Compared to GaAs-based HBTs, InP-based devices have a lower turn-on voltage and lower power dissipation, as well as a higher gain at low current densities [4]. For high power devices, InP is used as the collector to improve breakdown characteristics [5]. The favourable high field transport properties of InP are expected to improve breakdown voltage without a great sacrifice in frequency performance.

Similarly, InP-based high electron mobility transistors (HEMTs) with high transconductance, high speed, and low source resistance have been used for applications such as high-frequency, low-noise amplifiers [6].

Transmitters for optical communication systems are primarily InP-based lasers that emit light at a wavelength of 1.55 μm, a wavelength that minimizes absorption within silica fibres [7]. Optical detectors and receivers, such as p-i-n diodes and avalanche photodiodes, make use of wide bandgap InP layers to achieve low dark current and high gain [8]. InP substrates are advantageous in such applications because the 1.35 eV wide energy bandgap makes InP optically transparent to wavelengths greater than 0.92 μm.

Impact ionization is central to the operation of avalanche photodiodes. Separate absorption and multiplication avalanche photodiodes use one layer, often of InGaAs, to absorb incident light. Multiplication occurs in a separate InP layer by impact ionization. InP is chosen for the multiplication layer because it has a wide bandgap, so the dark current caused by band-to-band tunnelling is very small [9]. Both the noise and the gain-bandwidth of the photodiodes are affected by the impact ionization rate [10].

Impact ionization also affects the performance of HBTs, by causing non-linear behaviour that leads to breakdown. The collector current increases while the base current decreases by the same amount. The breakdown voltage of an HBT can be predicted if the impact ionization coefficient is known as a function of applied electric field [11].

Impact ionization rates have been studied for most important semiconductors, using a variety of devices and experimental methods. Most measurements of impact ionization or multiplication in InP have used modified avalanche photodiodes to measure hole-initiated and electron-initiated impact ionization rates at room temperature [10, 12, 13]. The impact ionization rates for InP have been measured for several ranges of doping

level, depletion width, and electric field strength, but the published results show significant scatter.

More recent measurements of impact ionization in materials such as GaAs and InGaAs [14, 15] have used HBTs to determine impact ionization coefficients. HBTs provide better control of the initial injected current, and more sensitivity in measurement due to the transistor current gain. InP has not previously been measured using HBTs because most HBTs with InP collectors are subject to collector current blocking, which is not compatible with impact ionization measurements. The material system chosen for this work has an $N^-$ InP emitter, a $p^+$ GaAsSb base and an N InP collector. This heterostructure has a staggered (type II) band lineup that eliminates current blocking at the base-collector junction [3]. Also, hole back-injection into the emitter is very low because of the large valence band discontinuity. This structure should allow accurate determination of the initial injected current.

The temperature variation of impact ionization coefficient is also an important concern. In high power applications, self-heating causes a temperature increase that affects device performance. The impact ionization coefficient at low temperatures is relevant for device operation with external cooling. The temperature variation of multiplication and impact ionization rates has been studied experimentally for a limited number of semiconductors, including InGaAs and GaAs [16, 17]. Theoretical predictions have been made for these materials and some others, including InP [18, 19]. The breakdown voltage in InP photodiodes over a temperature range of 20 K to 300 K has been reported [8], and the electron- and hole-initiated impact ionization coefficient for InP has been measured with avalanche photodiodes, over a temperature range of 25°C to 175°C (298 to 448 K) [20]. However, to our knowledge, direct measurements of the InP electron-initiated impact ionization coefficient using HBTs have not yet been reported.

## 1.2 Objective

The objective of this work is to characterize the electron-initiated impact ionization coefficient of indium phosphide over a temperature range of 125 K to 380 K, using InP/GaAsSb/InP staggered band lineup HBTs.

## 1.3 Outline of Thesis

Chapter 2 provides background relating to impact ionization. We define the multiplication factor and the impact ionization coefficient and give the equations that relate them. This is followed by a brief historical summary of theoretical approaches to impact ionization. Next, we present experimental methods for determining the multiplication factor, describing the older method of avalanche photodiodes and more recent methods using HBTs. Equations are included for HBT measurements using either the constant injected emitter current method or the constant applied base-emitter bias method. Finally, the equation for extracting $\alpha$, the coefficient for electron-initiated impact ionization, from the multiplication factor is presented.

Chapter 3 describes background related to the operation of HBTs, focussing on the aspects critical to impact ionization coefficient measurements. We justify the use of the InP/GaAsSb/InP material system, calculate the electric field profile in the collector under relevant bias conditions, and review the currents at each terminal of the device. Causes of collector current increase, other than impact ionization, are discussed and differentiated from impact ionization.

Chapter 4 is concerned with details of the experimental measurements. It includes specifications for the layers and devices used in this work, as well as the measurement methods and apparatus.

Chapter 5 contains the results of the measurement and analysis on InGaAs HBTs, to validate the method by comparison to published results. The extracted impact ionization coefficient should be independent of the applied base-emitter bias or the injected emitter current. We examine the data at each stage of analysis, to determine the valid range of bias conditions.

Chapter 6 presents the results of the measurement and analysis on InP HBTs, first at room temperature and then over a range of temperature. Sources of error are discussed, including a breakdown of contributions to the reverse-bias leakage current that affects the accuracy of the extracted impact ionization coefficients. We present graphs comparing the impact ionization coefficient measured in this work to previous results in the literature.

Chapter 7 concludes with a summary of results and suggestions for improvements to method employed in this work.

# Chapter 2
# Impact Ionization

## 2.1 Introduction

Impact ionization in a semiconductor occurs when charge carriers gain sufficient kinetic energy from a strong electric field to generate additional mobile carriers. Various scattering events act as a dissipative force which opposes the kinetic energy rise that results from the application of an electric field. Charge carriers in a semiconductor undergo energy and momentum scattering events caused by scattering with phonons and crystal impurities. A free carrier that gains enough energy may promote an electron from the valence band to the conduction band, thereby producing a new electron-hole pair in addition to the initiating electron or hole. This process is impact ionization.

Because of the probabilistic nature of scattering, only a fraction of carriers acquire enough kinetic energy to undergo impact ionization. The concept of an ionization threshold energy level has been used to indicate when impact ionization becomes possible. As shown in Figure 2.1, crystal momentum and energy must be conserved for the three quasi-particles involved, so the threshold energy depends strongly on the conduction and valence band structures. However, the actual ionization rate depends not only on the number of carriers that have acquired the minimum threshold energy but also on the probability that they will lose their energy by undergoing impact ionization rather than through some other scattering mechanism.

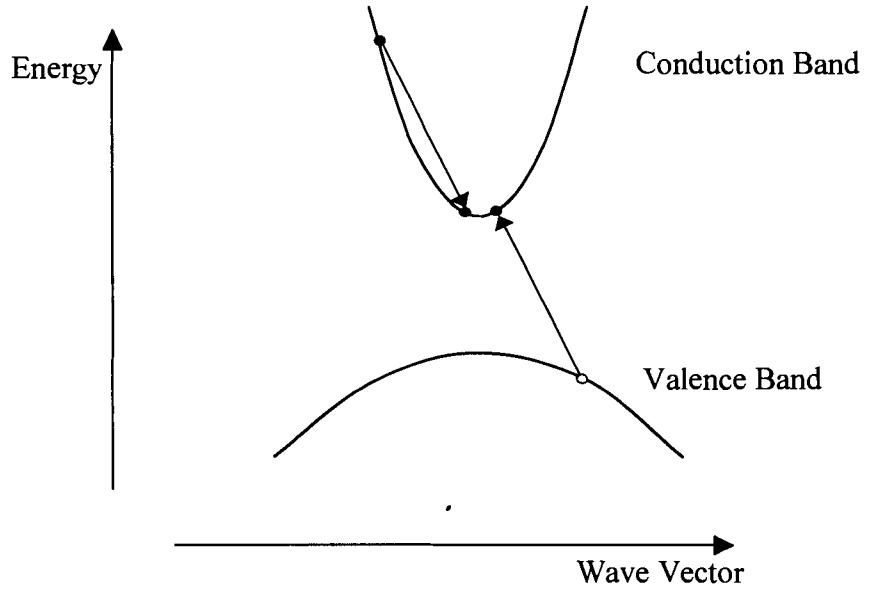


**Figure 2.1. Electron and hole transitions during impact ionization.**

Following an impact ionization event, the three resulting carriers are accelerated by the electric field and may in turn gain enough energy to undergo a second ionization event. This avalanche multiplication process creates additional electron-hole pairs, which may in turn produce even more electron-hole pairs. If the electric field is strong enough, a very large current results and junction breakdown occurs. In the context of transistor applications, such instabilities limit the operational range of the devices.

Section 2.2 defines two parameters conventionally used to characterize impact ionization: the multiplication factor and the impact ionization coefficient. To provide historical background, section 2.3 surveys several major approaches to the theoretical prediction of impact ionization coefficients. The remainder of the chapter examines the experimental approaches used to characterize impact ionization, including methods used to measure the multiplication factor with avalanche photodiodes and HBTs in section 2.4, and the extraction of impact ionization coefficient from multiplication data in section 2.5.

## 2.2 Characterization of Impact Ionization

The amount of impact ionization that occurs depends on many factors. The semiconductor band structure, the crystal orientation, the electric field strength, the

current density, and the temperature may all be important. Two parameters are frequently used to quantify impact ionization: the multiplication factor, M, and the impact ionization coefficient, $\alpha$. The multiplication factor measures the increase in current after travelling a distance in an electric field. It is the ratio of the final current to the initial current. The impact ionization coefficient measures the number of electron-hole pairs generated per unit distance travelled in an electric field. The multiplication factor is normally used with reference to a specific device, while the impact ionization coefficient more generally characterizes a semiconductor material. In general, both parameters show different values for electron-initiated and hole-initiated impact ionization because of differences in band structure.

### 2.2.1 Impact Ionization Coefficient, $\alpha$

The impact ionization coefficient $\alpha$, which is usually quoted in units of inverse centimetres, is the reciprocal of the average distance travelled by a charge carrier between impact ionization events. Alternatively, it indicates the number of electron-hole pairs expected per unit distance travelled in the constant electric field. The coefficient $\alpha_n$ (or simply called $\alpha$ by some authors) describes the likelihood of impact ionization caused by electrons, while $\alpha_p$ (also referred to as $\beta$) characterizes hole-initiated impact ionization. Over an incremental distance dx, the increase in electron current density is related to the impact ionization coefficients by the following equation:

$$dJ_n = J_n \alpha_n dx + J_p \alpha_p dx \tag{2.1}$$

Impact ionization coefficients are strongly dependent on the strength of the applied electric field, and are usually graphed on a logarithmic scale versus the inverse of electric field. Different forms of the relations between $\alpha$ and electric field have been proposed by various authors, as described in section 2.3.

### 2.2.2 Multiplication Factor, M

The current multiplication factor M measures the increase in current after travelling a distance, w, in an electric field. The multiplication factor must be quoted along with the details of the device for which it was measured. $M_n$ describes electron-initiated impact

ionization, and $M_p$ refers to hole-initiated impact ionization. For carriers travelling from the position x=0 to the position x=w, the original current, consisting of either electrons or holes, increases by a multiplication factor $M_n$ or $M_p$:

$$M_n = \frac{I_n(x=w)}{I_n(x=0)} \text{ or } M_p = \frac{I_p(x=w)}{I_p(x=0)} \tag{2.2}$$

### 2.2.3 Calculation of Multiplication Factor From Ionization Coefficient

If the values of the impact ionization coefficients $\alpha_n$ and $\alpha_p$ are known, the multiplication factor can be calculated for a given device structure. If the electric field varies across the device, the field profile determines the position-dependent value of ionization coefficient used in the following calculations. When an electron-hole pair is created by impact ionization, the electrons and holes are accelerated in opposite directions by the electric field. By current continuity, the total current is constant through the device, but the portion of the total current carried by holes versus electrons is position dependent. For example, if an electron current is injected into the depletion region of a reverse-biased p-n junction, then as electron-hole pairs are generated by impact ionization, the hole current decreases and the electron current increases as a function of position towards the n side, as shown in Figure 2.2.

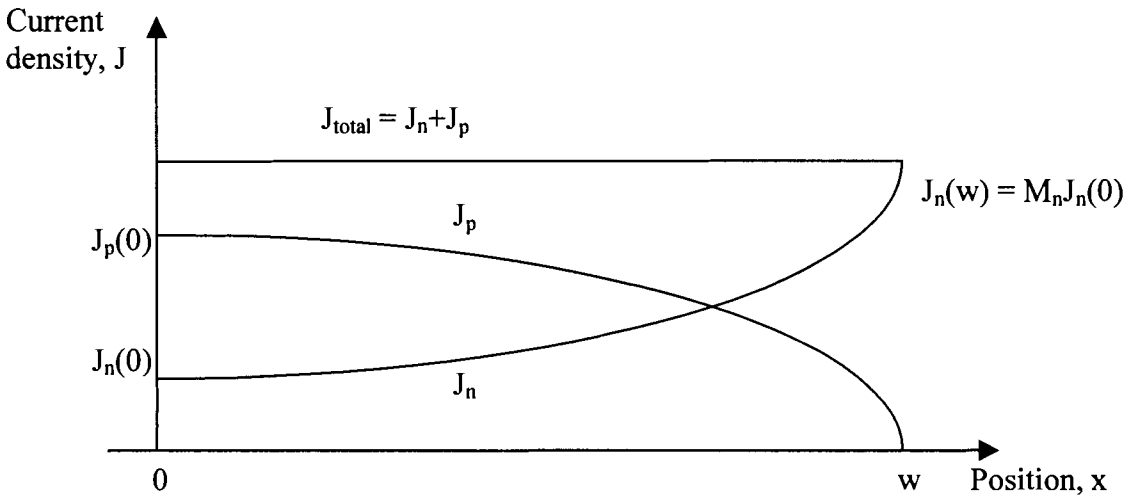


**Figure 2.2. Electron, hole and total current densities as a function of distance into the collector for electron-initiated impact ionization.**

Following the derivations by Shur [21] and Sze [22], the electron or hole current density can be written as a function of position using the impact ionization coefficients. Over the incremental distance dx, each electron will on average create $\alpha_n dx$ electron-hole pairs, and each hole will create $\alpha_p dx$ electron-hole pairs. This current distribution is described by the following differential equations:

$$\frac{dJ_n}{dx} = \alpha_n J_n + \alpha_p J_p \tag{2.3}$$

$$\frac{dJ_p}{dx} = -\alpha_n J_n - \alpha_p J_p \tag{2.4}$$

From current continuity, the total current J is constant for any position between x=0 and x=w:

$$J = J_n + J_p \tag{2.5}$$

Rewriting the differential equation to eliminate $J_p$ results in the equation for $J_n$

$$\frac{dJ_n}{dx} = \alpha_n J_n + \alpha_p (J - J_n) \tag{2.6}$$

$$\frac{dJ_n}{dx} + (\alpha_p - \alpha_n) J_n = \alpha_p J \tag{2.7}$$

which has the solution

$$J_n(x) = \frac{\int_0^x \alpha_p J \exp\left[\int_0^{x'} (\alpha_p - \alpha_n) dx''\right] dx' + J_n(0)}{\exp\left[\int_0^x (\alpha_p - \alpha_n) dx'\right]} \tag{2.8}$$

After evaluating this equation at x=w, rearranging and dividing through by $J_n(w)$, it can be used to relate the multiplication factor $M_n$ to the impact ionization coefficients.

$$\frac{1}{M_n} = \exp\left[\int_0^w (\alpha_p - \alpha_n) dx\right] - \int_0^w \alpha_p \exp\left[\int_0^{x'} (\alpha_p - \alpha_n) dx''\right] dx' \tag{2.9}$$

By expanding the first exponential term, the equation can be simplified to:

$$\frac{1}{M_n} = 1 - \int_0^w \alpha_n \exp\left[\int_0^{x'} (\alpha_p - \alpha_n) dx''\right] dx' \tag{2.10}$$

or, rewritten,

$$M_n = \frac{1}{1 - \int_0^w \alpha_n \exp\left[\int_0^{x'} (\alpha_p - \alpha_n) dx''\right] dx'} \tag{2.11}$$

An analogous equation relates the hole multiplication factor to the impact ionization coefficients:

$$M_p = \frac{1}{1 - \int_0^w \alpha_p \exp\left[\int_0^{x'} (\alpha_n - \alpha_p) dx''\right] dx'} \tag{2.12}$$

These equations give the electron and hole multiplication factors for any structure where the value of the impact ionization coefficients is known between x=0 and x=w. The multiplication factor M implicitly couples the material-dependent impact ionization coefficients to the electric fields in the device structure, because $\alpha$ is a function of the electric field. The inverse relation, giving the impact ionization coefficient when the multiplication factors are known, is structure-dependent. Additional information, such as the electric field profile in the device structure, must be known. The relation used to calculate $\alpha_n$ for the devices in this work is presented in section 2.5, after the discussion on experimental measurement of multiplication factor in section 2.4.

## 2.3 Theoretical Approaches

Many authors have attempted to predict impact ionization coefficients theoretically. The approach uses the Boltzmann transport equation, which describes the effects of electric field, collisions with phonons, and impact ionization on an initial distribution of particles. To predict impact ionization coefficients, the distribution of charge carrier energy as a function of applied electric field must be determined by numerically solving the Boltzmann transport equation. Because of different assumptions and approximations for the collision term and for the initial distribution function, some published results are found to apply better at low electric fields while others apply better at high fields. Later works also account for effects such as non-parabolic bands and temperature dependence, and differ in their use of the threshold energy concept. The results are usually given as a

general form for the equation describing the impact ionization coefficient as a function of electric field, with some parameters to be fitted to experimental data. This section summarizes the historical results achieved by various authors.

### 2.3.1 Wolff: Nearly Spherically Symmetric Distribution Function

Wolff, who in 1954 was the first to study impact ionization coefficients from a theoretical standpoint, assumed that electrons either lost energy in scattering with optical phonons, or in impact ionization events [23]. No other energy loss mechanisms were included. Wolff claimed that the mean free path for impact ionization would be much smaller than the mean free path for scattering with phonons, and thus overall the scattering would be nearly completely randomizing. From this claim he deduced a nearly spherically symmetric distribution function for the electron velocity, particularly at high electric fields. This solution gave an electric field dependence for the electron impact ionization coefficient of

$$\alpha(E) = A\exp\left[-\left(\frac{B}{E}\right)^2\right] \tag{2.13}$$

where A and B are experimentally determined coefficients, and E is the electric field strength.

### 2.3.2 Shockley: Lucky Electron Model

In 1961 Shockley proposed his 'lucky electron' model for low electric fields [24]. In this model, electrons that cause impact ionization must accelerate to the threshold energy without a single scattering event with an optical phonon. Because these energetic electrons have avoided all randomizing collisions, the electron distribution function has a high energy spike in the direction of the electric field. Like Wolff, Shockley assumed parabolic energy bands. The lucky electron model yields an equation for impact ionization coefficient of the form

$$\alpha(E) = A\exp\left(-\frac{B}{E}\right) \tag{2.14}$$

where A and B are again parameters fitted to experimental data.

### 2.3.3 Baraff: General Theory

Baraff combined the approaches of Wolff and Shockley to develop a general three-parameter theory [25]. He assumed an initial velocity distribution characterized by both a spherically symmetric part and a spiked part, then evaluated the Boltzmann equation numerically. Like the others, he assumed parabolic energy bands, and that the energy loss mechanisms are limited to impact ionization and scattering by optical phonons. Also, he assumed that the lattice temperature is low enough so no optical phonons are present and hence electrons cannot acquire energy by absorbing an optical phonon, and that scattering with optical phonons cause an energy loss per scattering event equal to a constant optical phonon energy $E_p$.

In addition, in his numerical solution Baraff assumed that the mean free path for optical phonon emission, $\lambda_p$, is independent of carrier energy; and that the mean free path for impact ionization, $\lambda_i$, is constant for carrier energies greater than the ionization threshold energy $E_i$. He used the concept of cross section to indicate the relative probability of each type of collision, given the energy of the carrier. Once a carrier reaches the threshold energy, Baraff assumed that the ionization cross section is the same as the phonon emission cross section. He stated that alpha depends only weakly on ionization cross section, as long as the ionization cross section is greater than one-quarter of the phonon emission cross section.

Baraff's results for impact ionization coefficient as a function of electric field are presented as a series of normalized curves of the form $\alpha\lambda_p$ versus $E_i/qE\lambda_p$. These curves are parameterized by $E_p/E_i$, the ratio of optical phonon energy to ionization threshold energy. The optical phonon mean free path, $\lambda_p$, can be determined by fitting the data from a set of experimental impact ionization measurements to a Baraff curve. Figure 2.3 shows examples of Baraff's curves for a general carrier.

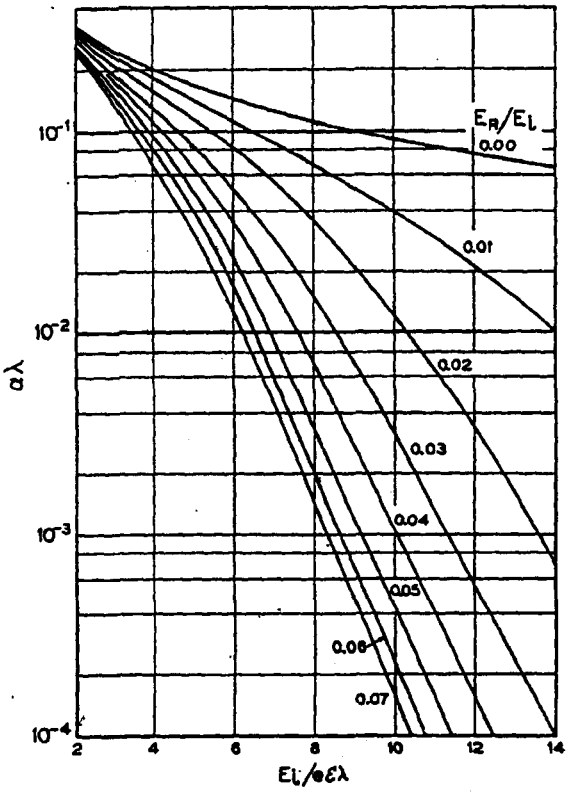


**Figure 2.3. Baraff's curves of $\alpha\lambda_p$ vs. $\varepsilon_i/qE\lambda_p$ for a general carrier parameterized by an optical phonon energy to ionization threshold energy ratio of $E_p/E_i$. [25]**

## 2.3.4 Crowell and Sze: Temperature Dependence

Crowell and Sze extended Baraff's work to include the temperature dependence of impact ionization rate. They added the effects of optical phonon absorption, which is important for materials such as GaAs in which the thermal energy kT at room temperature is significant relative to the optical phonon energy. The ionization threshold energy ($E_i$) and the optical phonon mean free path ($\lambda_p$) are still used as parameters, but to account for both phonon energy loss mechanisms, they replaced $E_p$ in Baraff's work by $\langle E_p \rangle$, the average energy lost per phonon collision [19]:

$$\frac{\langle E_p \rangle}{E_p} = \frac{1}{2N+1} = \tanh\left(\frac{E_p}{2kT}\right) = \frac{\lambda}{\lambda_0} \tag{2.15}$$

where N is the number of phonons per mode of vibration of energy $E_p$ and $\lambda_0$ is the high-energy, low-temperature asymptotic value of the phonon mean free path.

They note that the equation implies that the energy lost per unit path length is independent of temperature:

$$\frac{\langle E_p \rangle}{\lambda_p} = \frac{E_p}{\lambda_0} = \text{constant} \tag{2.16}$$

Both $<E_p>$ and $\lambda_p$ have the same relation with temperature, so the decrease in average energy lost per collision is balanced by the decrease in mean free path (alternatively, by the increase in number of collisions per unit path length).

They also suggested an approximation of the Baraff curves by the equation [19]:

$$\alpha\lambda_p = \exp\left[\left(11.5p^2 - 1.17p + 3.9\times10^{-4}\right)x^2 + \left(46p^2 - 11.9p + 1.75\times10^{-2}\right)x - \left(757p^2 - 75.5p + 1.92\right)\right] \tag{2.17}$$

where

$$p = \frac{\langle E_p \rangle}{E_p}, and\ x = \frac{E_i}{eE\lambda_p} \tag{2.18}$$

Crowell and Sze determined that for a given electric field, the impact ionization rate should decrease as temperature increases. They also concluded that in the low-field region the ionization rate is strongly dependent on temperature, but in the high-field region the temperature dependence is less pronounced. They argued that in a low field region, a carrier can only gain enough energy to cause ionization if it avoids collisions with phonons (similar to Shockley's lucky electron). When the optical phonon mean free path decreases (because of a temperature increase), the carriers are more likely lose energy in collisions with phonons and therefore the ionization rate decreases. At high electric fields, however, a larger fraction of carriers cause ionization. Crowell and Sze argue that at high fields the number of collisions per unit distance ($1/\lambda_p$) becomes less significant in determining the probability that a carrier will reach the ionization threshold energy; instead, the important quantity is the energy lost per unit distance, which is independent of temperature according their argument in equation 2.16.

### 2.3.5 Keldysh: Effect of Energy Dependent Phonon Scattering

Keldysh also used an analytic solution of the Boltzmann equation to determine energy-dependent ionization rates in 1965 [26]. He focussed on determining the impact ionization rate once the energy distribution function is known, by examining the

competition between impact ionization and phonon scattering as energy loss mechanisms for charge carriers that were above the threshold energy level. Along with the threshold energy, the Keldysh formula includes a second parameter that measures the threshold hardness to indicate the probability that impact ionization will occur instead of phonon scattering [18].

### 2.3.6 Dumke: Non-Parabolic Bands

The results described above are limited to semiconductors with parabolic energy bands, which excludes materials such as InSb and InAs. Further work by Dumke in 1968 expanded the assumptions used by the previous authors by allowing for non-parabolic conduction bands [27]. His work assumes that anisotropic polar-mode scattering is the primary energy loss mechanism. The scattering direction is not symmetric, and the electron energy distribution has a peak in the direction of the electric field.

### 2.3.7 Bude and Hess: Soft Energy Thresholds

In 1992 Bude and Hess performed full band Monte Carlo simulations and showed that the use of strict or hard energy thresholds to determine rates of impact ionization should be abandoned [18]. They replaced hard thresholds, based on the minimum carrier energy required to satisfy conservation of crystal momentum and energy in an impact ionization event, with numerically calculated effective thresholds. In their work, they defined the effective ionization threshold as the lowest energy for which the ionization rate is greater than $10^9$ $s^{-1}$; carriers with less energy do not contribute significantly to $\alpha$.

Bude and Hess argued that the parameters used extensively in previous work, including the ionization threshold, the phonon mean free path, and the average energy lost per phonon collision, were oversimplified and inapplicable because of the assumption of parabolic energy bands. The Keldysh formula, which gives the probability of impact ionization for carriers, assumes parabolic bands and a direct bandgap, and thus does not account for the full band structure. As a result, previous models failed to correctly predict the increase of ionization rate above the expected threshold energy level.

The focus of their work is to properly account for the density of states in the semiconductor, because the density of states influences both the effective threshold and

the average carrier energy. They conclude that for materials with a small energy bandgap, such as InAs and InGaAs, the threshold is soft and the threshold energy is close to the bandgap energy. For a wide bandgap material with a small density of states at low energy, such as InP, the threshold is harder and the threshold energy is much higher than the bandgap energy. In their work, Bude and Hess present calculated energy dependent ionization rates for several different compounds semiconductors, including InP.

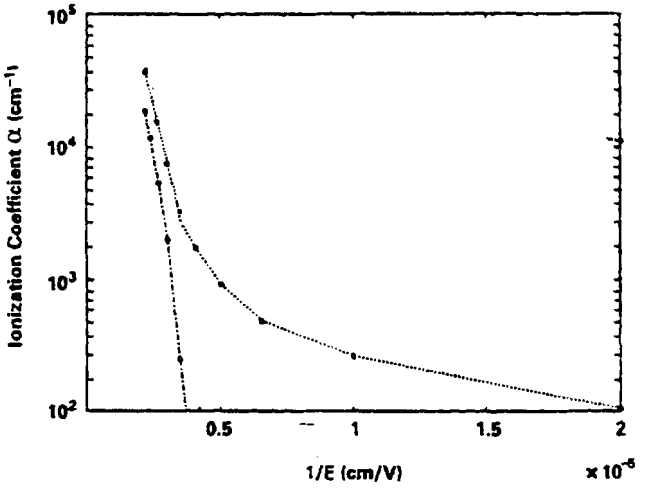


**Figure 2.4. Calculated electron-initiated impact ionization coefficient for InP as a function of inverse electric field. Dotted line: $In_{0.57}Ga_{0.43}As$; and Dot-dashed line: InP. Adapted by permission of Hess [18].**

## 2.4 Experimental Measurement of Multiplication Factor

Impact ionization coefficients can be determined experimentally in a number of ways. The usual method is to extract α as a function of electric field from a measurement of the multiplication factor, M or M-1, over a range of applied voltage. This section discusses several methods of measuring M-1, and reviews results for InP impact ionization coefficient measurements previously reported in the literature.

Several considerations are common to all methods of measuring the multiplication factor. First, the initiating current before impact ionization must be precisely known. Ideally, this current is composed entirely of one type of charge carrier, because the measurement is intended to determine either the hole-initiated or the electron-initiated multiplication factor (and hence the corresponding ionization coefficient). Second, the

amount of current increase due to multiplication is critical to the calculation. The bias-dependent current contribution from effects other than impact ionization, such as the reverse-bias leakage current $I_{cb0}$ and the Early effect in HBTs, must be accounted for or eliminated. These effects may be the limiting factors in the determination of impact ionization coefficient, if they are too large and the quantity of current increase due to impact ionization cannot be measured accurately. Third, the electric field magnitude and profile must be known in order to extract the ionization coefficient from the multiplication data, as discussed below in section 2.5, and to associate the ionization coefficient with the correct electric field value.

Once the first two basic quantities are known for a given set of conditions, the multiplication factor M can be calculated by dividing the final current by the initiating current. Other equations for M-1 will be given in the following sections. The variables in these equations are structure-dependent quantities that are more easily or more directly measured than the currents discussed above.

### 2.4.1 Measurements Using Avalanche Photodiodes

Prior to the 1990s, avalanche photodiodes with specially thinned substrates were the primary type of device used for impact ionization coefficient measurements [28]. Some measurements were performed on linearly graded diodes or on Schottky barrier diodes. However, these devices are considered less suitable than avalanche photodiodes because the electric field profile is more complex, and because the diodes may exhibit undesired photocurrents that affect the measurements [10].

The objective was to inject either a pure electron or a pure hole current to the same abrupt p-n junction, using an avalanche photodiode that could be illuminated from both sides (or from the top and bottom). The front and back surfaces were illuminated in turn by a laser, with all incident radiation absorbed before the depletion layer, and the injected hole or electron photocurrent would be treated as a sheet of charge diffusing towards the depletion layer.

The main difficulty was to precisely determine the amount and type of initiating current. This approach requires modelling of diffusion length in order to predict the amount of current that reaches the depletion region and initiates impact ionization. The

depletion region boundary moves depending on the applied bias, which changes the distance that the charge carriers must diffuse. Both surface and bulk recombination must be accounted for. The possibility that carriers may be regenerated from absorption of sub-bandgap radiation caused by recombination creates some uncertainty as to how well the 'pure injection' condition is maintained [13]. Another concern is that if the edge of the device is illuminated by the laser, the electric field that causes impact ionization will not be constant from the perimeter to the bulk of the device [13, 12, 20].

The data listed in Table 2.1 and plotted in Figure 2.5 have been reported in the literature for InP impact ionization coefficients, measured using avalanche photodiodes grown on (100) oriented InP. The wafers are grown by liquid phase epitaxy except for those used by Taguchi et al, which are grown by vapour phase epitaxy. The results show some variation in the common range of electric field. The values reported by Umebu et al and Taguchi et al agree well while the measurements reported by Cook et al show a different slope over a wider range of field. The earlier measurements by Armiento et al show a similar slope but with a lower magnitude of impact ionization coefficient. The values of ionization coefficient predicted by Bude and Hess are higher in magnitude than the rest.

| Author | Range of electric field, E (V/cm) | InP electron-initiated impact ionization coefficient, $\alpha_n$ ($cm^{-1}$) |
|---|---|---|
| Armiento et al, 1979 [10] | $4.85\times10^5$ to $6.37\times10^5$ | $1.07\times10^7\exp(-4.31\times10^6/E)$ |
| Umebu et al, 1979 [12] | $5\times10^5$ to $8\times10^5$ | $7.36\times10^6\exp(-3.45\times10^6/E)$ |
| Cook et al, 1981 [13] | $2.4\times10^5$ to $3.8\times10^5$ | $1.12\times10^7\exp(-3.11\times10^6/E)$ |
| | $3.6\times10^5$ to $5.6\times10^5$ | $2.93\times10^6\exp(-2.64\times10^6/E)$ |
| | $5.3\times10^5$ to $7.7\times10^5$ | $2.32\times10^5\exp(-7.16\times10^{11}/E^2)$ |
| Taguchi et al, 1985 [20] | $4\times10^5$ to $6\times10^5$ | $9.2\times10^6\exp(-3.44\times10^6/E)$ |

**Table 2.1. Literature reports of InP electron-initiated impact ionization coefficients measured with avalanche photodiodes.**

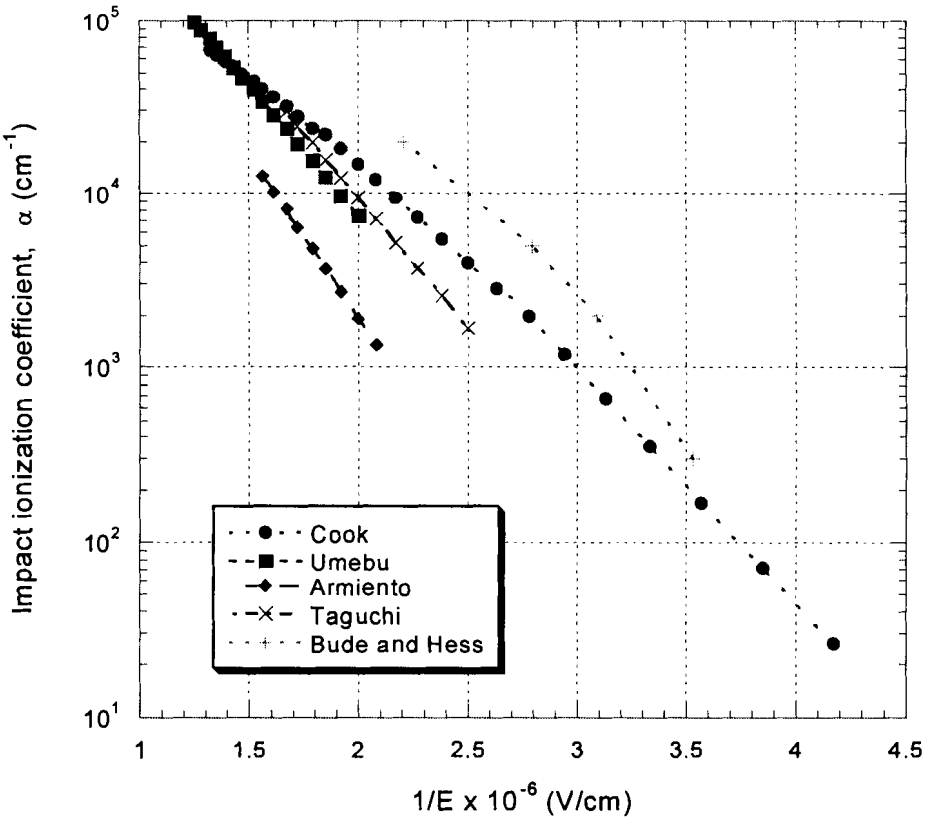


**Figure 2.5. InP electron-initiated impact ionization coefficients reported in the literature.**

## 2.4.2 Measurements Using HBTs with Constant Emitter Current

The advantage of using an HBT over a photodiode is that there is no need for a photocurrent. This eliminates much of the uncertainty in the impact ionization values that is caused by the difficulty in precisely knowing the magnitude and composition of the primary photocurrent. A disadvantage of HBTs is that electron- and hole- initiated multiplication cannot be measured in the same device.

In the constant emitter current method, the emitter current, $I_e$, is a parameter set by the external measurement system. The transistor is biased in constant current mode: the base-emitter voltage, $V_{be}$, is allowed to adjust as required to maintain a constant emitter current. Since a common-base configuration is used, the reverse bias across the base-collector junction, $V_{cb}$, can also be forced independently.

For n-p-n transistors, the initiating current is composed of injected electrons. The magnitude of the initiating current depends on the emitter current and the transistor gain. Electron-hole pairs are created by impact ionization within the base-collector depletion region. The electrons are swept to the collector contact while the holes drift back to the base and flow out of the base contact. Therefore, as $V_{cb}$ increases and more impact ionization occurs, the magnitude of the collector current increases and that of the base current decreases by an equal amount. As reported by Zanoni et al, the base current may become negative if enough holes are generated [14]. Here, currents are conventionally defined as positive if entering their respective contact. The change in either the collector current, $I_c$, or the base current, $I_b$, can be used to calculate the number of electron-hole pairs generated by impact ionization. From current continuity, at any fixed collector-base bias the total current must remain constant through the device. An impact ionization event generates an electron and a hole, which are swept by drift in opposite directions. As a result, although the total current is constant, the proportion of current carried by electrons vs holes varies with position as shown previously in Figure 2.2. When the applied collector-base bias is changed, the current is affected because the number of impact ionization events depends on the applied bias. The change in the number of electrons seen at the collector contact due to impact ionization is the same as the change in the number of holes seen at the base contact.

$$I_{cFinal} = MI_{c0} \tag{2.19}$$

$$\Delta I_c = (M-1)I_{c0} = |\Delta I_b| \tag{2.20}$$

The absolute magnitude of the change is the same for both currents, but since the base current is smaller than the collector current by a factor of the current gain, β, the change is a much larger proportion of the original base current.

In the absence of sources of current increase other than impact ionization, the equation used to calculate the multiplication factor from the measured base or collector currents is:

$$M-1 = \frac{\Delta I_c}{I_c(V_{cb}=0)} = \frac{|\Delta I_b|}{I_c(V_{cb}=0)} = \frac{|I_b(V_{cb}) - I_b(V_{cb}=0)|}{I_c(V_{cb}=0)} \tag{2.21}$$

For this equation to be valid, the open-emitter collector-base leakage current, $I_{cb0}$, must be negligible compared to the change in the base or collector current. For example, in measurements of InGaAs electron ionization coefficient by Neviani et al, $I_{cb0}$ remains below 5% of $\Delta I_b$ [16]. The current contribution from the Early effect must also not obscure the current increase due to impact ionization. This condition may be met depending on the magnitude of the ionization coefficient in the material, the base doping, the electric field range of the measurement, and by using a constant base-emitter bias instead of a constant emitter current, as discussed further in section 2.4.3. Other assumptions are that the self-heating of the device must be negligible, because the current gain in bipolar transistors is generally dependent on temperature, and that holes generated by impact ionization should exit at the base, rather than ending up in the emitter.

If $I_{cb0}$ is large relative to the change in collector or base current due to impact ionization, then it must be removed from the calculation of multiplication factor. In their measurement of InGaAs hole ionization coefficient, Buttari et al make the correction by measuring $I_{cb0}$ as a function of $V_{cb}$, and subtracting it from the total change in current [29]. In the numerator of equation 2.21, the change in current due to $I_{cb0}$ is subtracted, in order to isolate the contribution from impact ionization.

$$M-1=\frac{\Delta I_c - I_{cb0}(V_{cb})}{I_c(V_{cb}=0)}=\frac{\left|\Delta I_b - I_{bc0}\right|}{I_c(V_{cb}=0)} \tag{2.22}$$

In the low-field measurement of GaAs electron ionization coefficient by Canali et al, the Early effect limits the measurement at low field, even when the device is driven at constant $V_{be}$ [30]. Shamir and Ritter found the Early effect to be limiting for GaInAsP measurements but not for InGaAs measurements. They proposed a correction to the multiplication factor for the Early effect given by:

$$Err(M-1)\approx\frac{2\varepsilon\varepsilon_0 V_{cb}}{\beta_0 w_c Q_B} \tag{2.23}$$

$$Q_B = qN_B w_{B0} \tag{2.24}$$

where $\varepsilon$ is the relative dielectric constant, $\beta_0$ is the common emitter current gain at $V_{cb}$=0, $w_c$ is the width of the collector depletion region, $w_{b0}$ is the base width at $V_{cb}$=0, and $N_B$ is the dopant concentration in the base [31]. The Early effect contribution is minimized in a

device with high gain, high base doping, and low collector doping. It can also be reduced by measuring the ionization coefficient with the HBT at constant base-emitter voltage rather than constant emitter current, as discussed in section 2.4.3.

The constant emitter current configuration has several advantages over the constant base-emitter voltage configuration that is described in the next section. With a constant emitter current, the initiating current that enters the collector for impact ionization is more constant over the range of $V_{cb}$. The base current is less sensitive to self-heating or other temperature variation during the course of a measurement than for constant $V_{be}$ measurements. Although the constant base-emitter bias reduces the error caused by the Early effect, for the devices used in this work the Early effect is not a limiting factor. Due to the heavily doped base and lightly doped collector, most of the change in depletion width occurs on the collector side and the base depletion width changes very little with collector-base bias. Therefore, the constant $I_e$ configuration is the method used for measurements on InP in this work.

### 2.4.3 Measurements Using HBTs with Constant Base-Emitter Voltage

In the constant base-emitter voltage ($V_{be}$) method, the forward bias on the base-emitter junction is kept constant, thereby causing a current to be injected into the base. This method is sometimes used for low field measurements, especially for materials with low ionization coefficients, where the Early effect is the limiting factor for measurement accuracy.

For both constant $V_{be}$ and constant $I_e$, the total minority charge stored in the base is reduced by the Early effect when $V_{cb}$ is increased. As a result, the recombination current decreases, which adds an undesirable component to the calculated change in base current. The effect is worse for constant $I_e$ measurements than for constant $V_{be}$ measurements because the change in the amount of stored minority charge is greater. In addition, constant emitter current measurements also suffer from a decrease in $V_{be}$. Recombination in the base-emitter space charge region decreases as well, adding another source of error to the calculated change in base current.

In their study of multiplication in SiGe HBTs, Niu et al make measurements at constant base-emitter voltage because of the advantages in controlling the initiating

current when hole injection from the base into the emitter is a major component of the base current [32]. If some of the holes generated by impact ionization do not exit at the base, they are not measured as part of the change in base current and this causes an error in the determination of multiplication factor. The effect is large if hole back-injection into the emitter is a large contributor to the base current. However, in this work, the large valence band discontinuity (~0.78 eV) in the devices prevents hole back-injection from being a problem.

## 2.5 Extraction of Ionization Coefficient From M

The calculation of impact ionization coefficient, $\alpha$, can be more complex than the measurement of the multiplication factor. The extraction of $\alpha$ from M-1 depends on the structure of the device used to measure M-1. The magnitude of the electric field is an important parameter, while the electric field profile determines which equations must be used. This section presents the equations used to calculate $\alpha$ for the devices used in this work.

The simplest case occurs when the multiplication factor is measured across a constant electric field. This occurs in a p-i-n diode and, effectively, in some HBTs with nominally undoped or lightly doped collectors. In this case, the ionization coefficient $\alpha_n$ is nearly constant over the region of impact ionization. Hence, the value of $\alpha_n$ is easy to associate with an electric field strength, since the average and the maximum electric field values are the same or nearly the same. At low fields, the uncertainty caused by attributing the multiplication values to the maximum value of the electric field versus the average electric field strength can be the limiting factor, as reported by Canali et al for low field InGaAs electron ionization coefficient measurements [15].

The electric field profile in the device can be determined by solving Poisson's equation. Shamir and Ritter simply use

$$E_{avg} = \frac{V_{bi} + V_{cb}}{w} \tag{2.25}$$

where $E_{avg}$ is the average electric field in the collector, $V_{bi}$ is the built-in voltage of the base-collector junction, $V_{cb}$ is the applied reverse bias voltage, and w is the width of the

depletion region over which impact ionization occurred [33]. The equations for the maximum electric field and the average electric field for the HBTs used in this work are discussed in Chapter 3.

With some assumptions, the relation between impact ionization coefficient and multiplication factor (equation 2.11) can be simplified and the ionization coefficient can be extracted from the multiplication factor. Assuming that secondary impact ionization events are negligible, and that $\alpha_n$ is a function of the local electric field, then $\alpha_n$ can be calculated by simple division:

$$\alpha_n = \frac{M_n - 1}{w_c} \tag{2.26}$$

This equation can be used for measurements made with HBTs when the collector is nominally undoped, or lightly doped up to a concentration of $10^{16}$ $cm^{-3}$ [14, 29].

# Chapter 3
# HBT Operation

## 3.1 Introduction

This chapter provides the information required to understand how NpN heterojunction bipolar transistors (HBTs) are used to measure electron-initiated impact ionization coefficients. HBTs can be made from many different combinations of compound semiconductors, and section 3.2 discusses material considerations and describes the InP/GaAsSb/InP heterostructure system used in this work. Section 3.3 focuses on the depletion region and electric field at the base-collector junction. It includes equations to calculate the maximum electric field under an applied reverse bias, before and after the depletion region punches through to the subcollector. Next, section 3.4 describes the currents in a n-p-n HBT for the purpose of determining the initiating current used in impact ionization measurements. Effects other than impact ionization can cause transistor behaviour to deviate from the idealized case of constant collector current under an applied reverse bias. These effects, including the Early effect, the Kirk effect, and non-constant gain under self-heating, are reviewed from the perspective of impact ionization measurements in the final section of this chapter.

## 3.2 Material System

An HBT, like a bipolar junction transistor (BJT), is a three-terminal electronic device containing two p-n junctions. Current flows primarily through the emitter and collector terminals, with a much smaller current through the base terminal. The emitter current is controlled by the voltage applied across the base-emitter junction. In a BJT, the

emitter-base and the base-collector junctions are homojunctions: they are formed in the same semiconductor, by changing the doping type. In contrast, an HBT contains at least one heterostructure p-n junction, which consists of two different semiconductors in contact.

In both HBTs and BJTs, one side of a p-n junction is doped with donors to make it an n-type semiconducting material, and the other side is doped with acceptors to make it a p-type material. The doping levels are important design parameters because they affect many aspects of the transistor performance. For example, in a BJT, good current gain and high frequency performance are tradeoffs. To maximize one by changing the base doping has an undesirable effect on the other. However, in an HBT the different energy bandgaps of the two materials provide more flexibility to tailor the transistor's performance characteristics. In particular, a wide bandgap material is used for the emitter, thus achieving reasonable current gain. Then, the base doping can still be increased to improve the base conductivity and achieve high frequency operation without sacrificing gain.

This work was conducted using InP/GaAsSb/InP HBTs. In order to study impact ionization in InP using an HBT, the transistor must have an InP collector. However, most HBTs with InP collectors have a straddling, or type I, energy band lineup as shown in Figure 3.1 for the InP/InGaAs/InP system. The conduction band discontinuity causes an energy band spike at the base-collector junction and current blocking. The existence of a blocking potential makes it difficult to determine the value of electric field strength associated with a given level of impact ionization. Attempts to eliminate this spike have relied on doping schemes, which change the electric field, or on compositional grading of the semiconductors, which destroy the abrupt transition to InP required for impact ionization measurements. The InP/GaAsSb/InP material system has a staggered, or type II, energy band lineup, also shown in Figure 3.1. This heterostructure was developed to eliminate current blocking effects without requiring compositional grading to smooth out the energy band spike [34]. The abrupt junctions and lack of current blocking make the system well-suited to studying the electron-initiated impact ionization properties of InP.

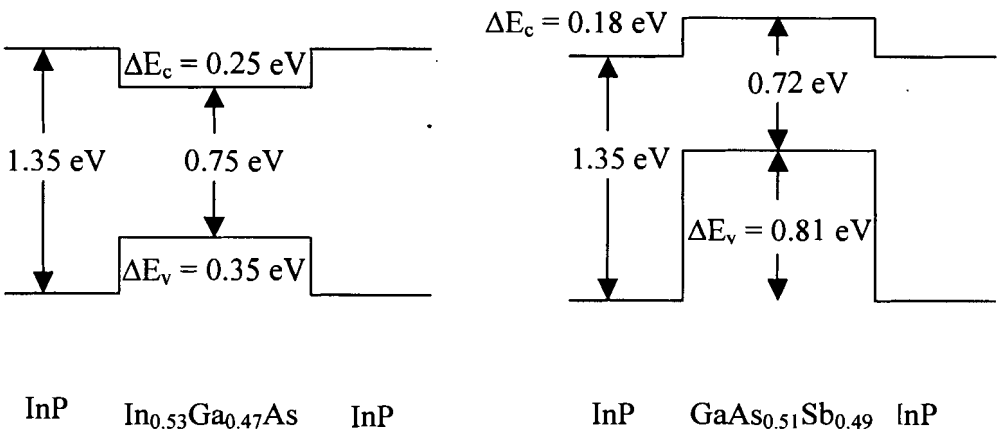


**Figure 3.1. Straddling and staggered band lineups for HBT material systems [35, 34].**

## 3.3 Depletion Region and Electric Field

The electric field profile in a transistor is very important in impact ionization measurements. The strength of the field determines the amount of impact ionization; usually, the impact ionization coefficient is given as a function of electric field. In measurements using HBTs, the impact ionization coefficient is assumed to be purely a function of the local electric field. This assumption fails when distances are very short and the field gradient is very large; then, the dead space effect must be considered. In many cases, the assumption is adequate and the average or the maximum electric field is treated as the independent variable for plotting impact ionization, depending on the doping level of the collector. Occasionally, results are reported using both the maximum electric field and the average electric field to provide an indication of the possible error due to the field variation across the collector.

Section 3.3.1 reviews basic equations for depletion width and electric field strength. These equations apply generally to any p-n junction in equilibrium. The discussion in section 3.3.2 refers specifically to the base-collector junction of a n-p-n HBT, and extends the equations to the conditions that may occur in impact ionization measurements.

### 3.3.1 Equilibrium p-n Junctions

In a p-n junction in equilibrium, the free charge distributes itself to create a balance between charge transport by diffusion and by drift. A depletion region of exposed space charge exists on either side of the junction and as a result there exists an electric field which gives rise to the 'built-in voltage', $V_{bi}$. Often, the change in dopant concentration is idealized as an abrupt step. The square-box depletion approximation also assumes abrupt changes in the exposed space charge, and no voltage drop across the quasi-neutral n and p regions. The existence of charge tails is accounted for by including the Gummel end correction factor in the equations presented below. This factor reduces the applied bias by 2kT/q. The space charge, electric field, and built-in voltage are shown in Figure 3.2.

The width of the depletion region depends on the concentration of acceptors, $N_A$, and the concentration of donors, $N_D$, on either side of the junction, and increases with an applied external reverse bias $V_r$ according to the following equation:

$$w = \sqrt{\frac{2\varepsilon_0\varepsilon_s}{q}\frac{N_A + N_D}{N_A N_D}\left(V_{bi} + V_r - \frac{2kT}{q}\right)} \tag{3.27}$$

where $\varepsilon_0\varepsilon_s=\varepsilon$ is the semiconductor permittivity, q is the elementary charge, k is Boltzmann's constant, T is the temperature in Kelvin and 2kT/q is the Gummel end correction factor to account for the slight deviation from the depletion approximation. In Figure 3.2, $w_p$ and $w_n$ refer to the depletion region widths in the p-type base and the n-type collector.

Similarly, the maximum electric field is given by the following equation:

$$E_{max} = \frac{q}{\varepsilon_0\varepsilon_s}\frac{N_A N_D}{N_A + N_D}w = \sqrt{\frac{2q}{\varepsilon_0\varepsilon_s}\frac{N_A N_D}{N_A + N_D}\left(V_{bi} + V_r - \frac{2kT}{q}\right)} \tag{3.28}$$

Since the doping and exposed charge are constant, the electric field changes linearly from $E_{max}$ to 0 over the width of the depletion region on either side of the p-n junction. The total voltage across the junction, $V_{bi} + V_r$, can be determined by integrating the electric field across the depletion region.

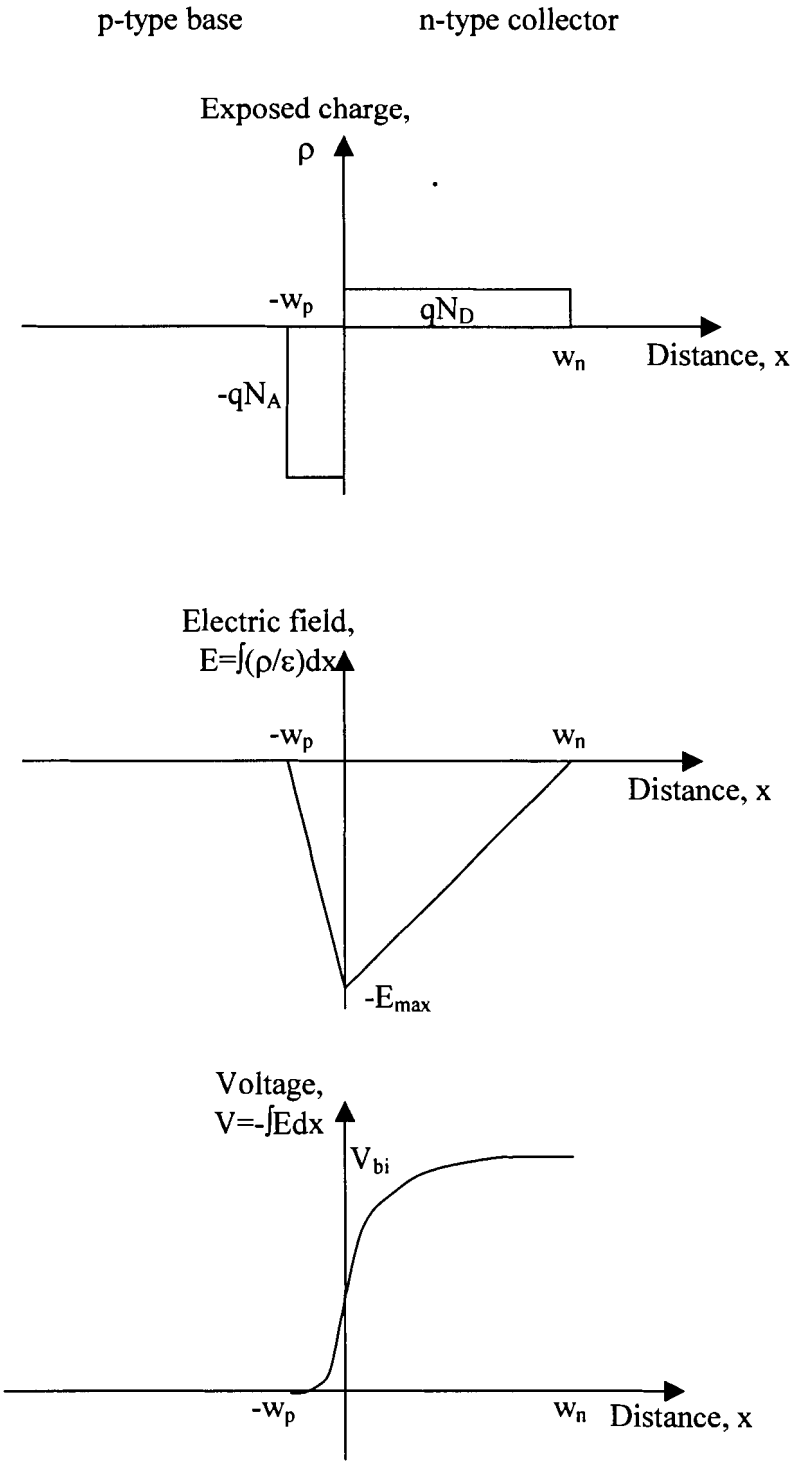


**Figure 3.2. Depleted space charge regions, electric field profile, and voltage distribution at the base-collector junction of an n-p-n HBT.**

### 3.3.2 Punchthrough to Subcollector

When a higher reverse bias is applied to the junction, the electric field increases as well. This section considers the situation in the base-collector junction of an n-p-n transistor, where the collector has a finite width $w_c$. In this case, the reverse voltage $V_r$ is also referred to as the collector-base bias $V_{cb}$. As long as the depletion width on the collector side remains less than $w_c$, the equations presented in the previous section apply. When the entire collector is depleted, the depletion region 'punches through' to the highly doped subcollector. In some transistors with thin collectors, this is the equilibrium situation which occurs before any external reverse bias is applied. For other devices, a very high reverse bias is needed. As $V_{cb}$ increases, $E_{max}$ and total depletion width both increase as shown in Figure 3.3.

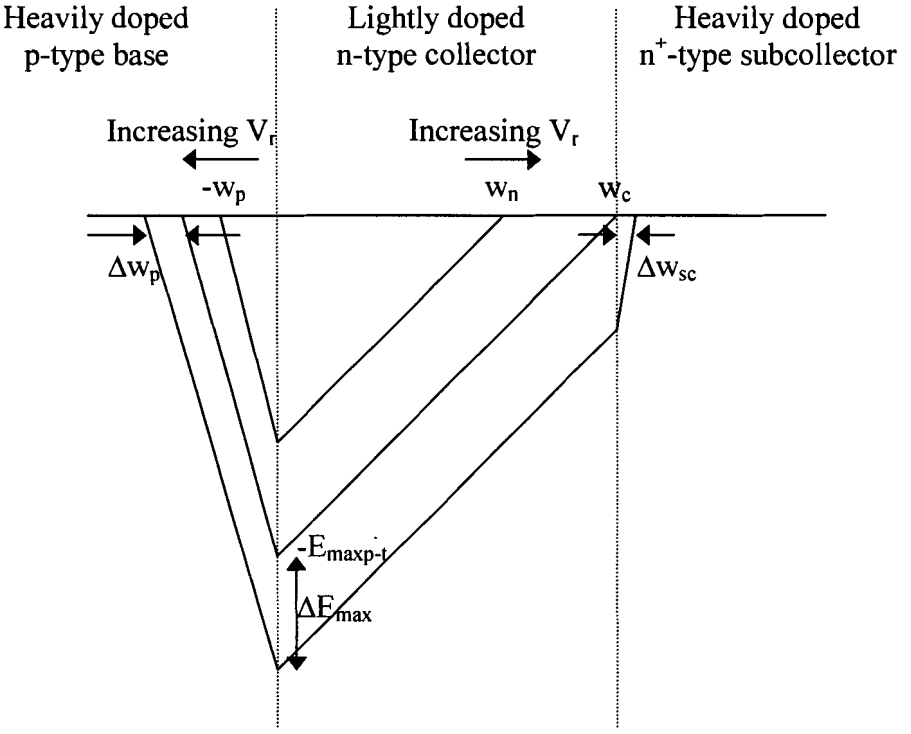


**Figure 3.3. Base-collector electric field profile in a n-p-n HBT with increasing reverse bias before, at, and after depletion region punchthrough to the subcollector.**

At punchthrough, the maximum electric field $E_{maxp\text{-}t}$ and the applied voltage $V_{p\text{-}t}$ are given by the following equations:

$$E_{\max\, p-t} = \frac{qN_D w_c}{\varepsilon_0 \varepsilon_s} \tag{3.29}$$

$$V_{p-t} = E_{\max\, p-t}\,\frac{w_{pp-t} + w_c}{2} + 2\frac{kT}{q} \tag{3.30}$$

where $V_{p\text{-}t}$ includes the built-in voltage, $V_{bi}$, the applied reverse voltage, $V_r$, and the Gummel end correction 2kT/q; the depletion width on the n-side is now the entire collection width, $w_c$; and the depletion width on the base side is $w_{pp\text{-}t}$.

An increase in reverse voltage beyond $V_{p\text{-}t}$ extends the depletion region and the electric field into the subcollector. The change in the maximum electric field, $\Delta E_{max}$, can be expressed in terms of the change in the p-type base depletion width, $\Delta w_p$, the subcollector depletion width, $\Delta w_{sc}$, or the total depletion width $\Delta w = \Delta w_p + \Delta w_{sc}$. Then, the increase in voltage $\Delta V$ can be written in terms of these changes, the magnitude of the electric field at punchthrough, and the collector width:

$$\Delta E_{\max} = \frac{qN_A \Delta w_p}{\varepsilon} = \frac{qN_{Dsc} \Delta w_{sc}}{\varepsilon} = \frac{qN_A N_{Dsc} \Delta w}{\varepsilon(N_A + N_{Dsc})} \tag{3.31}$$

$$\Delta V = E_{\max\, p-t} \Delta w_p + \frac{1}{2}\Delta E_{\max} \Delta w_p + w_c \Delta E_{\max} + \frac{1}{2}\Delta E_{\max} \Delta w_{sc} \tag{3.32}$$

This relation gives a quadratic equation for the change in depletion width $\Delta w$:

$$\frac{q}{2\varepsilon}\frac{N_A N_{Dsc}}{N_A + N_{Dsc}}\Delta w^2 + \frac{1}{N_A + N_{Dsc}}\left(E_{\max\, p-t} N_{Dsc} + \frac{w_c q N_A N_{Dsc}}{\varepsilon}\right)\Delta w - \Delta V = 0 \tag{3.33}$$

This equation can be solved for $\Delta w$ and combined with the equation 3.31 for $\Delta E_{max}$, to express $\Delta E_{max}$ as a function of $\Delta V$. Thus the maximum electric field $E_{max}$ can be calculated for any range of applied $V = V_{bi} + V_r - 2kT/q$, before or after punchthrough occurs.

## 3.4 Currents

Impact ionization measurement is primarily concerned with currents in the transistor. The initiating current at the base-collector junction must be accurately known, and the increase in collector current due to impact ionization must be determined. This section discusses currents in the n-p-n HBT. Basic background information is provided in section 3.4.1, followed by equations for the initiating current and change in currents which are crucial to impact ionization measurements in section 3.4.2.

### 3.4.1 Current Components in an HBT

To generate a current in a n-p-n HBT, the base-emitter junction is forward biased to inject minority charge carriers into each side of the base-emitter junction. The electron concentration injected into the p-type base is described by the Shockley boundary condition:

$$n_p(at\ depletion\ edge) = n_{p0} \exp\left(\frac{qV_f}{kT}\right) \tag{3.34}$$

where $n_{p0}$ is the equilibrium concentration of electrons in the p region without any applied bias, and $V_f$ is the forward bias. Thus, the minority carrier concentration in the base increases exponentially with a forward bias, $V_f$ or $V_{bc}$, applied to the base-emitter junction.

The injected minority carriers at the edge of the base depletion region set up a concentration gradient across the neutral base. As a result, a steady-state current exists because charge carriers diffuse across the base. This diffusion current is given by the following equation:

$$J_n = qD_n \frac{dn}{dx} = \frac{qD_n n_{p0}}{w_b}\left[\exp\left(\frac{qV_f}{kT}\right) - 1\right] \tag{3.35}$$

where $J_n$ is the electron current density in the base, $D_n$ is the diffusion coefficient for electrons in the semiconductor, and $w_b$ is the width of the base.

The charge carriers that reach the base-collector junction are swept into the collector by the junction built-in voltage and external reverse bias. This electron current,

controlled by a forward bias applied to the base-emitter junction, forms the primary component of the emitter and collector currents.

A major component of the base current comes from recombination in the base. Recombination occurs in the quasi-neutral base, in the bulk of the depleted space-charge region, and at the heterojunction interface. Some of the excess electrons in the base recombine with holes and to maintain charge neutrality these holes must be replaced; the supply of holes that enters through the base terminal contributes to the base current.

A second component of the base current and also the emitter current is minority carrier back-injection from the base to the emitter. Here, the advantage of a heterojunction over a homojunction is evident. In an HBT with a wide bandgap emitter, the equilibrium concentration of holes in the emitter is much smaller than the concentration of electrons in the base, as seen in the following equation:

$$\frac{n_{p0}}{p_{n0}} = \frac{N_A}{N_D}\frac{(N_C N_V)_p}{(N_C N_V)_n}\exp\left(\frac{-E_{Gp}+E_{Gn}}{kT}\right) \tag{3.36}$$

where $(N_C N_V)_{p,n}$ is the density of states in the conduction and valence bands, for the p- and n-type materials, $E_{Gp}$ is the energy bandgap in the narrow-gap p-type base, and $E_{Gn}$ is the energy bandgap in the wide-gap n-type emitter. The quantity of holes injected into the emitter depends on the equilibrium hole concentration, as governed by the Shockley boundary condition analogous to equation 3.34 for electron injection into the base. Hence, under a forward bias, the hole back-injection from the narrow bandgap base to the wide bandgap emitter is very small and can be neglected.

An important current is the reverse-bias collector-base current, $I_{cb0}$. This current is measured under a reverse bias between the collector and the base, with the emitter open-circuited. It is carried by thermally generated minority carriers, and depends on both the applied bias $V_{cb}$ and the temperature.

Of course, Kirchoff's current law applies so that:

$$I_e = I_c + I_b \tag{3.37}$$

### 3.4.2 Currents for Impact Ionization Measurements

For impact ionization measurements, the initiating current and the change in collector current with applied $V_{cb}$ must be accurately known. The calculations must account for the change in $I_{cb0}$. If $I_{cb0}$ is much smaller than the change in base or collector current, it can be neglected. However, if $I_{cb0}$ as a function of $V_{cb}$ is significant compared to $\Delta I_b$, then it must be subtracted from the measured current in order to calculate the change in current due to impact ionization. The initiating current and the change in collector and base currents are given by the following:

$$I_{init} = I_c(V_{cb} = 0) \tag{3.38}$$

$$\Delta I_c = I_c(V_{cb}) - I_{init} - I_{cb0}(V_{cb}) \tag{3.39}$$

$$|\Delta I_b| = |I_b(V_{cb}) - I_b(V_{cb} = 0) + I_{cb0}(V_{cb})| \tag{3.40}$$

## 3.5 Deviations From Ideal Collector Current

As described previously, most of the carriers injected from the emitter into the base diffuse across the base and are swept into the collector. The magnitude of the collector current depends primarily on the injected current, which is controlled by the voltage, $V_{be}$, applied to the base-emitter junction. In an ideal transistor, the collector current should remain constant regardless of the voltage, $V_{cb}$, applied between the base and collector. In reality, a number of effects cause non-ideal variations in the collector current: the Early effect, the Kirk effect, and non-constant gain versus temperature combined with device self-heating are some important examples. These effects and the implications for impact ionization measurements are reviewed in this section.

### 3.5.1 Early Effect

The Early effect is the name given to an increase in collector current caused by base-width modulation under an increase in base-collector reverse bias. When $V_{cb}$ is increased, the depleted space-charge region around the junction grows larger. Usually the base is more heavily doped than the collector, so most of the total change in depletion

width occurs on the collector side. However, to maintain electric neutrality, the depletion width must increase in both the collector and the base:

$$\Delta w_b N_A = \Delta w_c N_D \tag{3.41}$$

The expansion of the base depletion region results in a decrease in the effective base width that is traversed by the electrons. Since charge transport across the base occurs by diffusion, the change in effective base width affects the concentration gradient and hence the current density, as described in equation 3.35. When the reverse bias increases, the depletion width widens, the effective base width shrinks, the concentration gradient becomes steeper and the current density increases.

The Early effect can be seen in plots of collector current vs collector-emitter voltage, $V_{ce}$. As long as the collector-base junction is still reverse biased, the curves of $I_c$ vs $V_{ce}$ at a fixed value of $V_{be}$ are straight lines. The Early effect causes these lines to have finite slope, and the increase in collector current shows a linear relation with $V_{ce}$.

The change in currents during impact ionization measurements depends on the choice of bias conditions. If $V_{be}$ is held constant, then the base current shows only a small decrease, caused by the shrinkage in the neutral bulk area. In this case the emitter current increases almost as much as the collector current. If instead $I_e$ is kept constant, the base-emitter bias decreases because the injected minority charge must decrease to maintain the same concentration gradient in the base. Since the emitter current is held constant, the base current decreases while the collector current increases.

Because the Early effect causes an increase in the collector current, it is a source of error in impact ionization measurements. It can be distinguished from impact ionization because the Early effect shows a linear increase in collector current with $V_{ce}$, which can be subtracted from the total increase in collector current. However, the Early effect may be the limiting factor for measurements at low electric fields, when there is very little impact ionization.

### 3.5.2 Kirk Effect

The Kirk effect becomes noticeable when the collector current density is high enough for the charge carried by mobile carriers to be comparable to the fixed space

charge in the collector depletion region. The electric field gradient decreases and eventually reaches zero when the current density in the collector, $J_c$, is sufficiently high:

$$J_c = qN_D v_{sat} \tag{3.42}$$

At higher current density in a homojunction collector, the base region extends into the collector. This current-induced base pushout causes a decrease in current gain accompanied by a large increase in base transit time, reducing the device's high frequency performance.

The Kirk effect is important to impact ionization measurements because of the change in electric field caused by the mobile charge carriers. Measurements must account for the Kirk effect at high current densities in order to associate the measured value of multiplication with the correct electric field. If a constant electron velocity can be assumed, the effect is relatively easy to include in calculations of the electric field. The effective charge density contributed by the mobile charge, $n_c$, is related to the current density by the following equation:

$$n_c = \frac{J_c}{qv_{sat}} \tag{3.43}$$

where $v_{sat}$ is the saturation velocity of electrons travelling in the collector. The net exposed charge in the collector depletion region becomes $N_D - n_c$, and this quantity replaces $N_D$ in the equations for depletion width, maximum electric field, and applied voltage discussed in section 3.4.

### 3.5.3 Self Heating

The gain of a transistor usually varies with current density. The gain also depends on the operating temperature of the device. When a device operates at high power, it heats up; this temperature increase produces a change in gain, which causes a change in the base and collector currents. In the case of InP/GaAsSb/InP HBTs, the gain temperature coefficient is positive. As a result, positive feedback occurs when the device heats up, causing the gain and hence the collector current to increase, and resulting in further device heating which continues the cycle.

In impact ionization measurements, the temperature should be constant throughout the measurement. If a series of measurements involves increasing the applied reverse-bias voltage and hence the dissipated power, an increase in temperature could cause an increase in the collector current that is due to the change in gain rather than impact ionization.

An opposing effect is the decrease of the InP impact ionization coefficient at higher temperatures. If the equilibrium operating temperature is higher than the nominal value due to power dissipation, then the amount of multiplication will be lower and the true impact ionization coefficient for the assumed temperature will be underestimated.

The temperature rise can be calculated by considering the power dissipation and the thermal resistance of the device. Heat generated in the device is conducted through the substrate to the temperature controlled stage. The equilibrium temperature of the base-collector junction can be determined from the equation for conductive heat transfer:

$$\frac{Q}{t} = kA\frac{T_1 - T_0}{L} \qquad (3.44)$$

where Q/t is the rate of heat flow, k is the thermal conductivity, A is the cross-sectional area, $T_1$ is the temperature at the base-collector junction, $T_0$ is temperature of the stage, and L is the distance between the junction and the stage, i.e. the substrate thickness. The thermal resistance of the device, in °C/W, is:

$$R = \frac{L}{kA} \qquad (3.45)$$

The thermal conductivity, k, for InP is 0.68 W/cm°C [36].

The effect of self-heating can be avoided by allowing enough time between measurements for the device to cool. Pulsed measurements that apply high power for very short times can be used to minimize power dissipation and unwanted heating.

# Chapter 4
# Experimental Details and Apparatus

## 4.1 Introduction

This chapter includes information relating to the epitaxial layers, the fabrication and selection of devices, the equipment and the experimental setup used for the measurements of multiplication factor.

## 4.2 Epitaxial Layers

This section describes the growth conditions for the layers used for InP measurements, and gives details of the layer structures used for InP and InGaAs measurements.

### 4.2.1 MOCVD Growth

The epitaxial layers for the InP/GaAsSb/InP double heterojunction bipolar transistors (DHBTs) used in this work were grown by Metal Organic Chemical Vapour Deposition (MOCVD) in Dr. Simon Watkin's laboratory at SFU. The lab is equipped with a horizontal flow, low pressure Thomas-Swan MOCVD system. The carrier gas used is Pd-diffused $H_2$ at a pressure of 100 Torr. The InP/GaAsSb/InP transistor layer structures were grown using TMIn, TEGa, TMSb, TBAs and TBP as precursors; metal alkyl precursors are preferred where possible to reduce the hazard associated with using the more toxic, gaseous hydride precursors. $H_2S$ was used when n-type doping was required, and $CCl_4$ was used for p-type doping [34].

During GaAsSb growth, the susceptor temperature was kept at 560°C with a V/III ratio of approximately 2. The overall growth rate was about 1.0 μm/h for GaAsSb as well as for InP.

Sumitomo substrates were used, and layer structures similar to the one shown in Figure 4.1 were grown on exactly-oriented (001) InP:Fe, oriented to ±0.25°.

### 4.2.2 Layer Structures

The devices used for measurements of the InP impact ionization coefficient were InP/GaAsSb/InP double heterojunction bipolar transistors. The emitter consisted of 1500 Å of InP, the narrow base was 400 Å of heavily-doped GaAsSb, and the collector consisted of 5000 Å of nominally undoped InP. Details of the layer structure shown in Figure 4.1.

| | | |
|---|---|---|
| 2000 Å $In_{0.53}Ga_{0.47}As$ | (S: $1\times10^{19}$ $cm^{-3}$) | |
| 500 Å InP | (S: $3\times10^{19}$ $cm^{-3}$) | |
| 1500 Å InP | (S: $1\times10^{17}$ $cm^{-3}$) | $N^-$ Emitter |
| 400 Å $GaAs_{0.50}Sb_{0.50}$ | (C: $4\times10^{19}$ $cm^{-3}$) | $p^+$ Base |
| 5000 Å InP | (S: $2\times10^{16}$ $cm^{-3}$) | $N^-$ Collector |
| 500 Å $In_{0.53}Ga_{0.47}As$ | (S: $1\times10^{19}$ $cm^{-3}$) | $n^+$ |
| 5000 Å InP | (S: $3\times10^{19}$ $cm^{-3}$) | Subcollector |
| InP (100) Substrate | (Fe:SI) | |

**Figure 4.1. An epitaxial layer structure grown by MOCVD for N-p-N InP/GaAsSb/InP DHBTs and used for InP electron-initiated impact ionization measurements in this work (layer 2587).**

Measurements of the InGaAs electron-initiated impact ionization coefficient were performed on InP/InGaAs/InGaAs single heterojunction bipolar transistors. The device

layer structure consisted of a 1500 Å InP emitter, a 400 Å InGaAs base, and a 5000 Å InGaAs collector as shown in Figure 4.2.

| | | |
|---|---|---|
| 2000 Å $In_{0.53}Ga_{0.47}As$ | (S: $1\times10^{19}$ $cm^{-3}$) | |
| 500 Å InP | (S: $3\times10^{19}$ $cm^{-3}$) | |
| 1500 Å InP | (S: $3\times10^{17}$ $cm^{-3}$) | $N^-$ Emitter |
| 400 Å $In_{0.53}Ga_{0.47}As$ | (Be: $4\times10^{19}$ $cm^{-3}$) | $p^+$ Base |
| 5000 Å $In_{0.53}Ga_{0.47}As$ | (Si: $2\times10^{16}$ $cm^{-3}$) | $N^-$ Collector |
| 5000 Å $In_{0.53}Ga_{0.47}As$ | (S: $3\times10^{19}$ $cm^{-3}$) | $n^+$ Subcollector |
| InP (100) Substrate | (Fe:SI) | |

**Figure 4.2. An epitaxial layer structure for N-p-n InP/InGaAs/InGaAs HBTs and used for InGaAs electron-initiated impact ionization measurements in this work (layer 724psa1.7).**

## 4.3 Device Fabrication

Heterojunction bipolar transistors were fabricated from the epitaxial layers using a wet etch, optical lithography process previously developed in the CSDL. Large mesa-isolated devices were grown with emitter dimensions of 80 μm × 80 μm, 80 μm × 160 μm, 80 μm × 240 μm, and 80 μm × 320 μm. Smaller devices with air bridges were also fabricated with a variety of emitter dimensions including 6 μm × 20 μm, 4 μm × 12 μm, and 0.75 μm × 6 μm devices. There was no surface passivation treatment. The larger devices were probed directly, while the smaller devices were probed using the air bridges.

## 4.4 Device Selection

This section describes the DC measurements needed to select a device, and the differences in DC measurement results for large and small devices.

### 4.4.1 DC Measurements

DC measurements were performed on devices in order to locate a device with characteristics suitable for impact ionization measurements.

Measurements of the base and collector current vs base-emitter voltage were taken to produce a Gummel plot. From this data, the gain of the device as well as the ideality factors for the two junctions can be determined. If impact ionization measurements are performed using the change in the base current, $\Delta I_b$, then a high gain gives a more sensitive measurement. The Gummel plot also indicates the amount of leakage current for low values of base-emitter bias.

The breakdown voltage for applied $V_{cb}$ was measured. The breakdown voltage is arbitrarily defined as the reverse bias voltage at which the current increases to 100 μA. In a suitable device, breakdown occurs by current increase due to impact ionization, and not because the device is leaky due to a defect. A typical I-V characteristic showing a very low current at low $V_{cb}$, then an exponential increase in current with further increase in $V_{cb}$, indicates an appropriate device. The actual voltage required to reach the electric field strength necessary for breakdown depends on the width of the collector. If the collector is nominally undoped, then impact ionization measurements are usually associated with the average electric field in the collector.

### 4.4.2 Device Size

The DC measurements on large and small devices for the same layer show the expected difference in maximum current density. Higher current densities were achieved with small devices, since the smaller area reduces the probability of a defect existing within the device. As a result, higher gain (associated with higher current density) was achieved.

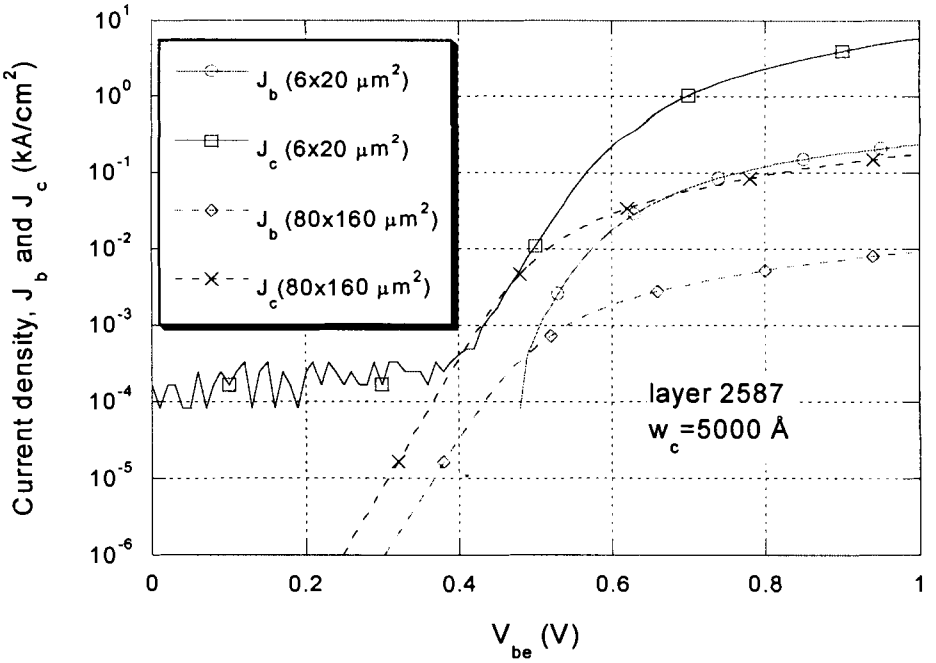


**Figure 4.3. Gummel plot for device with 6×20 μm$^2$ emitter area compared to 80×160 μm$^2$ emitter area. The smaller device reaches higher current density. The low current measurements for the small device were limited by the resolution setting of the HP4156.**

The existence or lack of air bridges did not affect the measured data. However, applying the probe tip directly to the device increased the risk of puncturing the metallization layer and damaging the semiconductor below, making the transistor useless for high-bias measurements.

## 4.5 Measurement Apparatus

Measurements for this work were taken using a temperature controlled probe station. The probe station is produced by MMR and has a temperature range of 80 K to 400 K when no power load is applied to the device under test. The stage is continuously cooled by a Joule-Thomson refrigerator by expansion of nitrogen at a maximum pressure of 1800 psi. The stage also contains a resistive heater and a silicon diode temperature sensor. The MMR controller reads the stage temperature and varies the power dissipation of the resistive heater in order to reach the desired temperature set point. Devices are mounted on the stage with a thin layer of thermal grease, to improve thermal contact.

Before taking a measurement, the temperature was allowed to stabilize for 60 to 120 seconds, by which time the stage remains within 0.10°C or better of the desired target temperature. However, the refrigerator is not always able to maintain the desired temperature if the device is tested at a high power level. A typical measurement had a maximum power dissipation of up to 45 mW ($V_{cb}$=15 V and $I_c$ = 3 mA). Some additional measurements were taken at higher currents, up to 40 mA, but these were not used to extract impact ionization coefficients. If the device heats too quickly, the response time of the controller may not be fast enough; this problem can be partially addressed by using pulsed measurements with pauses that are long enough for the temperature to drop. The problem is especially acute at very low temperatures, when the refrigerator does not have enough cooling power to maintain a low temperature while the device is under power.

The MMR is connected via shielded triaxial cables and a switching box to an HP 4156 semiconductor parameter analyzer. This model is capable of applying DC bias conditions in several modes, including steady and pulsed measurement modes. Hold times and delays were also used on some measurements.

# Chapter 5
# InGaAs Measurements and Analysis

## 5.1 Introduction

The electron impact ionization coefficient in InGaAs has been studied experimentally under many conditions: by Canali's group at electric fields as low as $2\times10^7$ V/m [15], by Neviani over a temperature range of -100°C (173 K) to 50°C (323 K) [16], and over a wider temperature range from 77 K to 413 K by Ritter [37]. The experimental measurements give results which show good agreement with theoretical predictions by Bude and Hess [18]. Because the electron ionization coefficient in InGaAs has been measured previously, measurements were taken on InGaAs-based HBTs in order to verify the experimental and data analysis procedures before applying these procedures to measurements on InP-based HBTs.

This chapter presents the results of measurements of the InGaAs electron-initiated impact ionization coefficient. The multiplication factor, which should not depend on injected current, appears to vary when measured over a range of base-emitter bias. At high and low biases, the current contribution from impact ionization is obscured by other effects. The most appropriate range of base-emitter bias for impact ionization measurements is determined from a discussion of these effects. The final results are compared to published values for the impact ionization coefficient as a function of inverse electric field.

## 5.2 Examination of Method and Valid Data Range

Electron-initiated impact ionization coefficients are determined with HBTs under a set of specific conditions which include the device temperature, the electric field strength in the collector, and the injected emitter current or the applied base-emitter bias. Theory predicts that the impact ionization coefficient will depend on temperature and electric field strength. Other measurement conditions, including the injected emitter current, $I_e$, and the applied base-emitter voltage, $V_{be}$, are not expected to directly affect the final extracted value of ionization coefficient. However, over some range of $V_{be}$ or $I_e$, effects other than impact ionization may dominate the data. The range of conditions that is invalid for a measurement can be determined and screened out by examination of the data at several stages of the analysis. The following sections present the data for measurements on InGaAs-based HBTs and discuss the trends that exist in the data over the range of base-emitter bias.

As described in chapter 2, the direct measurements of base and collector current are analyzed in several stages to extract the value of electron initiated impact ionization coefficient. The following sections examine the data at each stage of analysis. All data is taken using a device on layer 724psa1.7, with an emitter area of 6×20 $\mu m^2$. The InGaAs base width is 400 Å and the collector width is 5000 Å, as described in section 4.2.2. The relevant effects are discussed in order to determine the best range of $V_{be}$ for extracting the ionization coefficient.

### 5.2.1 Base Current and Collector Current

The plot in Figure 5.1 shows the collector current as a function of the base emitter voltage, measured at several values of collector-base reverse bias, $V_{cb}$. The magnitude of the base-collector reverse leakage current ($I_{cb0}$), measured at $V_{be}$=0, can be seen from the plot. As expected, $I_{cb0}$ increases with the reverse bias $V_{cb}$. The collector current, $I_c$, must be distinguishable from $I_{cb0}$ before a multiplication factor can be calculated. This requirement limits the usefulness of low values of $V_{be}$ for measuring the multiplication factor. The lowest value of $V_{be}$ for useful measurements depends on the magnitude of the leakage current $I_{cb0}$ at any $V_{cb}$. For example, the voltage at which $I_c$ is one order of

magnitude greater than $I_{cb0}$ (i.e. clearly growing exponentially beyond $I_{cb0}$) is 0.27 V for $V_{cb}$=1.0 V, and 0.41V for $V_{cb}$ of 4.0 V. This may serve as a lower limit on $V_{be}$; however, the magnitude of the change in current ($\Delta I_b$ or $\Delta I_c$) should also be considered, as discussed further on.

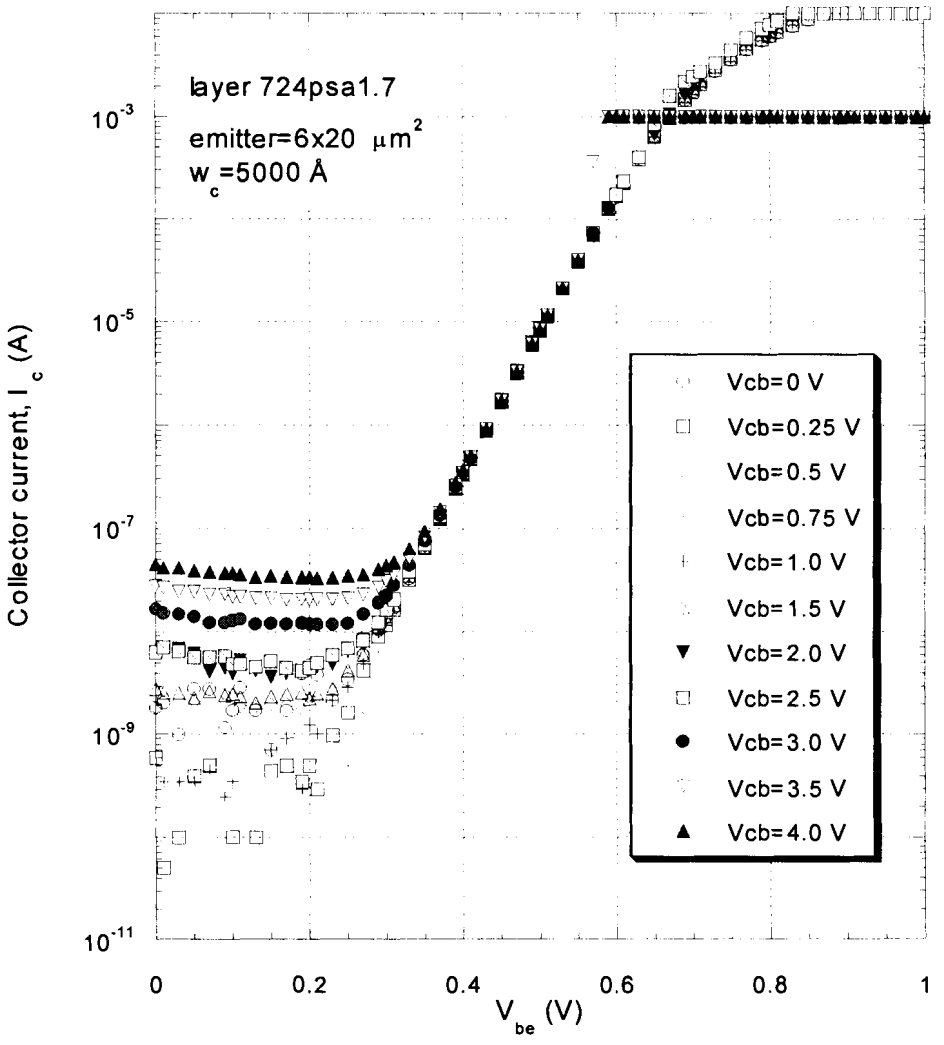


**Figure 5.1. Collector current vs base emitter voltage; the reverse-bias leakage current $I_{cb0}$ increases with $V_{cb}$.**

A second limitation occurs at high base-emitter bias. At high $V_{be}$, the compliance levels set for a measurement will also invalidate some high current data. For example, in Figure 5.1 the data at a reverse base-collector bias of 3.5 V and 4.0 V was measured with a compliance of 1 mA, to prevent excessive power dissipation that would burn out the device. For lower reverse bias, the compliance was 10 mA.

When the collector current reaches the compliance level, it is not able to increase further with higher $V_{be}$. However, current continuity must still be maintained, so the increase in injected emitter current causes a rapid increase in base current as shown in the Gummel plot of Figure 5.2. The increase in the base current gives rise to an apparent negative multiplication value, since impact ionization would decrease, not increase, the base current.

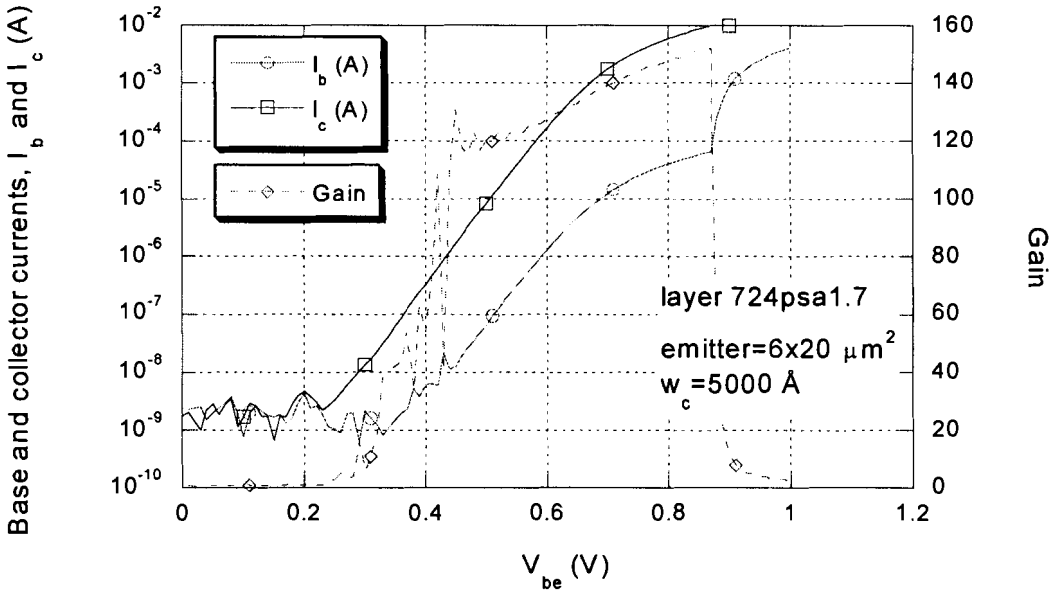


**Figure 5.2. Gummel plot showing limitation of collector current by externally set compliance level and rapid increase in base current.**

Clearly, once the current has reached the compliance level, the data is not useful for multiplication calculations. The effect of compliance is very visible in a plot of the measured currents or in the numerical data. The numerical value of $I_c$ saturates, and the behaviour of the base current shows a discontinuity in slope and a rapid increase. Data affected by compliance is easily removed from consideration in the determination of impact ionization coefficients.

For the InGaAs measurements on the device shown in Figure 5.1, all data measured with $V_{be}$ greater than 0.85 V were affected by the collector current compliance of 10 mA. In addition, when $V_{cb}$ was greater than 3 V the compliance level was reduced to 1 mA to protect the device. For these measurements, the data was affected when $V_{be}$ was as low as 0.59 V.

### 5.2.2 Change in Base and Collector Currents, $\Delta I_b$ and $\Delta I_c$

As discussed in chapter 2 and 3, the change in base current, $\Delta I_b$, is the difference between the base current at some value of $V_{cb}$ and the base current measured when $V_{cb}=0$, for a fixed value of $V_{be}$.

$$\Delta I_b(V_{cb}) = I_b(V_{cb}) - I_b(V_{cb} = 0) \tag{5.46}$$

If the dominant cause of $\Delta I_b$ is impact ionization, then $\Delta I_b$ should increase exponentially with $V_{be}$, because it is proportional to $I_e$. If the contribution from $I_{cb0}(V_{cb})$ is significant, it should be subtracted. Figure 5.3 shows the change in the base current, $\Delta I_b$, focussing on the region of non-exponential increase where $I_{cb0}$ is dominant. The start of the exponential increase in $\Delta I_b$ is also visible.

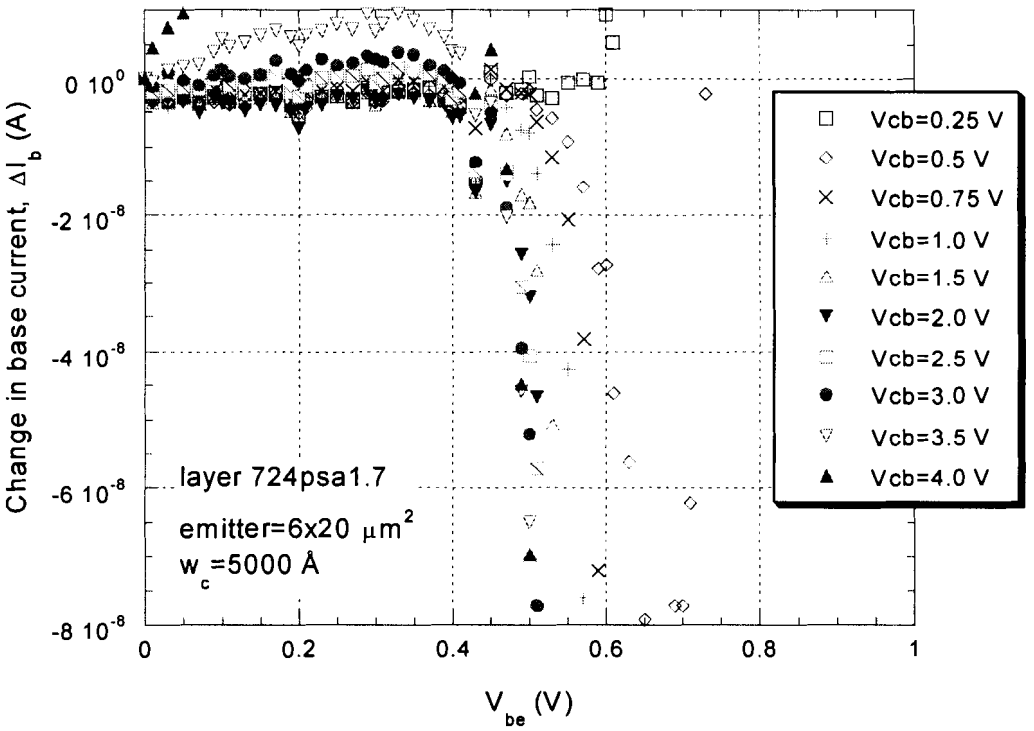


**Figure 5.3. Change in base current, $\Delta I_b$, as a function of the base-emitter bias, $V_{be}$. The constant $\Delta I_b$ section (at low $V_{be}$) marks the boundaries of the low injected current regime.**

At low $V_{be}$, the dominant contributor to $\Delta I_b$ is $I_{cb0}$, the open-emitter base-collector reverse bias leakage current. The magnitude of $I_{cb0}$ can be seen along the y-axis, where $V_{be}=0$ V. $I_{cb0}$ increases with applied $V_{cb}$ and adds a constant contribution to $\Delta I_b$,

independent of the injected current. At low $V_{be}$, any small component of $\Delta I_b$ caused by impact ionization is obscured by the larger value of $I_{cb0}$.

At higher $V_{be}$, in the range where $\Delta I_b$ is predominantly caused by impact ionization, $I_{cb0}$ still causes an error in the calculation of multiplication factor. At any $V_{cb}$, part of $\Delta I_b$ can be attributed to impact ionization, and part of $\Delta I_b$ is due to the increase in $I_{cb0}$ with $V_{cb}$. The $I_{cb0}$ contribution can be measured and subtracted, so that the increase of current used to calculate the multiplication factor becomes:

$$|\Delta I_b| \text{ for multiplication factor} = |I_b(V_{cb}) - I_b(V_{cb} = 0)| - I_{cb0}(V_{cb}) \qquad (5.47)$$

The removal of the $I_{cb0}$ component reduces the magnitude of $\Delta I_b$, as shown in Figure 5.4, and the multiplication factor is calculated only from the change in base current that is not due to $I_{cb0}$.

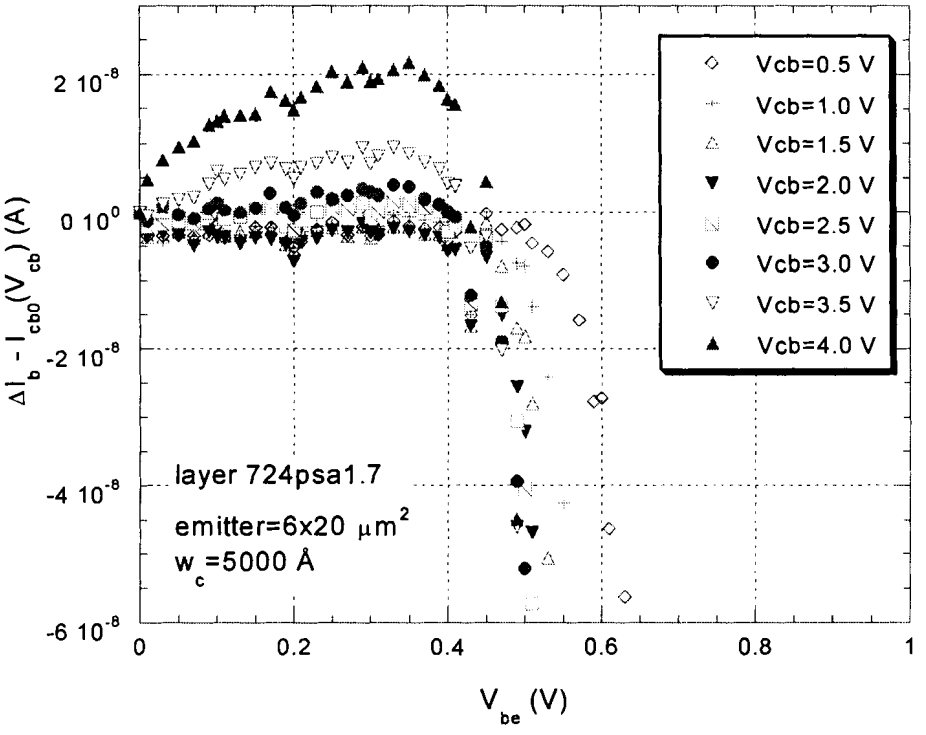


**Figure 5.4. Change in base current, $\Delta I_b$, after removing effect of $I_{cb0}$.**

From Figure 5.4 it is evident that a second effect is involved. The change in current due to impact ionization or to $I_{cb0}$, measured at with respect to the current at $V_{cb}$=0, gives a positive $\Delta I_c$ and a negative $\Delta I_b$. After removing the current change due to $I_{cb0}$, the plot of

Figure 5.4 would be expected to show a negative current with exponentially increasing magnitude at higher $V_{be}$, and a nearly zero current at lower $V_{be}$. Instead, $\Delta I_b$-$\Delta I_{cb0}$ is positive and increasing at low $V_{be}$, especially for higher values of $V_{cb}$; the increase probably continues at higher $V_{be}$ but is obscured by the large current caused by impact ionization at $V_{be}$>0.4 V. There appears to be a current component that acts in opposition to the current flow caused by impact ionization or reverse leakage current. This current is approximately linear with $V_{be}$ and the rate of increase is larger with $V_{cb}$. The current contribution in opposition to impact ionization gives a reduced multiplication factor at higher $V_{be}$; the multiplication factor will not be constant with $V_{be}$ as expected for impact ionization. This effect will be more noticeable at higher $V_{cb}$.

This decreasing magnitude in $\Delta I_b$ (and decreasing magnitude of $\Delta I_c$) with $V_{be}$ cannot be associated with $I_{cb0}$, which ought to be independent of $V_{be}$, nor with impact ionization, which increases rather than decreases the magnitude of $\Delta I_b$.

### 5.2.3 Multiplication Factor

Figure 5.5 shows a plot of multiplication factor, M-1, calculated from data over a range of applied base-emitter voltage. As discussed in the following sections, the trends in behaviour of multiplication factor with $V_{be}$ can be divided into three regimes: low, moderate, and high $V_{be}$. Measurements taken with constant emitter current $I_e$, rather than constant applied base-emitter bias, show similar trends at low, moderate, and high $I_e$.

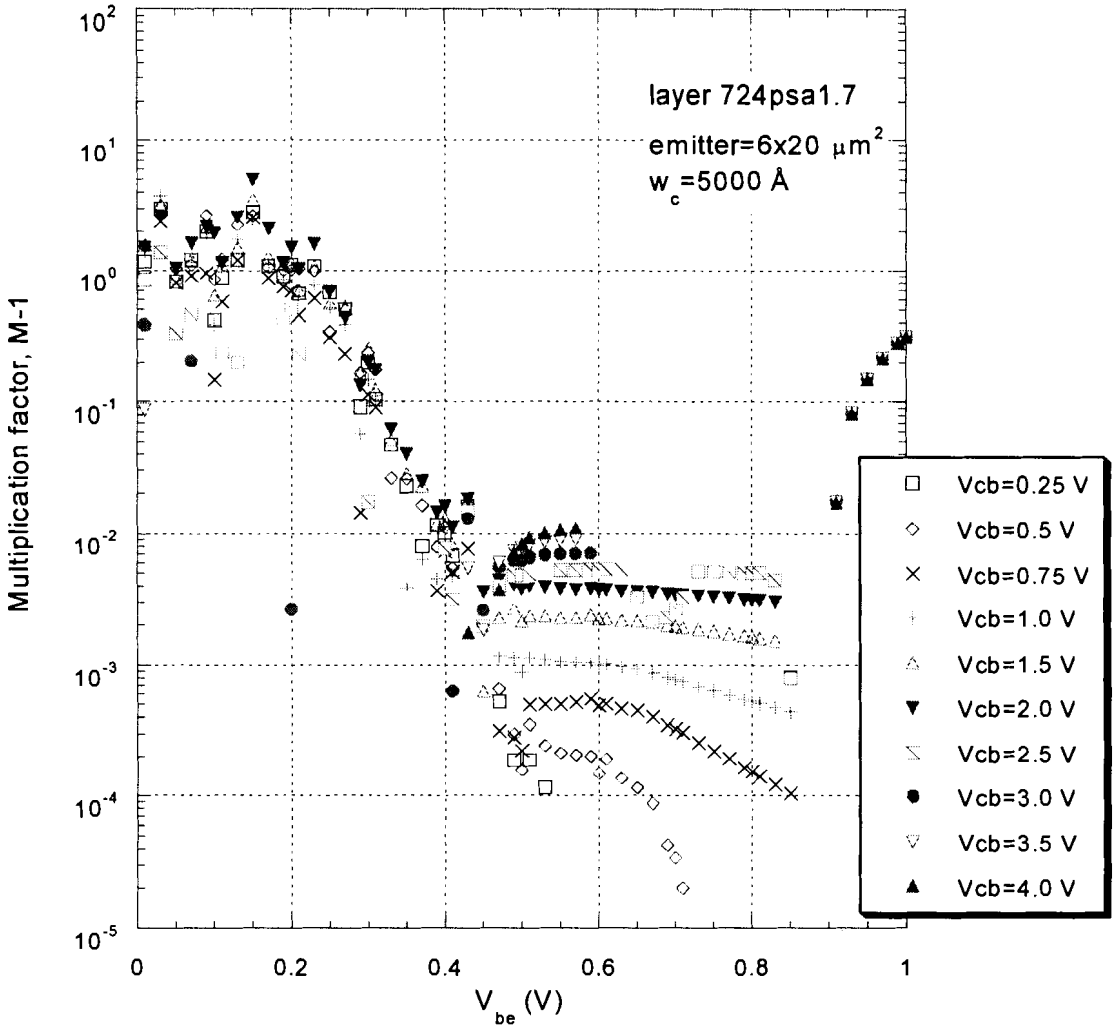


**Figure 5.5. Extracted multiplication factor for InGaAs as a function of base-emitter bias, at different base-collector voltages. The data can be divided into three regimes with different trends for M-1 vs $V_{be}$.**

### 5.2.3.1 Low Base-Emitter Bias

In the low base-emitter bias or current regime, the multiplication factor extracted using the equations described in chapter 2 depends on the applied bias, and is much larger than the multiplication factor at higher $V_{be}$. At low $V_{be}$ ($V_{be}$<0.2 V), the multiplication factor is scattered and at its maximum value; at slightly higher $V_{be}$, the multiplication factor decreases exponentially with $V_{be}$. The multiplication factor does not show a strong trend based on the collector-base voltage, $V_{cb}$. For the device of Figure 5.5, this regime extends from $V_{be}$=0 V up to approximately 0.4 V.

The extracted multiplication factor in the low $V_{be}$ regime is not related to impact ionization at all. The cause of the trends in the low base-emitter bias regime can be seen from the plot of $\Delta I_b$ at low $V_{be}$, in Figure 5.3. The quantity $\Delta I_b$-$I_{cb0}$, which is used in the numerator in the calculation of multiplication factor, is nearly constant at low $V_{cb}$, and decreases slightly at higher $V_{cb}$. As seen on Figure 5.2, the collector current, in the denominator of the expression for multiplication factor, is very small and constant while $V_{be}$ is less than 0.2 V. This corresponds to the scattered values of M-1 at very low $V_{be}$. Above $V_{be}$=0.2 V, the collector current in the denominator increases exponentially with $V_{be}$, while $\Delta I_b$, in the numerator, is still approximately constant. Therefore the apparent multiplication factor decreases exponentially as $I_c$ increases.

The impact ionization coefficient cannot be determined using the data at low $V_{be}$, while $I_{cb0}$ is the dominant component of $\Delta I_b$. The procedure for extracting the multiplication factor is not valid until $\Delta I_b$ also begins to increase exponentially with $V_{be}$, due to impact ionization, in proportion with the collector current. The increase in $\Delta I_b$ beyond $I_{cb0}$ marks the end of the low current regime. The value of $V_{be}$ for which this condition is met depends on $V_{cb}$, but is just over 0.4 V. Data measured at lower $V_{be}$ is not useful for impact ionization calculations.

### 5.2.3.2 Moderate Base-Emitter Bias

Over the moderate $V_{be}$ or $I_e$ range, the multiplication factor is nearly independent of $V_{be}$ or $I_e$. Multiplication also clearly increases with applied $V_{cb}$, which is expected from the relation between impact ionization and electric field strength. On close examination, as seen in Figure 5.6, the plot of multiplication factor vs $V_{be}$ at any $V_{cb}$ has a slight negative slope. This slope is due to the current component visible in the low $V_{be}$ regions of the plot of $\Delta I_b - I_{cb0}$ vs $V_{be}$ (Figure 5.4). At all $V_{be}$, the current component is opposite to the current contribution from impact ionization, so it reduces the calculated value of multiplication factor.

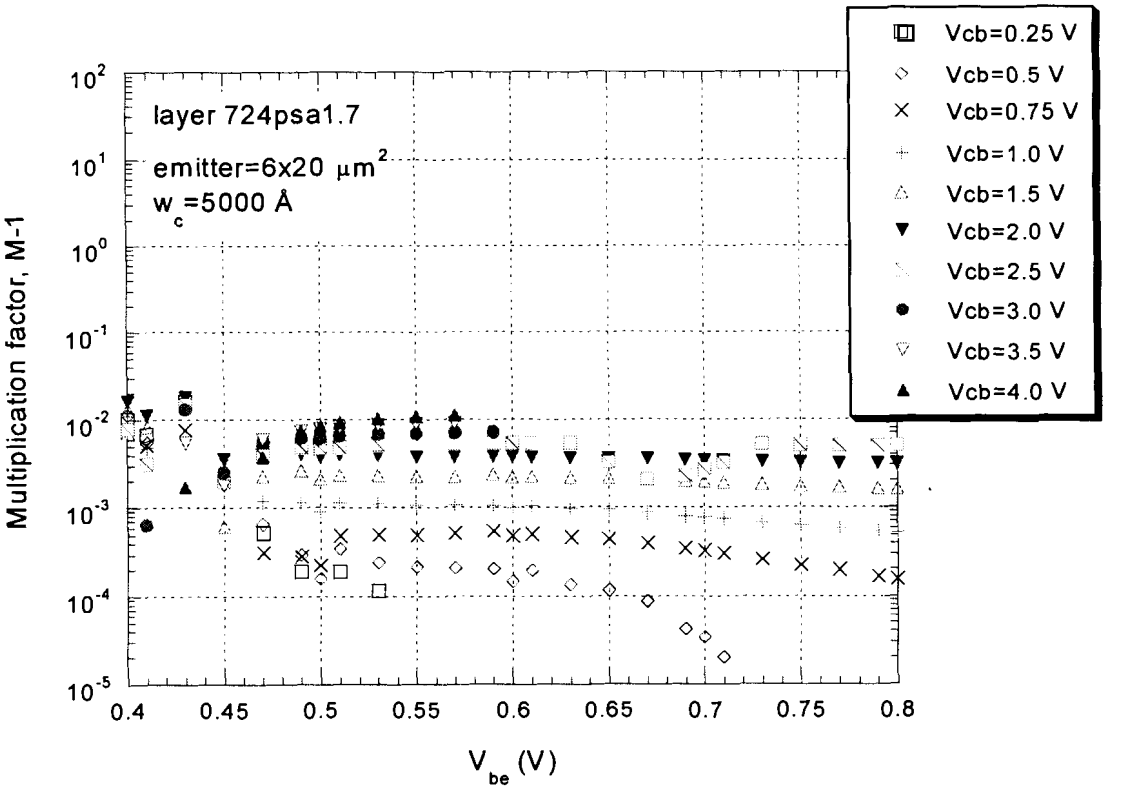


**Figure 5.6. Multiplication factor at moderate $V_{be}$ range.**

Within the moderate range of base-emitter bias, there are still other current effects that tend to reduce the multiplication value. The decrease in extracted M-1 can be predicted by the behaviour of $\Delta I_b$, which shows a linearly decreasing magnitude with $V_{be}$ in the moderate bias range.

Therefore, the best range of data for extracting the impact ionization coefficient is the moderate range of $V_{be}$, at a low $V_{be}$ where the decrease in M-1 is still small, but high enough such that the main contributor to $\Delta I_b$ is impact ionization rather than $I_{cb0}$.

### 5.2.3.3 High Base-Emitter Bias

When the base-emitter bias is high, the extracted multiplication factor again depends on bias conditions: M-1 increases with $V_{be}$. In Figure 5.5, some values of extracted M-1 at high $V_{be}$ appear to converge for different collector-base bias conditions; other values of M-1 become negative and are not shown on the logarithmic plot.

The behaviour in this range is associated with the limitation of collector current by the system compliance setting, as seen in Figure 5.1. The collector current is limited and

the base current increases rapidly. This increase in base current gives rise to an apparent negative multiplication factor, since impact ionization causes a decrease, not an increase, in the base current. These values are not plotted in Figure 5.6. The positive values of multiplication factor occur at high $V_{cb}$, when the collector current has hit a compliance level but measurements at low $V_{cb}$ had a higher compliance. The extracted values are nearly identical because the current values are the same.

All data measured with $V_{be}$ above 0.85 V was affected by the collector current compliance. In addition, data for $V_{cb}$ was greater than 3 V is affected when $V_{be}$ is as low as 0.59 V, but the extracted multiplication values have become negative and do not appear on the logarithmic plot of Figure 5.5.

### 5.2.4 Impact Ionization Coefficient

The electron-initiated impact ionization coefficient for InGaAs vs the inverse of the maximum applied electric field is shown in Figure 5.7, for several values of base-emitter bias. The data reported by Ritter, showing a weak field dependence in the same range of low electric field, is also plotted.

The impact ionization coefficient calculated for base-emitter bias levels of just over $V_{be}$=0.42 V until $V_{be}$=0.75 V appears to be nearly independent of bias, as expected for impact ionization. This range of data corresponds to the range of nearly constant multiplication factors in Figure 5.6. The slight variation (generally a smaller coefficient with $V_{be}$) is in accord with the decreasing $\Delta I_b$ caused by a current contribution in opposition to the impact ionization current.

The coefficient calculated for data measured at $V_{be}$=0.4 V shows a different behaviour. The data give a larger magnitude for the impact ionization coefficient, and the coefficient drops off more slowly with decreasing electric field (i.e. it has a weak field dependence). This behaviour is in contrast to the lower values of impact ionization coefficient which decrease by two orders of magnitude over measured range in electric field.

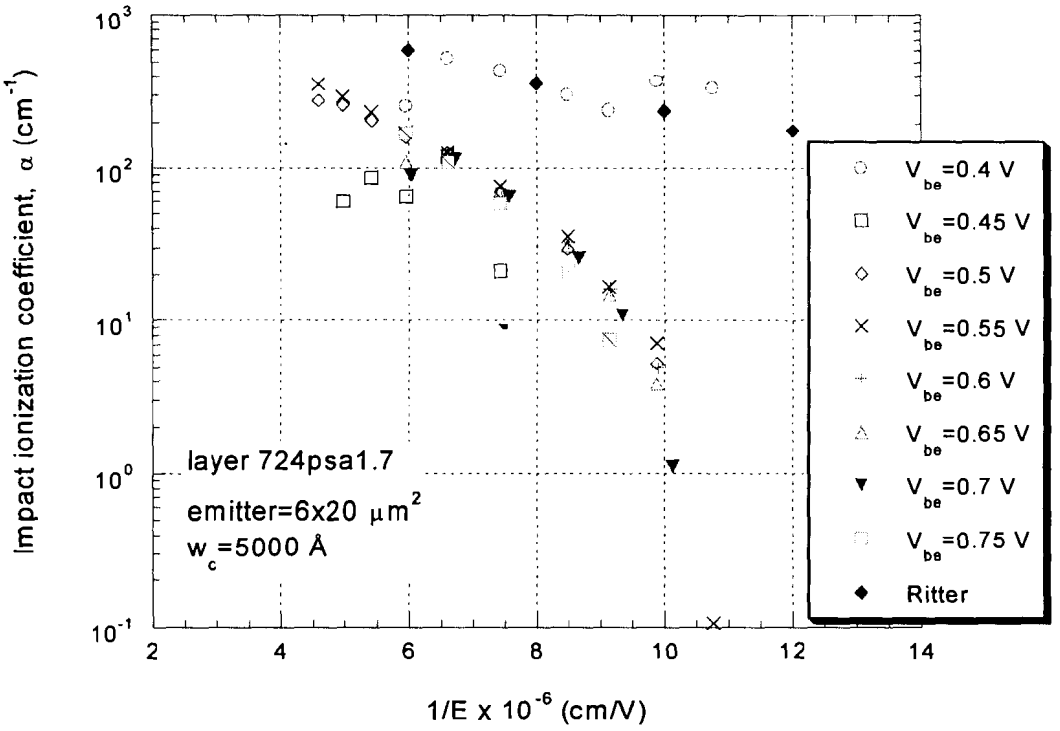


**Figure 5.7. Electron-initiated impact ionization coefficient for InGaAs, calculated from a range of applied base-emitter bias, compared to results published by Ritter which show a weak low-field dependence.**

## 5.3 Comparison of Results

It appears that the data measured at $V_{be}$=0.4 V gives the best match to other published results. However, according to the analysis of the data, the change in current at this bias level is not primarily due to impact ionization. The plot of $\Delta I_b$ is not in the exponential range, and the small additional current caused by impact ionization is overshadowed by $I_{cb0}$.

At base-emitter biases just above $V_{be}$=0.4 V, the measurements in this work result in impact ionization coefficients that are nearly bias-independent, but lower in magnitude and with a stronger field dependence than the reported data from other sources. The smaller value is in agreement with the apparent decrease in $\Delta I_c$ or $|\Delta I_b|$ with $V_{be}$, which causes a smaller value of multiplication than expected.

# Chapter 6
# InP Measurements and Analysis

## 6.1 Introduction

This chapter discusses the extraction of electron-initiated impact ionization coefficients in InP from an InP-GaAsSb-InP HBT. The approach is parallel to that used for InGaAs in chapter 5: the valid current and bias ranges are determined by examining the data at various stages of analysis; then the valid data are used to calculate numerical results for the impact ionization coefficient as a function of inverse electric field. The room temperature results are compared to previously published results. The procedure is then applied to a set of measurements that span a temperature range of 125 K to 380 K.

An important consideration in the InP measurements is the behaviour of the reverse bias leakage current $I_{cb0}$. This chapter contains a discussion of the components which may contribute to $I_{cb0}$, including the diode saturation current $I_{c0}$, thermal generation of electron-hole pairs in the depletion region, tunnelling between the valence and conduction bands, and surface leakage.

The section on temperature dependence includes an examination of the reverse bias leakage current over a range of temperature, and the collector-base breakdown voltage, for devices on two different layer structures.

## 6.2 Room Temperature Measurements

This section examines the room temperature InP data at each stage of analysis: first, the base and collector currents, then the change in base and collector currents, $\Delta I_b$ and $\Delta I_c$, followed by the multiplication factor and finally the impact ionization coefficient. Data presented in section 6.2 are taken using device 11j2 on layer 2587, with an emitter

area of 80 μm × 160 μm. The layer 2587 has a GaAsSb base width of 400 Å and an InP collector width of 5000 Å, as described previously in section 4.2.2.

### 6.2.1 Base Current and Collector Current

The following section presents the Gummel plot and gain of the device, and discusses the negative base current seen in the measurements. The voltage at which the base current becomes negative depends strongly on the emitter current; this dependence is an early indication of the effect that the reverse-bias leakage current, $I_{cb0}$, will have on the calculations.

#### 6.2.1.1 Gummel Plot

Figure 6.1 is a Gummel plot showing the base and collector current versus the base-emitter voltage, measured with $V_{cb}$=0. The plot shows the region of exponential increase of current with $V_{be}$. The linear portion of the plot gives a base current ideality factor of 1.1 and a collector current ideality factor of 1.0. Resistive effects cause the change of slope seen at approximately $V_{be}$=0.5 V. There is no indication of limitation by saturation current or measurement resolution at low $V_{be}$, indicating that the junctions are of good quality. The current gain is also shown in the plot of Figure 6.1.

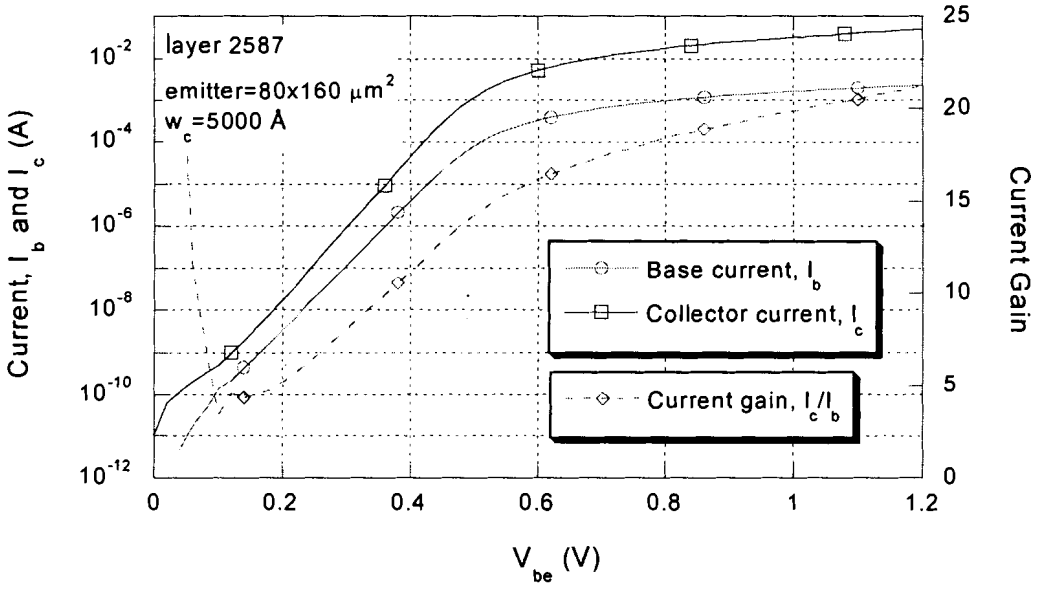


**Figure 6.1. Gummel plot and current gain for InP device.**

### 6.2.1.2 Negative Base Current

When a collector-base reverse bias is applied and impact ionization occurs in the collector-base depletion region, the base current, $I_b$, decreases because holes generated by impact ionization flow into the base, and reduce the amount of base current required due to recombination in the base. Figure 6.2 is a plot of the base current through the device as a function of the reverse collector-base bias $V_{cb}$, for a range of injected emitter currents, $I_e$. At $V_{cb}$=0, $I_b$ is a portion of the emitter current. However, as $V_{cb}$ increases, the amount of base current begins to decrease and eventually becomes negative.

Figure 6.2 shows that a larger emitter current requires a larger reverse bias before the sign of $I_b$ becomes negative. A voltage of 5.25 V is required before the base current goes negative when the emitter current is 1 μA, but 10 V are required at $I_e$ =10 μA and 13.5 V are required at $I_e$=300 μA. For emitter currents of 1 mA or more, the base current does not become negative in the range of reverse bias applied up to 15 V.

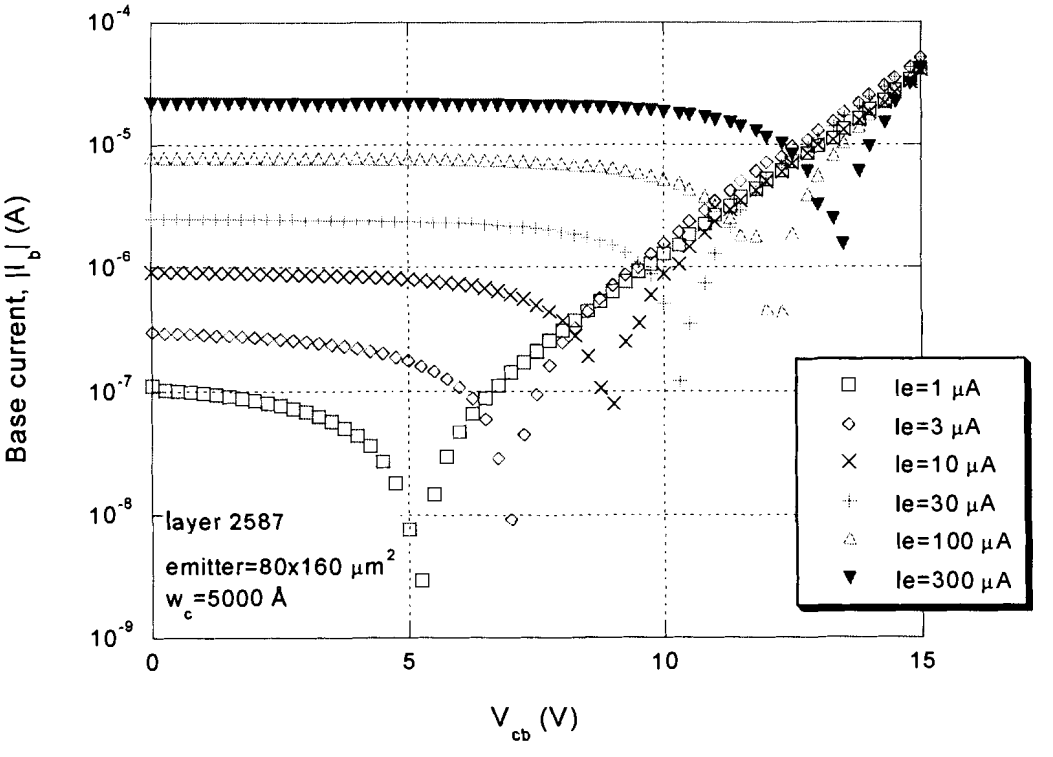


**Figure 6.2. Base current versus collector-base reverse bias for InP device at room temperature; at higher emitter currents, a larger reverse bias is required to reach negative base current.**

The value of $V_{cb}$ at which the base current becomes negative depends on the injected emitter current, $I_e$. One possible explanation for this dependence is the variation of current gain with $I_e$. However, as seen from Figure 6.2, a higher $V_{cb}$ is needed for a higher $I_e$, and this cannot be explained by the variation in current gain. The multiplication factor required for the base current to be negative is:

$$M - 1 \geq \frac{1}{\beta} \tag{6.48}$$

where β is the current gain. Because the current gain increases with $I_e$, as shown in Figure 6.2, the required multiplication to give a negative base current should decrease with emitter current, not increase as it appears to (assuming that multiplication increases with $V_{cb}$, and gain is constant or increases with $V_{cb}$). Therefore, the non-constant gain is not the cause of the increase in $V_{cb}$ required to make $I_b$ negative when the injected emitter current is larger.

A second possible explanation suggested by the current-dependent behaviour is a reduction of the junction electric field due to the charge on the mobile carriers. Since the current gain, β, increases with $I_e$, the required M-1 for negative base current actually decreases, as discussed previously. However, if the multiplication value at a given $V_{cb}$ decreased with increasing emitter current, because of a reduction in the electric field, then at higher $I_e$, a higher $V_{cb}$ might still be required to achieve the multiplication value needed for negative base current. Decreased multiplication at higher $I_e$ is consistent with a reduced junction electric field at higher currents.

However, this explanation cannot explain the large change in $V_{cb}$ over the range of emitter current. The current densities involved are actually very low and the charge on the mobile carriers, when compared to the contribution from the depletion region space charge, does not make a significant difference to the electric field. The data plotted in Figure 6.2 refers to a device with an emitter area of 80×160 $\mu m^2$, with a corresponding emitter current density ranging from 0.01 to 2 $A/cm^2$. For comparison, the current density required to reach a zero electric field gradient was given previously in chapter 3:

$$J_c = qN_D v_{sat} \tag{3.16}$$

For a collector doping level of $N_D=2\times10^{16}$ $cm^{-3}$ and assuming a saturation velocity of $10^7$ cm/s, the critical current density is $J_c=32$ $kA/cm^2$. At current densities up to 2 $A/cm^2$, the maximum electric field decreases by less than 0.01%. The additional reverse bias voltage required to compensate for this drop in the electric field is negligible. Therefore, reduction of the electric field by mobile carriers does not explain the large increase in reverse-bias voltage required to reach a negative base current for higher emitter currents.

A third explanation for the negative base current occurring at higher $V_{cb}$ for larger emitter currents involves the reverse bias leakage current, $I_{cb0}$. $I_{cb0}$ increases as a function of $V_{cb}$ and contributes to the reduction of the base current. The base current becomes negative at the value of $V_{cb}$ where the current contribution from $I_{cb0}$ plus the contribution from impact ionization equals the magnitude of the base current at $V_{cb}=0$. Unlike impact ionization, $I_{cb0}$ is not proportional to the injected current. At lower base currents, the contribution from $I_{cb0}$ contributes a larger proportion of the base current and a smaller multiplication factor is required. Figure 6.3 shows the contributions to the change in base current at the value of $V_{cb}$ where the base current becomes negative. At higher emitter currents, the current that must be provided by impact ionization is a larger fraction of the total current required.

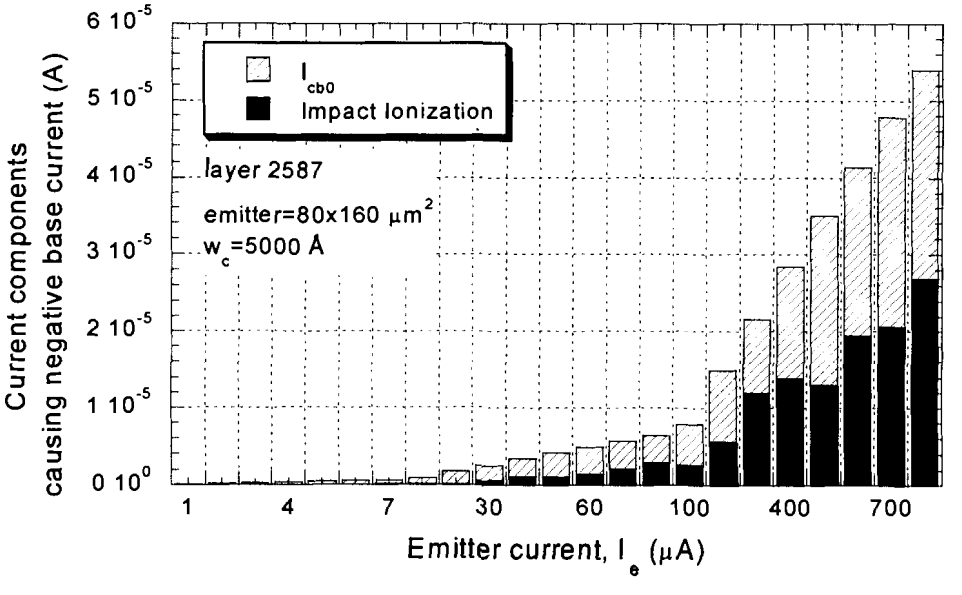


**Figure 6.3. Components of change in base current, $\Delta I_b$, at the reverse collector-base voltage where the base current becomes negative, for increasing emitter current.**

Negative base currents were also reported by Zanoni et al [14] during impact ionization measurements on AlGaAs/GaAs HBTs. They report that at higher values of $V_{cb}$, the reversal of $I_b$ occurs at lower $I_e$. This behaviour is opposite to the results in Figure 6.2, where low $I_e$ values showed reversal of $I_b$ at low $V_{cb}$. The limit of the behaviour in Zanoni's measurements occurs at $V_{cb}$ = 8.6 V, below which $I_b$ does not become negative at any (high) value of $I_e$.

### 6.2.2 Change in Base and Collector Currents, $\Delta I_b$ and $\Delta I_c$

As with the measurements on InGaAs, the $\Delta I_b$ data show the range of bias conditions for which $\Delta I_b$ is proportional to $I_e$. This condition is met for different current ranges depending on $V_{cb}$. Unlike InGaAs, the data do not show a section where $\Delta I_b$ is constant, followed by exponential growth of $\Delta I_b$. Instead, $\Delta I_b$ versus $I_e$ increases gradually, with the slope increasing slowly as well.

The second condition used in the InGaAs measurements, that $I_{cb0}$ should form a small part of $\Delta I_b$ or $\Delta I_c$, is still applicable to InP. From Figure 6.4, $I_{cb0}$ is nearly equal to $\Delta I_b$ for small values of emitter current, approximately up to $I_e$=30 μA. A close examination of $I_{cb0}$ would be useful to determine what components it has, and how this would affect the calculation of the impact ionization coefficient. $I_{cb0}$ is discussed further in section 6.3.3.

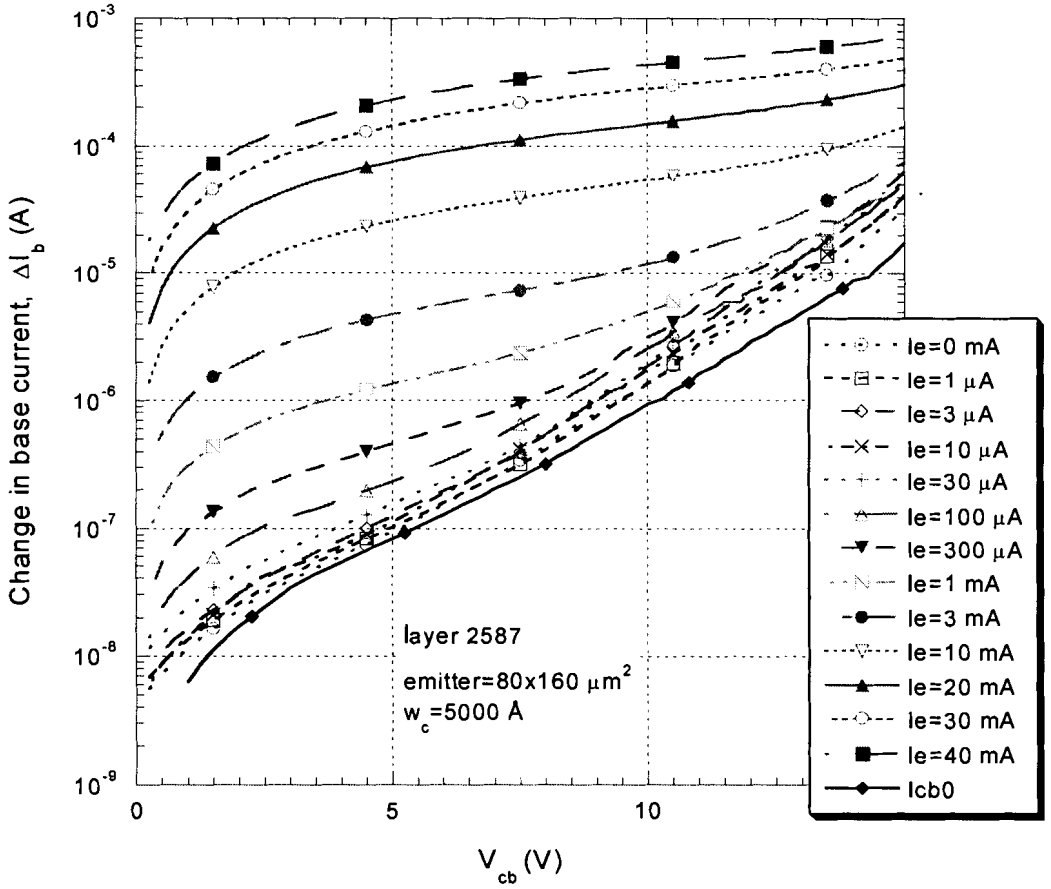


**Figure 6.4. Absolute value of $\Delta I_b$ versus collector-base bias at selected emitter current levels, for InP device at room temperature.**

## 6.2.3 Multiplication Factor

The plot in Figure 6.5 illustrates the variation of extracted multiplication coefficient with emitter current for measurements on a InP-GaAsSb-InP HBT. The contribution of the reverse bias leakage current $I_{cb0}$ has been removed, and the results corrected for the Early effect using Shamir and Ritter's correction as discussed in chapter 2:

$$Err(M-1) \approx \frac{2\varepsilon\varepsilon_0 V_{cb}}{\beta_0 w_c Q_B} \tag{2.24}$$

$$Q_B = qN_B w_{B0} \tag{2.25}$$

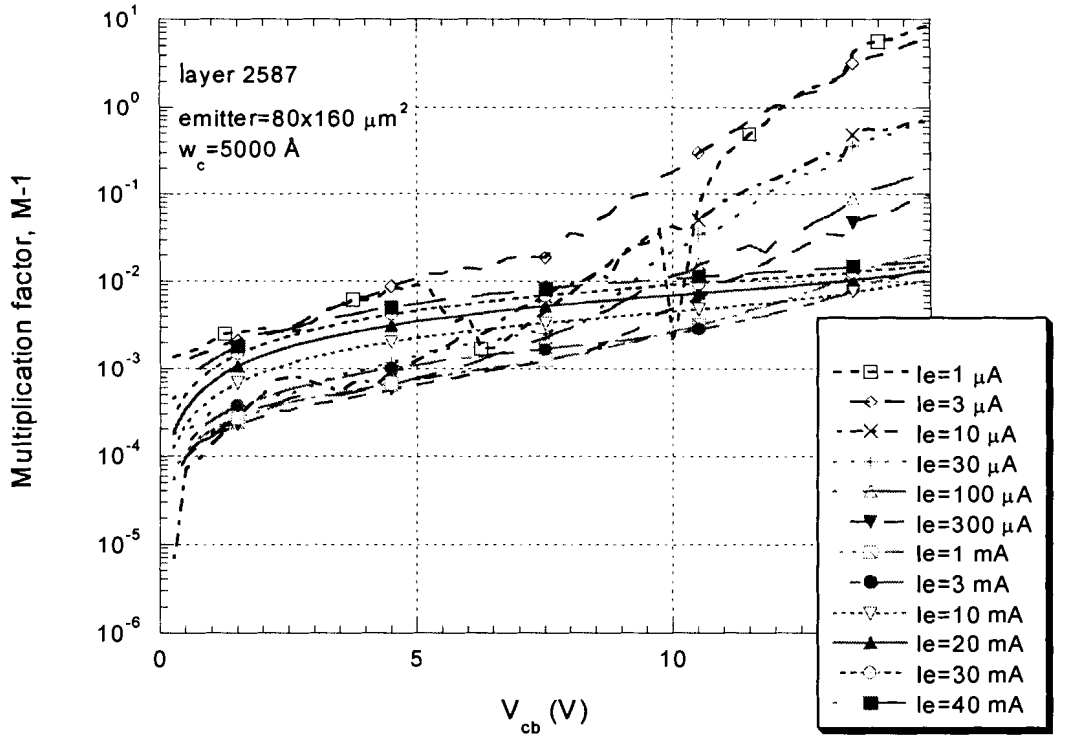


**Figure 6.5. Multiplication factor as a function of $V_{cb}$ at selected emitter current levels, for InP device at room temperature.**

As the emitter current $I_e$ is increased, the multiplication factor first decreases then stabilizes for an applied $V_{cb}$ of less than 8 V, then increases again with current. The multiplication factor is nearly constant over two orders of magnitude of applied emitter current, from 20 μA to 3 mA, for $V_{cb}$ less than 8 V. At higher $V_{cb}$, the multiplication continues to decrease with current until 2 to 5 mA (not shown on plot), when it begins to increase.

The behaviour shown in Figure 6.5 is similar in many respects to that in Figure 5.6, the corresponding plot for the InGaAs collector device. The measured data shows that the calculated multiplication factor is constant over a two order of magnitude range of bias current from 20 μA to 3 mA, for lower applied base-collector voltages. Over this range, the multiplication factor is constant, and also at its minimum value. At higher $V_{cb}$, the multiplication factor is at its minimum value and constant over a smaller range of current, from 2 to 5 mA. As with the InGaAs measurements, the calculated multiplication factor for InP is at its lowest magnitude in the current range for which it is also constant. The

constant multiplication factor with emitter current suggests that impact ionization is the dominant effect, and the multiplication factor at its minimum value indicates that impact ionization coefficient is less likely to be overestimated due to current contributions from other sources.

### 6.2.4 Impact Ionization Coefficient

Based on the trends seen in the plot of multiplication factor, it appears that a current bias range of approximately 20 μA to 3 mA is the best range for extracting the impact ionization coefficient on this device. The results are plotted in Figure 6.6 for the range of collector base voltage, in terms of the average electric field for each bias.

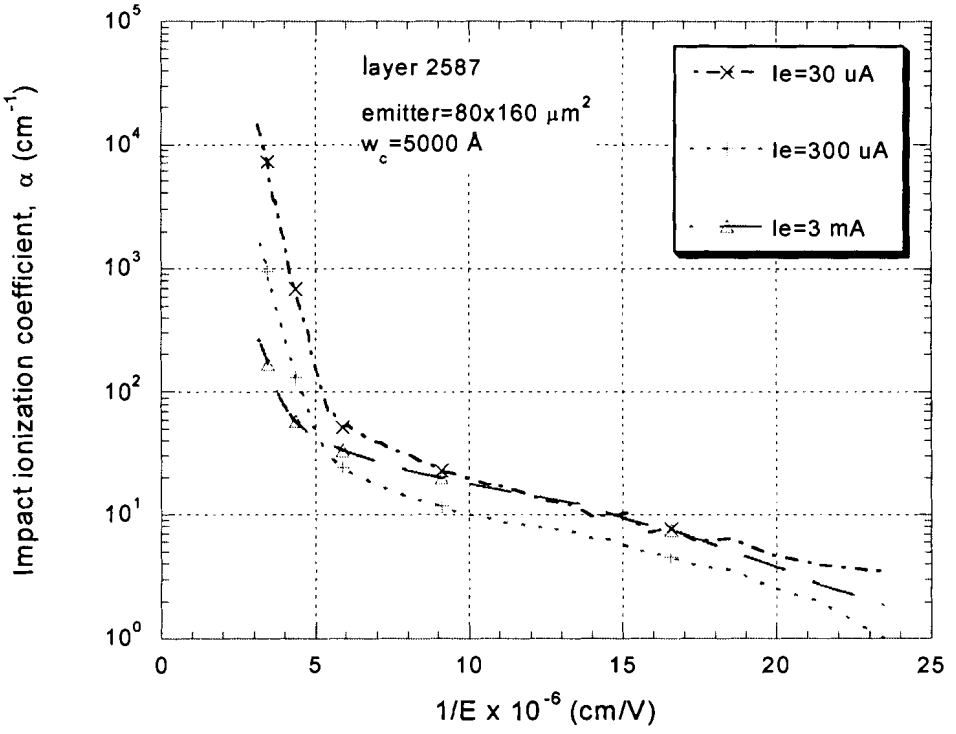


**Figure 6.6. Extracted values of electron-initiated impact ionization coefficient versus inverse electric field, for InP at room temperature.**

As seen in the plot of multiplication factor, the agreement between values measured at different current levels is good at lower applied base-collector voltages (lower $V_{cb}$, i.e. lower electric field and higher 1/E) but there is some variation in multiplication and hence impact ionization coefficient at higher electric fields. The values of impact ionization

shown here are the lowest measured values over the range of injected current, to minimize the probability of other current contribution effects.

The next plot, in Figure 6.7, shows a comparison of the measured impact ionization coefficient versus 1/E with other values that have been reported in literature. The plot shows measurements by Umebu et al [12], Cook et al [13], and Armiento et al [10], along with theoretical predictions by Bude and Hess [18]. The data of Umebu and Armiento are measured in a range of higher electric field, due to the limitations of the photodiode used in their measurements, but Cook's data extend to the lower electric field values covered by our measurements. From Figure 6.7, the measurements taken at $I_e$=300 μA agree well with those of Cook at high electric field values around $4\times10^5$ cm/V. The data measured at 3 mA give a lower impact ionization coefficient; if Armiento's data are extrapolated to lower electric fields it would give approximately the same values but at a steeper slope.

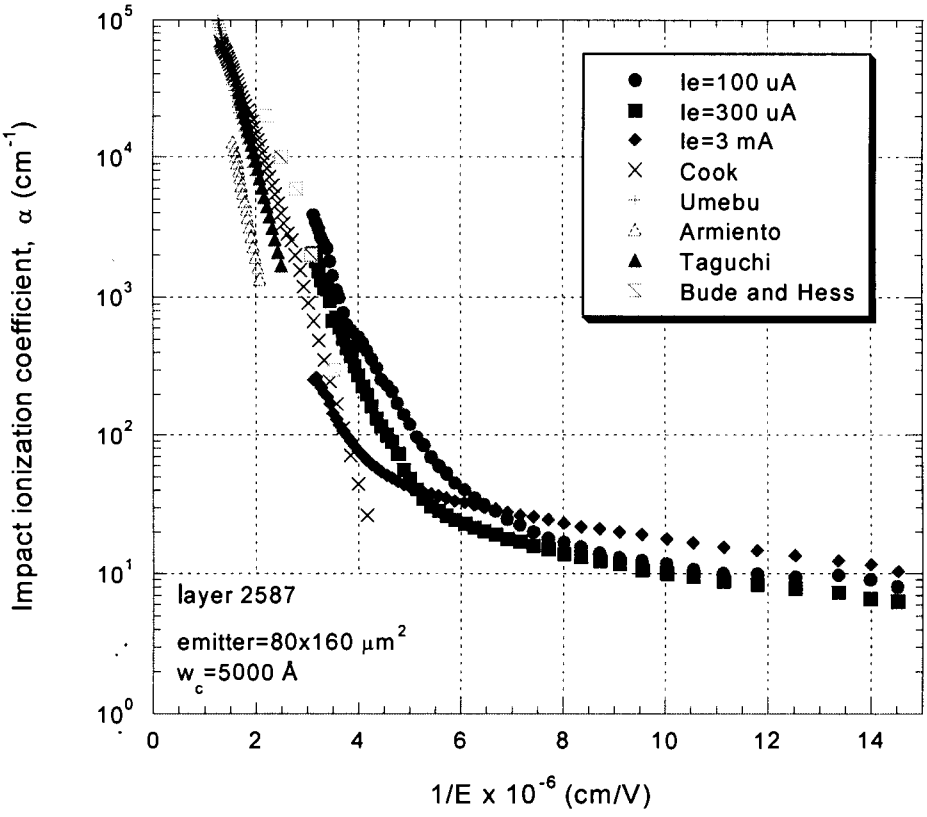


**Figure 6.7. Extracted electron-initiated impact ionization coefficients for InP at room temperature, compared to other results reported in literature.**

Figure 6.7 shows that the InP electron-initiated impact ionization coefficient has a low-field 'tail' where it changes slope and becomes less dependent on electric field at low electric fields. This work is the first time that such a tail has been observed in InP. The change in slope is similar to the behaviour seen in InGaAs. The appearance of the low-field tail agrees with the statement by Bude and Hess that the idea of hard thresholds should be abandoned for all materials, including InP, that they discuss in their paper [18]. Their numerical calculation of InP impact ionization coefficient, as shown directly in Figure 2.4 and replotted in Figure 6.7, does not indicate the presence of a low-field tail because their Monte Carlo simulations did not extend to sufficiently low values of InP impact ionization coefficient: their results are plotted only to $\alpha$=100 $cm^{-1}$, at an inverse field of $4\times10^{-6}$ cm/V. Bude and Hess argue that the rise of impact ionization rate with carrier energy is limited by the small low-energy density of states available in the conduction band. The impact ionization rate increases more rapidly only at higher energies, when intervalley final states become available. Large intervalley separations therefore indicate that a material should show soft impact ionization thresholds, and the similarity in density of states between InP and InGaAs shown by Bude and Hess suggests that InP should also feature a soft threshold characteristic.

## 6.3 Sources of Error

This section discusses the sources of error in each measurement of electron-initiated impact ionization coefficient that affect either the calculated multiplication value, or the electric field that is associated with the measurement. The assumptions that are typically made with this type of measurement are re-examined, as well as the possibility of self-heating and current crowding. The possible sources of the reverse-bias leakage current, $I_{cb0}$, are examined in more detail.

### 6.3.1 Electric Field

The value of electric field to associate with each impact ionization measurement is subject to some uncertainty. Several authors quote the maximum electric field at the base-collector junction [15]. The maximum electric field is often used with the assumption that

the electron-initiated impact ionization coefficient is a function of the local electric field [15, 16]. However, if the electrons travel a significant distance in the collector ("dead space") before gaining enough energy to cause impact ionization, then using the maximum field strength at the base-collector junction overestimates the field responsible for the impact ionization. For lightly-doped collectors, such as the ones in this work with a collector dopant concentration of $2\times10^{16}$ $cm^{-3}$, Buttari states that the average field in the collector region should be used because the ionization rate at the far end of the collector is not negligible compared to the ionization rate near the junction [29]. The difference between the maximum electric field and the average electric field across the collector provides an estimate of the error in the electric field value.

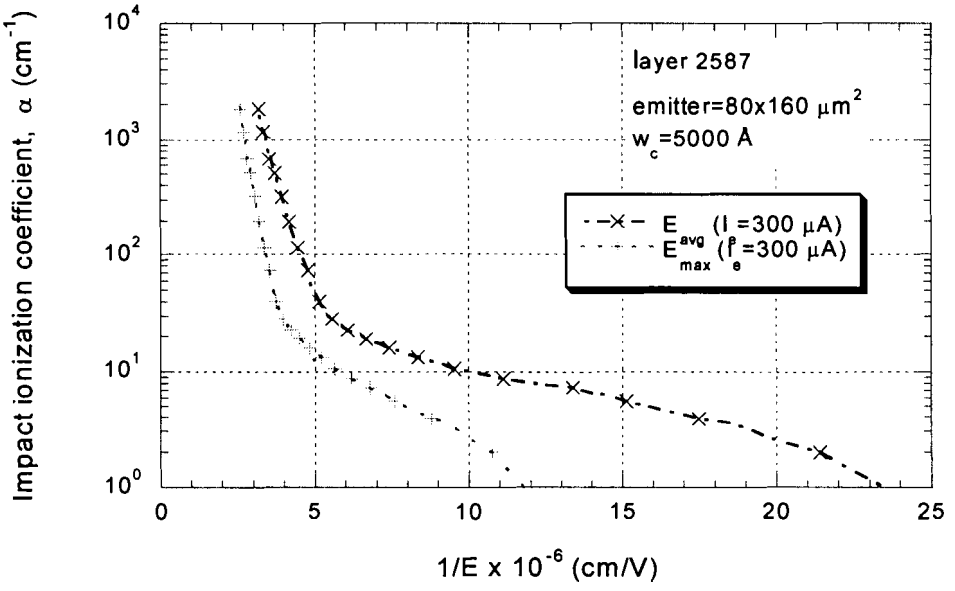


**Figure 6.8. Impact ionization coefficient for $I_e$=300 μA from Figure 6.6, versus the average and the maximum electric field in the collector.**

## 6.3.2 Multiplication Value

The calculated multiplication factor contains some uncertainty if the base current changes for any reason other than impact ionization. As discussed in chapter 2, the Early effect causes a change in the base current. An increase in the base-collector reverse bias causes a decrease in the minority carrier charge stored in the base, and hence a decrease in base recombination. This decrease is larger for constant emitter current type measurements than for constant base-emitter bias type measurements; however, the

constant emitter current has the advantage of a smaller uncertainty in the initiating current. In these devices, the Early effect is small because most of the change in the depletion width occurs in the lightly doped collector rather than the heavily doped base.

Several assumptions that are typically made in the calculation of multiplication factor and impact ionization have been reconsidered in this work. In some previous studies, the reverse bias leakage current $I_{cb0}$ is considered negligible relative to the change in the base current [14, 15]. However, in this work, as in Buttari's [29], $I_{cb0}$ is not negligible and the change in $I_b$ that is due to $I_{cb0}$ must be subtracted before the multiplication factor is calculated. The uncertainty in the resulting $\Delta I_b$ increases from the subtraction of the two values. The causes of non-negligible $I_{cb0}$ are discussed further in the next section.

A second assumption is that secondary ionization is insignificant. The advantage of HBTs for ionization measurements is that the initiating current is known to be a pure electron (or hole) current, with a well-known magnitude. The usual assumption made for impact ionization measurements is that there is no secondary ionization; i.e. the electron and hole generated by the first impact ionization event will not undergo impact ionization themselves. If this assumption is not valid, then the electron-initiated impact ionization coefficient cannot be extracted without knowing the hole-initiated impact ionization coefficient, because the holes will also cause ionization, and the contribution from the primary and secondary electron-initiated ionization events cannot be separated from the secondary hole-initiated ionization events. At high electric fields, when it is more likely that the generated charge carriers will be able to accelerate quickly enough to undergo secondary impact ionization, multiple ionization events can occur and the device approaches avalanche breakdown. In this case the calculated value of multiplication factor will be higher than expected, and the electron-initiated ionization coefficient will be overestimated. At low electric fields, it is also possible that hole-initiated impact ionization will occur. This may be the cause of the low electric field 'tail' in the electron-initiated impact ionization coefficient: the multiplication factor appears to be higher than expected because hole-initiated impact ionization is contributing to the multiplication factor, and masking the low value of electron-initiated impact ionization.

### 6.3.2.1 Device Self-Heating

Self-heating of the device, for example over a series of measurements with increasing base-collector bias for a fixed emitter current level, can affect the multiplication value of the later measurements. When the power dissipation is high, the temperature increase in the device will decrease the amount of multiplication and the true impact ionization coefficient for the assumed temperature will be underestimated. As discussed in section 3.5.3, the thermal resistance of the device is given by:

$$R = \frac{L}{kA} \tag{3.19}$$

The thermal conductivity for InP is 0.68 W/cm°C. For a device with an area of 80×160 $\mu m^2$ and a substrate thickness, L, of 350 μm, the thermal resistance is 400°C/W. At the maximum collector-base bias of 15 V, and with a collector current of 3 mA, the power dissipation of 45 mW leads to a maximum temperature rise of 18°C. The extent of the error caused by this temperature change can be judged from the plot of temperature dependent impact ionization coefficients, shown in Figure 6.21. The effect of a temperature change is worse at lower temperatures: at 150 K the impact ionization coefficient is only fifty to sixty percent of its value at 125 K, while it remains nearly constant between 275 K and 300 K.

The effect of self-heating on a series of measurements can be reduced by taking the measurements on a temperature controlled stage, and by allowing time for the device to cool between measurements.

### 6.3.2.2 Current Crowding

Current crowding is the non-uniform distribution of emitter current, caused by resistance of the base layer that leads to a potential difference across the base. The variation in base-emitter voltage causes the emitter current density to increase towards the periphery of the device. If strong current crowding occurs, then the assumption of an average current density is not valid.

Typically, the effect of current crowding remains small as long as the potential drop across the intrinsic base is less than the thermal voltage, kT/q. The potential drop across the base depends on the sheet resistance of the base, the geometry of the base and contact,

and the magnitude of the base current. An acceptable collector current can then be calculated from the maximum base current and the current gain. A conservative estimate uses the base resistance for a one-sided base contact, calculated from:

$$R_B = \frac{1}{3} R_S \frac{W}{L} \tag{6.49}$$

where $R_S$ is the base sheet resistance in ohms per square (Ω/□), W is the width or maximum distance from the contact, and L is the length of the contact. The collector current at which current crowding begins to have an effect is given by:

$$I_C = \frac{kT}{q} \frac{\beta}{R_B} \tag{6.50}$$

where β is the current gain.

The thermal voltage at 295 K is 25 mV. The GaAsSb base layer, 400 Å thick with a doping of $4\times10^{19}$ $cm^{-3}$, has a typical sheet resistance of 1400 Ω/□. An aspect ratio, W/L, of 0.5 and a current gain of 20 indicate that current crowding will not have a significant effect for a collector current of 2 mA. The consistent impact ionization coefficient data is reported across current levels of 30 μA to 3 mA, so current crowding should not be a concern.

The InGaAs device discussed in chapter 5, with a lower sheet resistance of 750 Ω/□ and an aspect ratio of 0.3, can tolerate a collector current of up to 7 mA before current crowding becomes significant.

### 6.3.3 Current Sources: $I_{cb0}$

The reverse-bias leakage current, $I_{cb0}$, is an additional current contribution to $\Delta I_b$ that should be examined. A significant difference between the InGaAs and InP measurements is that $I_{cb0}$ forms a larger portion of $\Delta I_b$ for the InP devices. $I_{cb0}$ is approximately equal to $\Delta I_b$ for injected emitter currents of up to 30 μA on the large (80 μm × 160 μm emitter area) device. The magnitude of $I_{cb0}$ at high $V_{cb}$ is in the 10 μA range, which is larger than expected. Typically, devices with an InGaAs collector have an $I_{cb0}$ of no greater than 5% of delta $I_b$, in the fA or at low nA range. Since the sensitivity of the impact ionization coefficient measurement depends on how accurately $\Delta I_b$ is

known, the high $I_{cb0}$ should be investigated. The following section examines some components of $I_{cb0}$: the diode saturation current, thermal generation in the depletion region, inter-band tunnelling, and surface leakage.

### 6.3.3.1 Saturation Current $I_{c0}$ or $J_s$

According to the ideal diode equation, the current density in a p-n junction under reverse bias should saturate at $-J_s$, the diode saturation current density. $J_s$ is temperature dependent but should not vary with applied bias.

The value of the saturation current, $I_s$, can be determined from the Gummel plot of $I_b$ and $I_c$ versus $V_{be}$, with reverse bias $V_{cb}$ = 0 V. Under forward bias, when $I_b$ and $I_c$ are significant, the forward currents can be approximated by the diode equation:

$$I = I_s \exp\left(\frac{V_{be}}{nkT}\right) \tag{6.51}$$

which gives a linear plot of $\log(I_b)$ and $\log(I_c)$ versus $V_{be}$. The value of the saturation current $I_s$ is determined by extrapolating the linear portion of the current versus voltage plot to $V_{be}$=0 as shown in Figure 6.9.

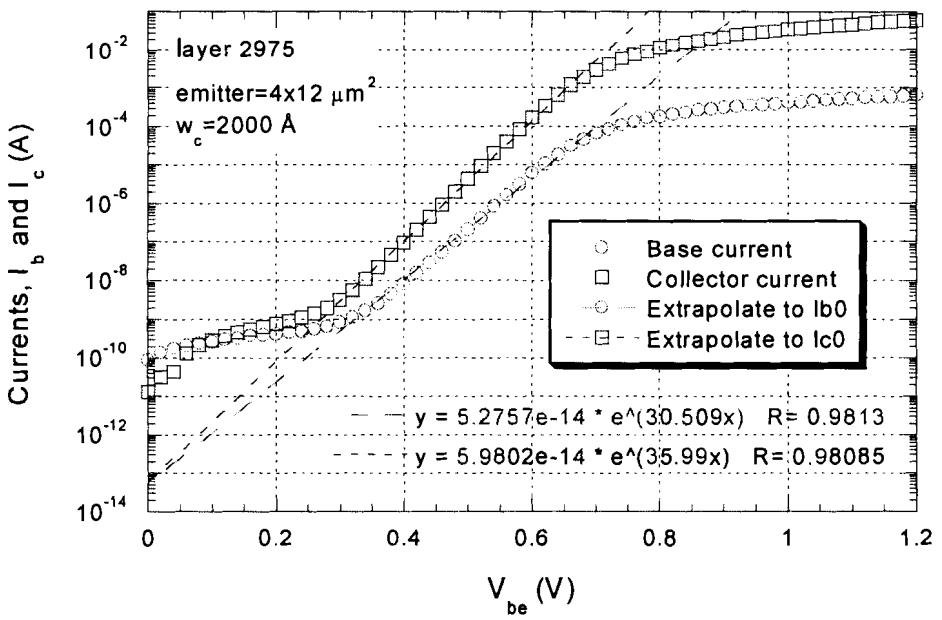


**Figure 6.9. Determination of $I_{c0}$ by extrapolating linear portion of $I_c$ to $V_{be}$=0.**

The saturation current in a $p^+n$ junction is given by:

$$J_s \approx \frac{qD_p p_{n0}}{L_p} \approx q\sqrt{\frac{D_p}{\tau_p}}\frac{n_i^2}{N_D} \tag{6.52}$$

where $D_p$ is the hole diffusion coefficient, $L_p$ is the hole diffusion length, $\tau_p$ is the hole lifetime, $p_{n0}$ is the equilibrium hole density on the n side, $n_i$ is the intrinsic carrier concentration and $N_d$ is the acceptor doping concentration. The temperature dependence of these quantities are:

$$D_p \propto T^3 \tag{6.53}$$

$$\frac{1}{\tau} \propto T^{\gamma} \tag{6.54}$$

$$n_i^2 \propto \exp\left(-\frac{E_g}{kT}\right) \tag{6.55}$$

Therefore the saturation current density relation to temperature is:

$$J_s \propto T^{(3+\gamma/2)} \exp\left(-\frac{E_g}{kT}\right) \tag{6.56}$$

The diffusion coefficient and hole lifetime contribute a temperature dependent term of $T^{(3+\gamma/2)}$, where $\gamma$ is a constant. This term is negligible compared with the exponential contribution from the intrinsic carrier concentration. From these relations, a plot of $\log(J_s)$, or $\log(J_s/T^3)$ versus 1/T should be linear with a slope of $-E_g/k$ [38].

The plot of $I_s/T^3$ versus 1/T is shown in Figure 6.10 with $I_s/T^3$ plotted on a logarithmic scale. This plot is based on measurements from device b5e7 on layer 2975, with an emitter size of 4x12 $\mu m^2$ and a collector width of 2000 Å. The plot shows a good linear fit to the data over a temperature range of 125 K to 380 K. The slope of –8660 K indicates a bandgap of $E_g$=0.75 eV, which is in good agreement with the 0.72 eV bandgap of GaAsSb.

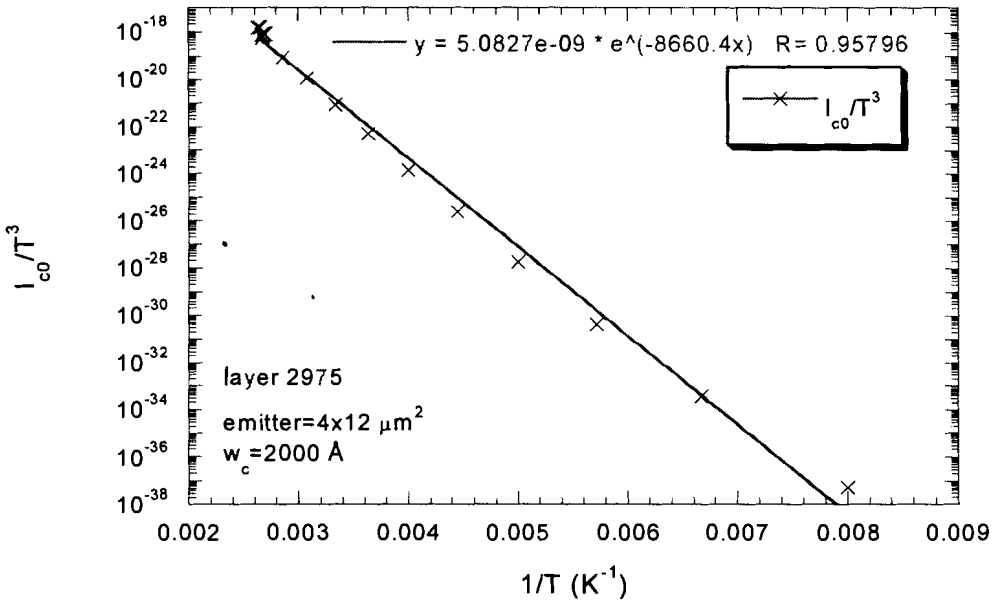


**Figure 6.10. Extraction of energy bandgap based on saturation current as a function of temperature between 125 K to 300 K.**

The saturation current appears to behave as expected over the range of 125 K to 380 K. The extracted energy bandgap agrees well with the accepted bandgap for GaAsSb. The saturation current adds a component to the reverse bias leakage current that is dependent on temperature, but not on the reverse bias.

### 6.3.3.2 Thermal Generation of Electron-hole Pairs

The measured value of $I_{cb0}$ is usually several orders of magnitude larger than the saturation current. One source of the additional current is thermal generation of electron-hole pairs in the depletion region.

The amount of current generated in the depletion region is given by Sze as [39]:

$$J_{gen} = \frac{qn_i w}{\tau_e} \tag{6.57}$$

where w is the depletion width, $n_i$ is the intrinsic carrier concentration, and $\tau_e$ is the effective lifetime of generated electron hole pairs. The temperature dependence of the generated current comes from the intrinsic carrier concentration:

$$n_i \propto \exp\left(-\frac{E_g}{2kT}\right) \tag{6.58}$$

$$J_{gen} \propto \exp\left(-\frac{E_g}{2kT}\right) \tag{6.59}$$

The reverse bias $V_{cb}$ affects the generated current through the change in depletion width:

$$J_{gen} \propto (V_{bi} + V_{cb})^{1/2} \tag{6.60}$$

where $V_{bi}$ is the built-in voltage across the base-collector junction.

From these equations, the contribution to reverse-bias leakage current caused by thermal generation shows a square root dependence on $V_{cb}$. However, as shown in the plot of $I_{cb0}$ versus $V_{cb}$ in Figure 6.11, the reverse-bias leakage current does not follow this square root dependence, particularly at high $V_{cb}$. Therefore, the increase in $I_{cb0}$ at higher values of $V_{cb}$ cannot be explained by thermally generated carriers. The $I_{cb0}$ data in the plot are from measurements on device 11j2 on layer 2587, seen previously in section 6.2.

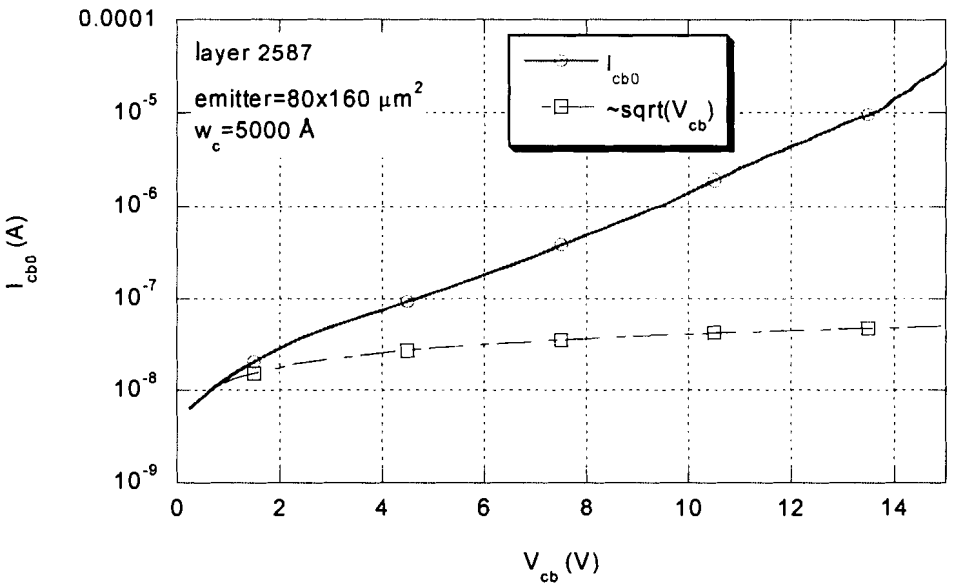


**Figure 6.11. Reverse bias leakage current versus collector-base reverse bias, compared to square root dependence of leakage current from thermally generated carriers.**

### 6.3.3.3 Tunnelling

Another possible source of current is tunnelling between the valence and the conduction bands. In a homojunction, the tunnelling distance depends on the energy bandgap of the material and the strength of the electric field. As the applied reverse voltage increases, the bands bend more strongly and the distance that a valence band electron must tunnel to reach the conduction band decreases. If the distance between equal-energy states in the valence and conduction bands is small enough, about 100 Å or less, then an appreciable tunnelling current will exist. Typically in silicon, with its bandgap of 1.12 eV, significant tunnelling occurs at an electric field strength of $10^6$ to $10^7$ V/cm [40].

The tunnelling current density for a homojunction is given by [41]:

$$J_{tunnelling} = \left(\frac{2m^*}{E_g}\right)^{1/2} \frac{q^3 EV}{\pi h^2} \exp\left(\frac{-\pi^2}{heE}(2m^* E_g^3)^{1/2}\right) \tag{6.61}$$

where m* is the effective tunnelling mass, V is the applied voltage, and E is the electric field in the junction. The electric field can be calculated exactly for a p-i-n junction with an intrinsic region of width w:

$$E = \frac{V_g + V}{w} \tag{6.62}$$

$$V_g = \frac{E_g}{q} \tag{6.63}$$

For a step junction, the field varies across the junction, but the tunnelling current can still be estimated using the equation above. The upper bound of the possible tunnelling current is calculated using the maximum electric field in the junction, and the lower bound is calculated using the average electric field in the junction.

In a heterojunction with a staggered band lineup, such as the GaAsSb-InP junction, the conduction band discontinuity narrows the distance between the highest energy level of the valence band to the same energy level in the conduction band, as shown in Figure 6.12. As in the homojunction case, the distance decreases further with stronger electric field.

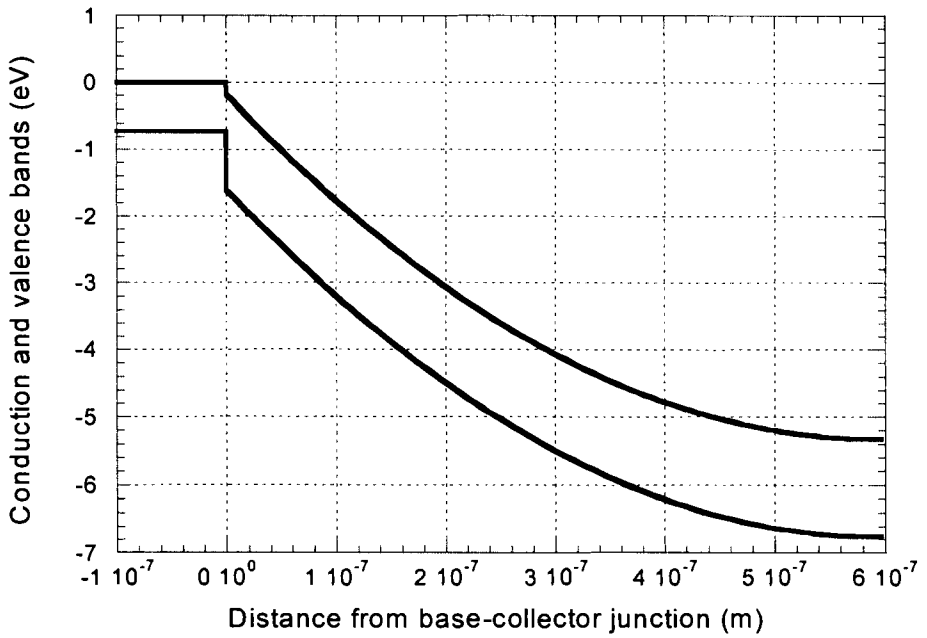


**Figure 6.12. Relative positions of conduction and valence bands under a reverse bias of 4 V.**

In a heterojunction the tunnelling current cannot be calculated by a direct application of equation 6.61, because the bandgap is not constant as it is in a homojunction. One possibility for estimating the current is to use, as the bandgap, the smallest energy difference between the valence band and the conduction band. For staggered bands, this occurs exactly at the base-collector junction, between the valence band of the base and the conduction band of the collector. For GaAsSb and InP the band offsets give a value of 0.54 eV for this minimum energy gap between the bands.

However, this value of bandgap occurs only at one position, at the base-collector junction. On its own it does not indicate the physical distance through which the electron must tunnel, between states of equal energy in the valence and conduction band, given the strength of the electric field. This distance is important because tunnelling probability decreases exponentially with distance, and must be calculated from the electric field strength, the minimum 'bandgap' at the collector-base junction, and the collector bandgap.

For an applied reverse bias of 4 V, the distance between equal energy states of the conduction and valence bands is 30 nm, which is large for tunnelling. The physical

distance decreases to about 100 Å at a bias of 16 V. At low $V_{cb}$, the large tunnelling distance suggests that the contribution from tunnelling to the reverse bias leakage current is small.

### 6.3.3.4 Surface Leakage

Surface leakage is another source of current that may affect the extracted impact ionization coefficient value. In unpassivated mesa devices, the reverse-bias leakage current is composed of a contribution from the perimeter of the mesa and a contribution from the bulk material. Surface leakage from the perimeter of InGaAs mesa devices has been attributed to the formation of conducting oxides, excess arsenic or trap states on the sidewall of the mesa [42]. The surface leakage through the perimeter of the mesa adds a current contribution that is not due to impact ionization in the bulk material. However, the contribution cannot easily be measured and subtracted from the calculation of impact ionization coefficient. As a result, the impact ionization coefficient is overestimated, and the extracted value varies depending on the perimeter to surface area ratio.

The effect on reverse bias leakage currents is shown for two devices with different perimeter to area ratios, in Figure 6.13. The devices, 11j2 and 41a6x20 on layer 2587, have emitter dimensions of 80×160 $\mu m^2$ and 6×20 $\mu m^2$ respectively, and corresponding perimeter to area ratios of 0.0375 $\mu m^{-1}$ and 0.43 $\mu m^{-1}$. The 6×20 $\mu m^2$ device, with its larger perimeter to area ratio, shows a leakage current density that is higher by over an order of magnitude. Therefore, for the same injected emitter current density, the overestimation of multiplication factor is smaller for the 80×160 $\mu m^2$ device than the 6×20 $\mu m^2$ device.

The measurement of impact ionization coefficient for the bulk material could be improved by passivating the devices to remove the surface damage that causes the surface leakage current.

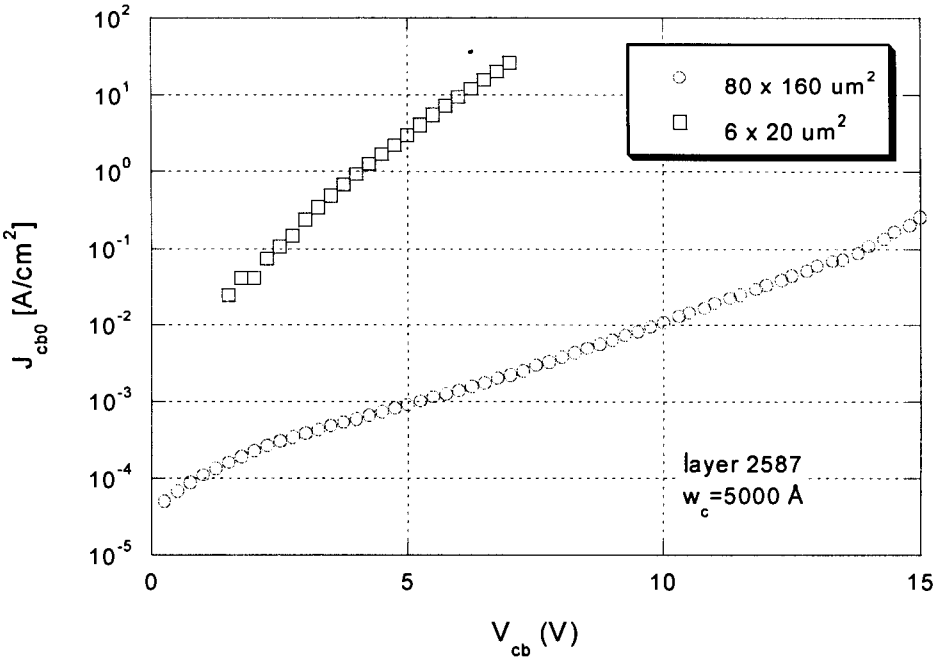


**Figure 6.13. Reverse-bias leakage current density as a function of $V_{cb}$; the leakage current density differs for two devices with different perimeter to area ratios.**

## 6.4 Temperature Dependent Measurements

The procedure followed in the room temperature measurements is applied to measurements taken over a range of temperature. As before, the behaviour of the reverse-bias leakage current, $I_{cb0}$, must be tracked so that the correct current and voltage conditions for impact ionization coefficient measurements can be determined. $I_{cb0}$ shows variation with temperature, but without clear trends across the temperature range.

Other parameters also show a temperature dependence. The breakdown voltage, which is arbitrarily defined as the voltage for which the reverse bias leakage current reaches 100 μA, is plotted for two different devices over a temperature range of 125 K to 375 K.

The room temperature measurements on the device used for temperature dependent measurements are compared to results from the previous section. Finally, the temperature dependent results are presented. The electron-initiated impact ionization coefficient of InP shows a strong dependence on temperature. Over the measured temperature range of

125 K to 380 K, the impact ionization coefficient decreases by about an order of magnitude.

### 6.4.1 $I_{cb0}$ and Breakdown Voltage Measurements

This section shows the behaviour of $I_{cb0}$ and collector-base breakdown voltage over the temperature range for the measured device, which must be removed from the $\Delta I_b$ data for impact ionization coefficient calculations. Data for a second device on a layer structure with a thinner collector are also shown for comparison

#### 6.4.1.1 Device for Impact Ionization Measurements

Impact ionization measurements over a range of temperature were performed on device 41a6x20 on layer structure 2587. This device has an emitter area of 6 μm × 20 μm. The layer 2587 was also used for the room temperature measurements. As described previously in section 4.2.2, this layer has a base width is 400 Å and a collector width of 5000 Å.

$I_{cb0}$ over a temperature range is shown in Figure 6.14 and the breakdown voltage is shown in Figure 6.15. These values of $I_{cb0}$ are important because the impact ionization measurements were made on this device, and this leakage current must be removed from the analysis.

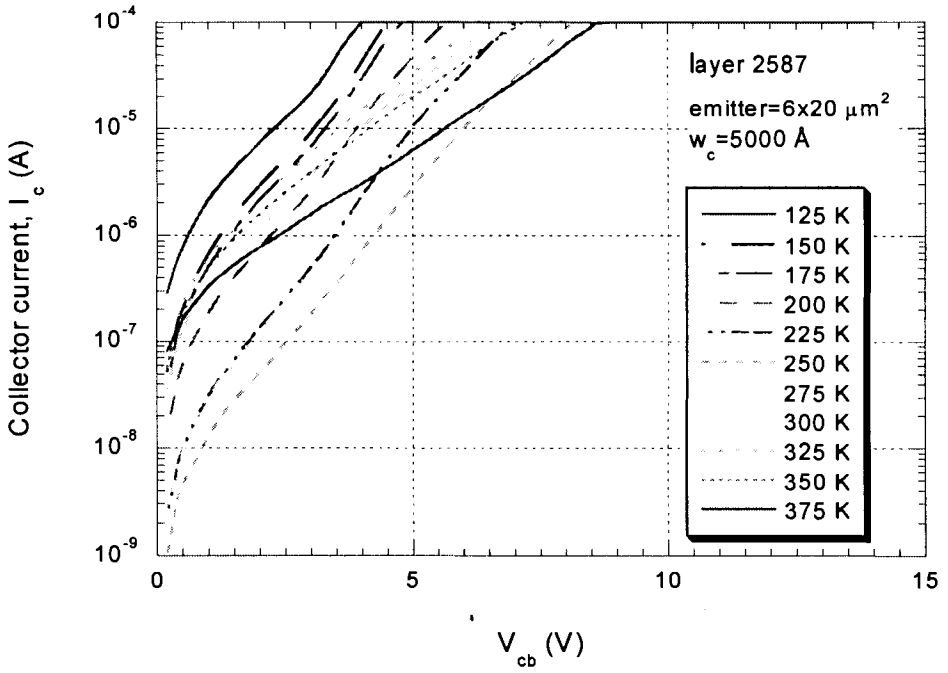


**Figure 6.14. Reverse-bias leakage current for InP device 41a6x20 on layer 2587, showing collector-base breakdown over a temperature range of 125 K to 375 K.**

Two parameters can be used to describe the behaviour of the reverse bias leakage current: the leakage current at small $V_{cb}$<1V (the intercept), and the rate of increase of $I_{cb0}$ with higher $V_{cb}$ (the slope of the plot in Figure 6.14). The temperature trends for these parameters for the measured device are:

- $I_{cb0}$ for $V_{cb}$<1 V increases as temperature decreases, from 250 K to 125 K. It is minimum between 250 and 300 K, then increases with temperature to 380 K.
- The slope of $I_{cb0}$ versus $V_{cb}$ is constant between 125 K and about 300 K, then decreases as temperature increases from 300 to 380 K.

The behaviour of the $I_{cb0}$ curves can also be divided into temperature ranges. Between 125 K to 250 K, the $I_{cb0}$ versus $V_{cb}$ curves are parallel, with lower values of $I_{cb0}$ corresponding to higher temperature over the whole range of Vcb (0 to 7 V). Between 250 K and 350 K there is no apparent trend in either intercept or slope. The $I_{cb0}$ versus $V_{cb}$ curves lie in a band and do not differ significantly in value. At around 325 K, the slope of $I_{cb0}$ versus $V_{cb}$ begins to decrease. At 325 K, the slope is greatest. Due to the large slope, $I_{cb0}(T, V_{cb})$ is highest at high $V_{cb}$ for 325 K but lowest at low $V_{cb}$ for the same

temperature. Conversely, the lowest $I_{cb0}$ at high $V_{cb}$ occurs at the highest temperature measured, at 380 K. However, at low $V_{cb}$ the 380 K measurement has the highest $I_{cb0}$ above 200 K.

The consequence of the $I_{cb0}$ temperature dependence is that impact ionization coefficient measurements on this device are most reliable at low $V_{cb}$ for low temperatures, and at higher $V_{cb}$ at high temperatures. Although $I_{cb0}$ is subtracted from the current in the calculation of impact ionization coefficient, the higher values of $I_{cb0}$ increase the uncertainty in the impact ionization coefficient. Therefore, the uncertainty is greater for measurements at low temperature, and at low $V_{cb}$ at high temperature. Projection of trends between 250 K to 350 K is difficult as there is no clear trend in the behaviour of $I_{cb0}$ between these temperatures.

A slice of the $I_{cb0}$ versus $V_{cb}$ behaviour is shown in the plot of breakdown voltage versus temperature in Figure 6.15. The collector-base breakdown voltage is defined as the collector-base voltage at which the reverse-bias leakage current reaches 100 μA.

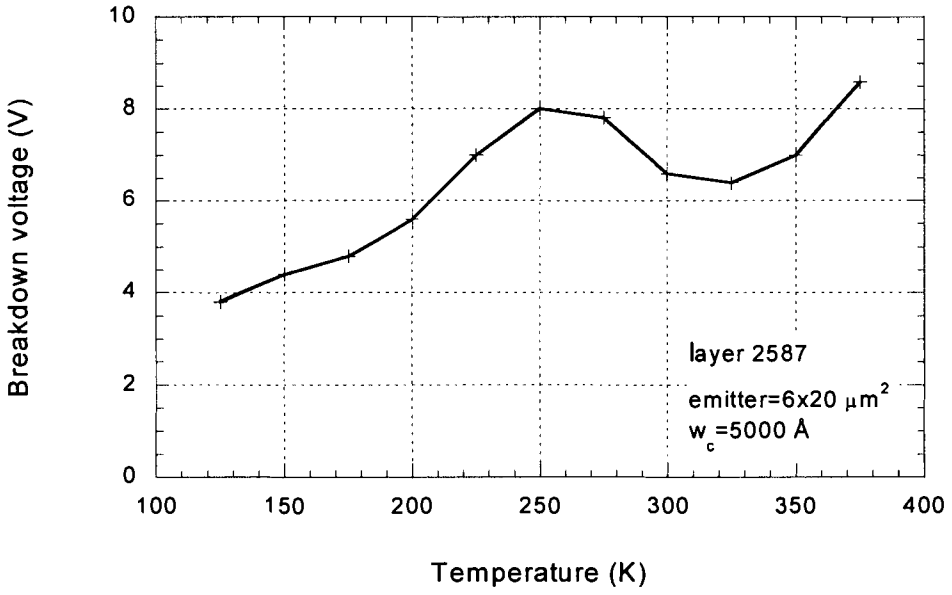


**Figure 6.15. Collector-base breakdown voltage versus temperature for InP device 41a6x20 on layer 2587.**

The breakdown voltage increases from 100 to 250 K, in the region of parallel $I_{cb0}$ versus $V_{cb}$ lines and decreasing $I_{cb0}$ with temperature. It reaches a local maximum at 250 K, but decreases again in the region of no clear trends, between 250 K and 325 K. Finally,

as the slope of $I_{cb0}$ versus $V_{cb}$ decreases, the breakdown voltage begins to increase again, reaching its maximum value in the measurement range at 380 K.

### 6.4.1.2 Other Devices (b5e7 on layer 2975)

The data for $I_{cb0}$ in the previous section are important because they are the values that must be subtracted in calculations of the impact ionization coefficient. However, the temperature behaviour seen is not necessarily typical. This section presents the $I_{cb0}$ versus $V_{cb}$ and breakdown voltage behaviour with temperature, for a second device and layer structure. The device b5e7 on layer 2975 has an emitter area of 4 μm × 12 μm, a 300 Å wide base, and a 2000 Å wide collector. It shows a lower breakdown voltage due to the narrow collector, but better temperature stability.

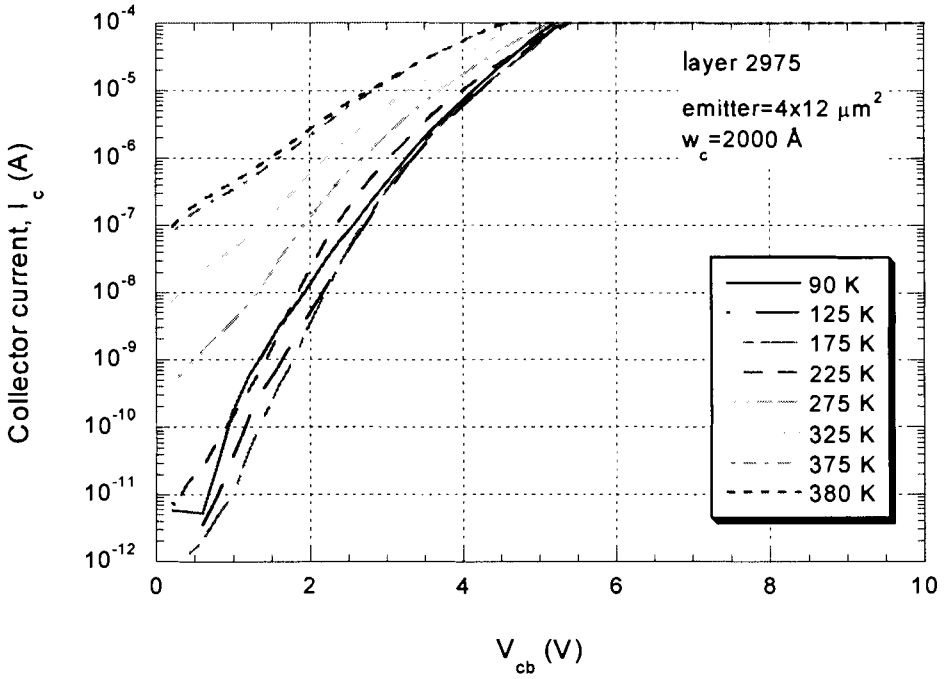


**Figure 6.16. Reverse-bias leakage current for InP device b5e7 on layer 2975, showing collector-base breakdown for temperatures from 90 K to 380 K.**

The trends shown in Figure 6.16 are much more regular than the data in Figure 6.14. The data show a steady trend of increasing $I_{cb0}$ at low $V_{cb}$ with temperature, and a decreasing slope. Despite the decrease in slope with temperature, the increase of $I_{cb0}$ at low $V_{cb}$ is high enough that the breakdown voltage is highest at low temperature and

remains steady until 250 K, when it decreases slightly by less than 0.5 V with temperatures up to 380 K, as shown in Figure 6.17.

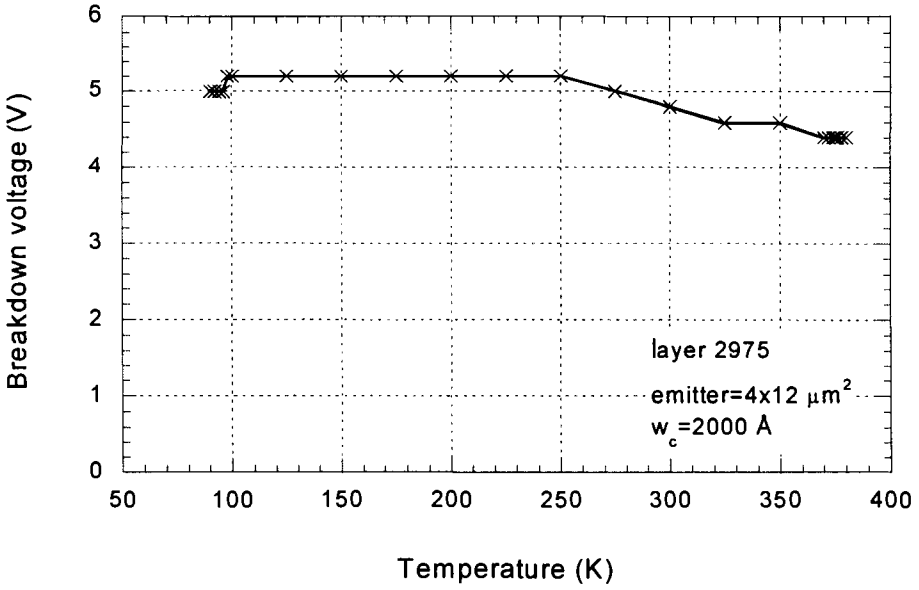


**Figure 6.17. Collector-base breakdown voltage versus temperature for InP device b5e7 on layer structure 2975.**

## 6.4.2 Room Temperature Results for 41a6x20 Device (Comparison)

The measurements over a range of temperature were performed on device 41a6x20 on layer 2587, the device for which $I_{cb0}$ and breakdown voltage were discussed in section 6.4.1.1 . This section presents the electron-initiated impact ionization coefficient measurements at 295 K, for comparison to the room temperature results presented earlier for device 11j2 on layer 2587. The layer structure of the two devices is the same; however device 41a6x20 has an emitter area of 6×20 $\mu m^2$, while device 11j2 has a much larger emitter area of 80×160 $\mu m^2$.

### 6.4.2.1 $\Delta I_b$ and $\Delta I_c$

The plot in Figure 6.18 presents data to evaluate the condition that $I_{cb0}$ should form a small part of $\Delta I_b$ or $\Delta I_c$. In behaviour similar to that of device 11j2, $I_{cb0}$ for device 41a6x20 is nearly equal to $\Delta I_b$ for small values of emitter current. However, for the 41a6x20 device, $I_{cb0}$ appears to increase with $V_{cb}$ more quickly than $\Delta I_b$. At low $V_{cb}$, $\Delta$Ib is larger than $I_{cb0}$ for all values of emitter current, but at $V_{cb}$=4 V, $\Delta I_b$ is greater than $I_{cb0}$

only for injected emitter current values of more than 300 μA. As before, the calculated values of multiplication and impact ionization coefficient have less uncertainty for operation parameters where the difference between $\Delta I_b$ and $I_{cb0}$ is larger.

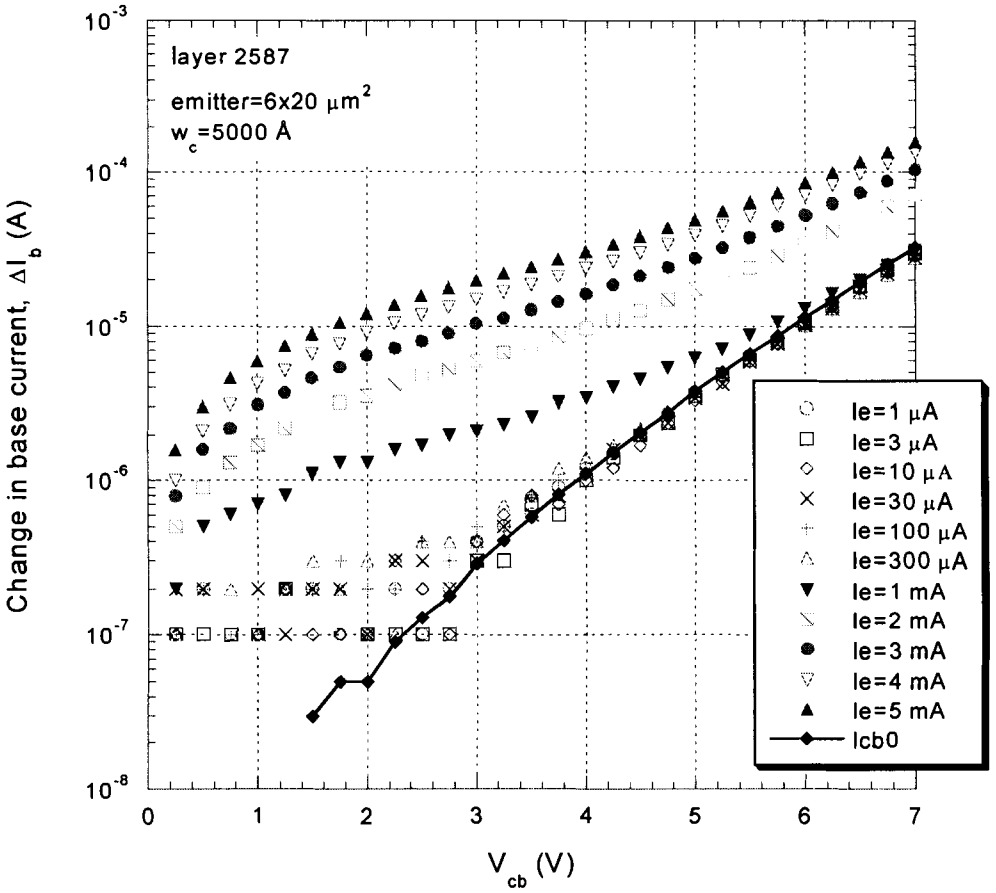


**Figure 6.18. Absolute value of $\Delta I_b$ versus collector-base bias $V_{cb}$, compared to the magnitude of the reverse-bias leakage current $I_{cb0}$, for InP device 41a6x20 at 295 K.**

### 6.4.2.2 Multiplication Factor, M-1

The multiplication factor should be independent of injected current. As seen in Figure 6.19, the multiplication factor lies in a band of one order of magnitude for currents between 30 μA and 5 mA. The multiplication factor is scattered for lower values of emitter current, even up to 300 μA, because $I_{cb0}$ is a high percentage of $\Delta I_b$ and the multiplication factor is calculated from the difference between $I_{cb0}$ and $\Delta I_b$.

The multiplication factor is nearly at its lowest value at an emitter current of 1 mA, and the data show relatively little scatter. The multiplication factor increases with

higher emitter current by less than a factor of 2 for emitter currents of up to 5 mA. With decreasing current, the multiplication is smaller by a factor of 2 and much more scattered at $I_e$=300 μA, but returns to the same value of multiplication as 1 mA for an emitter current of 100 μA. Based on the results for the larger 11j2 device, it could be expected that the region of current-independent multiplication factor would occur at lower emitter currents. Also, the more reliable data should be the higher current data because the current contribution from impact ionization is much higher than the contribution from the reverse bias leakage current, $I_{cb0}$. However, the lack of a range of emitter currents over which the multiplication factor is constant indicates that the data are not highly reliable for accurately extracting the impact ionization coefficients.

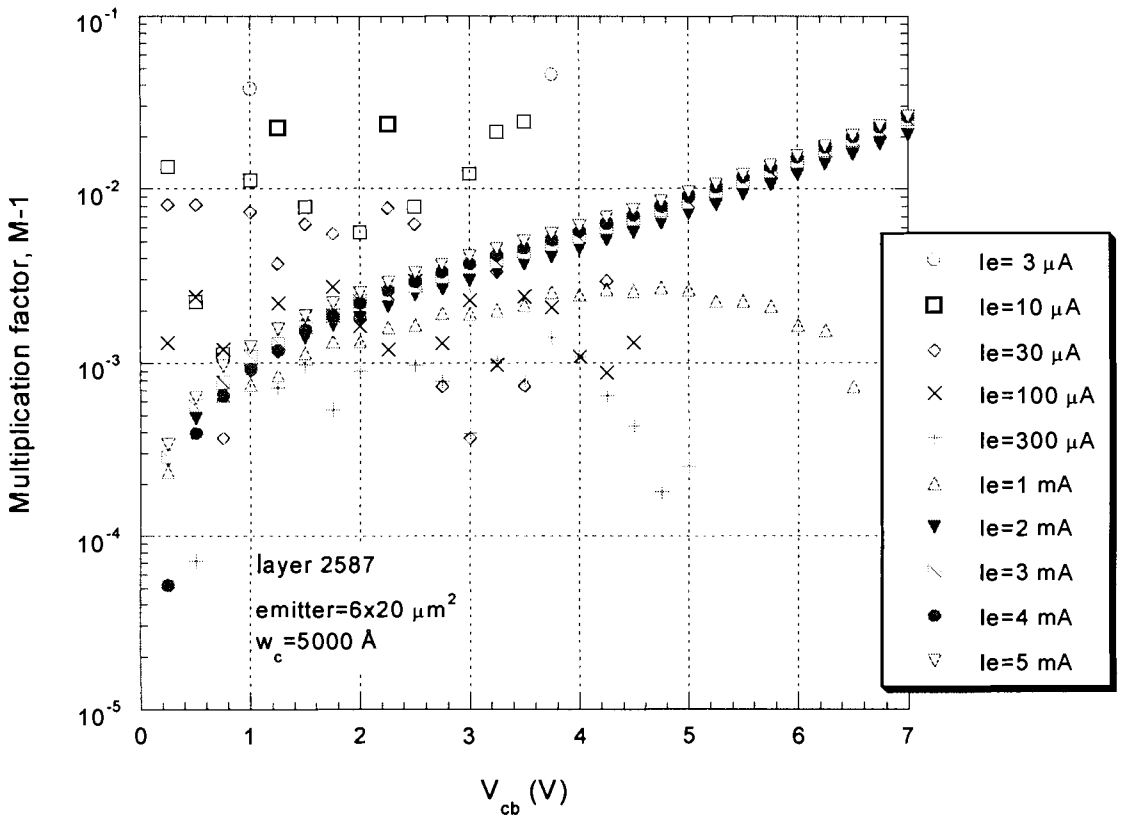


**Figure 6.19. Multiplication factor versus reverse bias voltage over a range of emitter current, for InP device 41a6x20 at 295 K.**

### 6.4.2.3 Impact Ionization Coefficient

Figure 6.20 compares the measured impact ionization coefficients from the two devices. The lowest values of impact ionization coefficient from 41a6x20 are about 1

order of magnitude higher than the lowest values from 11j2, at these low electric field values. The slope is similar between measurements on the 11j2 device and on the 41a6x20 device. Emitter currents of 300 μA to 1 mA give the closest values of impact ionization coefficient at 295 K. As discussed in section 6.3.3.4 , the overestimation of impact ionization coefficient for the smaller device, with its higher perimeter to area ratio, is consistent with a large surface leakage component in the reverse-bias leakage current. This leakage current obscures the multiplication due to impact ionization and increases the error in the measurement.

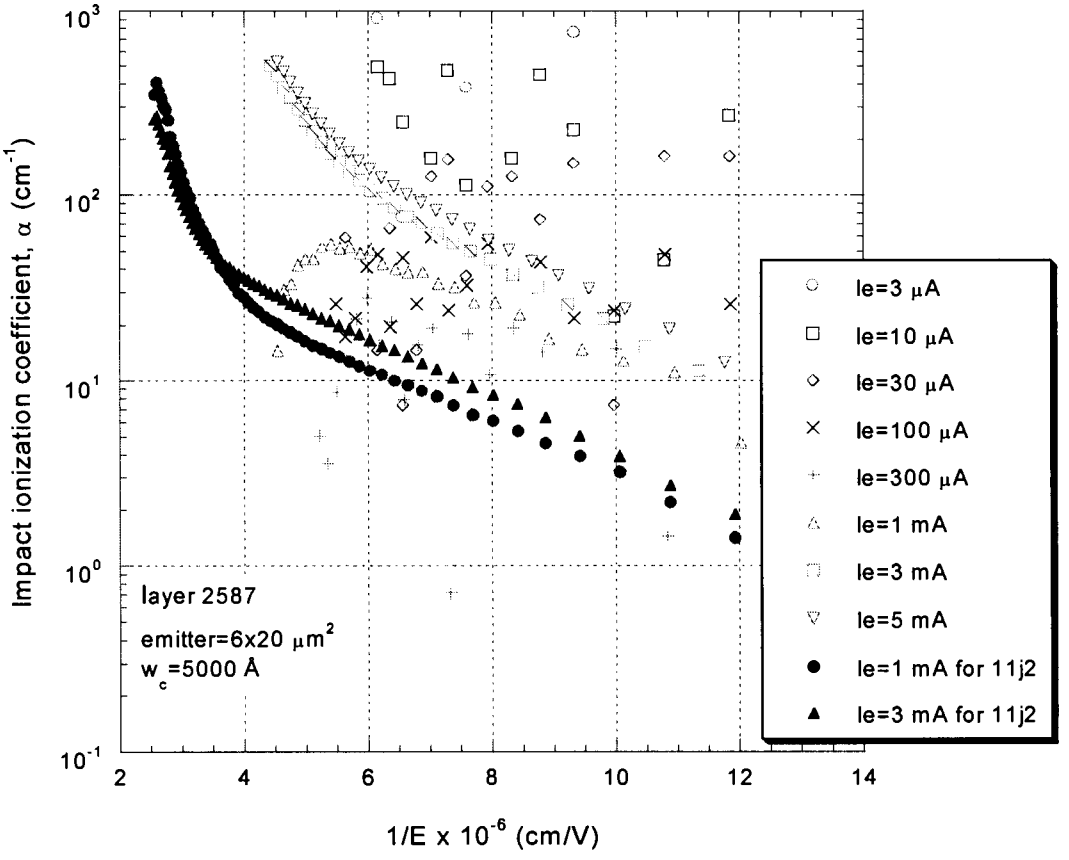


**Figure 6.20. Impact ionization coefficient for device 41a6x20 (6×20 μm² emitter area) at 295 K, compared to lowest values of impact ionization coefficient on device 11j2 (80×160 μm² emitter area) at room temperature.**

### 6.4.3 Temperature Results for 41a6x20 Device

The plot in Figure 6.21 shows the calculated electron-initiated impact ionization coefficient measured at an emitter current of 1 mA to 5 mA. The numerical value of electron-initiated impact ionization coefficient has a large error bar associated with each measurement due to the surface leakage of the device. However, the surface leakage does not obscure the temperature trend. The surface leakage is expected to increase with temperature [43]; this behaviour is opposite to the change in current shown in the data. The trend with temperature is clear: the impact ionization coefficient decreases by more than an order of magnitude over the temperature range of 125 K to 380 K.

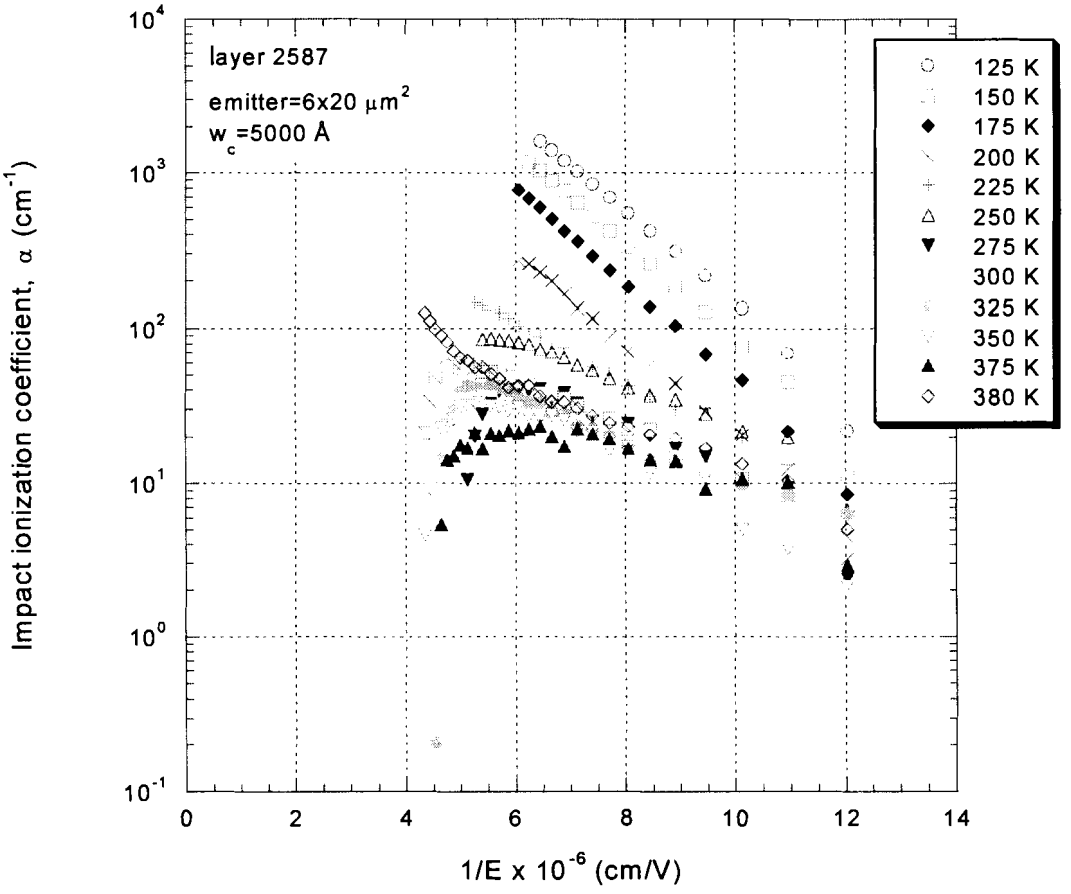


**Figure 6.21. Electron-initiated impact ionization coefficients for InP measured on device 41a6x20 at an emitter current of 1 mA, over a temperature range from 125 K to 380 K.**

## 6.5 Conclusions

The results of measuring the electron-initiated impact ionization coefficient of InP using a InP-GaAsSb-InP DHBT are presented in this chapter.

At room temperature, the multiplication factor shows the least dependence on the injected emitter current over the range of 20 μA to 2 mA, at a reverse bias of less than 8 V. The measurements on device 11j2 at an emitter current of 300 μA show good agreement with coefficients reported in the literature, in the overlapping region of higher electric field. However, there is significant scatter in the values of impact ionization coefficient extracted from measurements taken at other emitter current levels and on other devices, as seen in Figure 6.7 and in Figure 6.20.

In addition, the low field results include an unexpected change in slope of impact ionization coefficient versus inverse electric field. A possible explanation is that the assumption that the hole impact ionization coefficient is negligible in these measurements is incorrect. The contribution from hole impact ionization may cause an overestimation of the multiplication factor that is then attributed to the electron impact ionization coefficient; as a result the coefficient is higher than expected causing the unexpected slope and change of slope.

The large magnitude of the reverse bias leakage current, $I_{cb0}$, obscures the behaviour of impact ionization. In particular, it is difficult to separate the surface leakage current contribution from the impact ionization current; as a result, the extracted value of impact ionization coefficient is not precise and varies depending on the perimeter to area ratio of the device as seen in Figure 6.13.

Although the surface leakage increases the error bars so that the numerical value of the impact ionization coefficient is not reliable, the temperature trends are not obscured. This measurement of electron-initiated impact ionization coefficient in InP using DHBTs confirms the trend of impact ionization coefficient with temperature. Between 125 K and 380 K the impact ionization coefficient decreases by more than one order of magnitude.

The high bias measurements at moderate emitter current appear to be the most reliable, because they have a component of current clearly due to impact ionization. However, at room temperature the measurements on device 41a6x20 on layer 2587 are

not in good agreement with the previously measured coefficients on device 11j2 on the same layer structure. This discrepancy is likely due to surface leakage. The temperature dependent measurements are also subject to the problems of large $I_{cb0}$ and possibly non-negligible hole-initiated impact ionization.

HBTs should allow better measurements of impact ionization coefficients at low-field conditions than avalanche photodiodes. The use of a GaAsSb base with InP collector removes the difficulty of the current spike at the collector-base junction, so the electric field profile at the junction is well known. However, in order to measure the impact ionization coefficient accurately, the reverse bias leakage current $I_{cb0}$ must be very small. Passivating the devices may assist in reducing the surface leakage current. In addition, the electron-initiated impact ionization coefficient can be easily extracted from the measured currents only if the hole-initiated impact ionization coefficient is negligible. Otherwise, a value must be assumed for the hole-initiated impact ionization current.

# Chapter 7
# Conclusions and Recommendations

## 7.1 Conclusions

Impact ionization measurements were first performed using avalanche photodiodes; however, the precise amount and type of initiating charge is difficult to determine. A newer measurement technique uses HBTs at either constant emitter current or constant base-emitter bias. HBTs should allow better measurements of impact ionization coefficients at low-field conditions than avalanche photodiodes. The constant base-emitter bias method is preferable if the Early effect is large in the devices; otherwise, the constant emitter method current allows better control of the initiating current.

Impact ionization measurements depend on the ability to determine the injected current and the electric field profile across the depletion region. Heterojunction bipolar transistors are useful because the electric field profile is well-known, the injection current consists purely of electrons or holes, and the magnitude of the initiating current can be controlled. The staggered band lineup of InP-GaAsSb-InP HBTs allows for current injection into the InP collector. The carriers do not need to overcome a base-collector energy spike, which would make it difficult to determine the electric field. The reverse bias leakage current, $I_{cb0}$, is important to the measurements and preferably should be small compared to the change in base current. Other non-ideal behaviours of the HBT, such as the Early effect and the Kirk effect, can contribute to the change in base current. Surface leakage is also problematic, because measurements taken on devices with different perimeter to area ratios will give different results for the impact ionization coefficient, and the increase in current that is due to impact ionization cannot be determined accurately.

The electron-initiated impact ionization coefficient in InGaAs was measured using HBTs. The leakage current $I_{cb0}$ must be subtracted from the change in base current, $\Delta I_b$, because $I_{cb0}$ forms a substantial portion of the increase in current that would otherwise be attributed to impact ionization. The appropriate range of bias conditions is determined by examining the current levels as the reverse bias across the collector-base junction, $V_{cb}$, is increased. The increase in base (or collector) current, relative to the base current at zero reverse bias, should be proportional to the injected emitter current. This is not the case at low levels of injected emitter current, or low values of base-emitter bias, where the total increase in base current is nearly independent of the applied bias. This trend indicates that the increase in base current is dominated by the behaviour of the reverse bias leakage current, and the initial collector current is too small to generate substantial number of charge carriers from impact ionization. At high values of $I_e$ or $V_{be}$, the increase in base current is also non-linear with respect to the injected emitter current. Often there is indication of current limiting due to the compliance settings of the measurement apparatus. These two limiting behaviours define the range of moderate emitter current or base-emitter bias that is suitable for impact ionization measurements.

Measurements on the InP HBT at room temperature are also affected by the large reverse bias leakage current, $I_{cb0}$. The surface leakage clearly has an effect, visible in the different multiplication factors and leakage currents measured on two devices that differ only in their perimeter to area ratios. The InP electron-initiated impact ionization coefficient plot shows good agreement with measurements taken at an emitter current of 300 μA at higher electric fields. However, at very low electric fields the InP electron-initiated impact ionization coefficient plot shows a different slope from other data in the literature. The behaviour seen in the InP HBTs may be explained by a contribution to the total current from hole-initiated impact ionization, which would mask the low levels of electron-initiated current. The method of measuring the electron-initiated impact ionization coefficient is not accurate unless hole-initiated impact ionization is negligible.

The temperature dependent measurements show the expected behaviour with temperature. Although the numerical values of impact ionization coefficient are subject to large error bars due to the surface leakage and hole ionization effects, the temperature

trend is clear. The impact ionization coefficient increases at lower temperature, because there is less vibration of the lattice atoms to interfere with the charge carrier acceleration, and the carriers reach critical velocity more easily. The results of the experiment did not produce numerical results that are consistent with the previous room temperature measurement, but the impact ionization coefficient decreases by over an order of magnitude over a temperature range of 125 to 380 K.

## 7.2 Recommendations

In this work, the primary barrier to achieving consistent numerical values for the electron-initiated impact ionization coefficient was the reverse bias leakage current, $I_{cb0}$. The magnitude of the leakage current is large compared to the change in base or collector current caused by impact ionization. In addition, the surface leakage was significant, causing results to vary depending on the device dimensions. To achieve more reliable measurements, the leakage current of the devices must be reduced. Passivation of the mesa devices is one possible technique that should reduce the surface leakage current.

# List of References

1. Mehran Matloubian, "Applications of InP-Based Transistors for Microwave and Millimeter-Wave Systems" in *InP-Based Materials and Devices*, ed. Osamu Wada and Hideki Hasegawa, Toronto: John Wiley and Sons, 1999, p. 38.

2. Herbert Kroemer, "Heterostructure Bipolar Transistors and Integrated Circuits," *Proceedings of the IEEE*, vol. 70, no.1, pp. 13-25, 1981.

3. C.R. Bolognesi, N. Matine, X. Xu, J. Hu, M.W. Dvorak, S.P. Watkins, and M.L.W. Thewalt, "Low-Offset NpN InP/GaAsSb/InP Double Heterojunction Bipolar Transistors with Abrupt Interfaces and Ballistically Launched Collector Electrons," *Device Research Conference Digest, 56th Annual*, pp. 30-31, June 1998.

4. Mehran Matloubian, p. 53.

5. Hin-Fai Chau, Edward A. Beam III, Yung-Chung Kao, and William Liu, "InP-Based Heterojunction Bipolar Transistors" in *Current Trends in Heterojunction Bipolar Transistors*, ed. M. F. Chang, New Jersey: World Scientific, 1996, p. 322.

6. Mehran Matloubian, p. 45.

7. Govind P. Agrawal, *Fiber-Optic Communication Systems*, Toronto: John Wiley and Sons, 1992, p. 5.

8. C.H. Tan, K.F. Li, S.A. Plimmer, J.P.R. David, G.J. Rees, J. Clark and C.C. Button, "Improved excess noise and temperature dependence of multiplication characteristics in thin InP avalanching regions," *International Conference on Indium Phosphide and Related Materials*, pp. 295 – 298, 1999.

9. Kenko Taguchi, "Photodiodes and Receivers Based on InP Materials" in *InP-Based Materials and Devices*, ed. Osamu Wada and Hideki Hasegawa, Toronto: John Wiley and Sons, 1999, p. 517.

10. C.A. Armiento, S.H. Groves, and C.E. Hurwitz, "Ionization coefficients of electrons and holes in InP," *Applied Physics Letters*, vol. 35, no. 4, pp. 333 – 336, Aug. 1979.

11. S.M. Sze, *Physics of Semiconductor Devices,* Toronto: John Wiley and Sons, 1981, p. 100.

12. I. Umebu, A.N.M.M. Choudhury, and P.N. Robson, "Ionization coefficients measured in abrupt InP junctions," *Applied Physics Letters*, vol. 36, no. 4, pp. 302 – 303, Feb. 1980.

13. L.W. Cook, G.E. Bulman, and G.E. Stillman, "Electron and hole impact ionization coefficients in InP determined by photomultiplication measurements," *Applied Physics Letters*, vol. 40, no. 7, pp. 589 – 591, Apr. 1982.

14. Enrico Zanoni, Roger Malik, Paolo Pavan, Julien Nagle, Alessandro Paccagnella, and Claudio Canali, "Negative Base Current and Impact Ionization Phenomena in AlGaAs/GaAs HBT's," *IEEE Electron Device Letters*, vol. 13, no.5, pp. 253 – 255, May 1992.

15. C. Canali, C. Forzan, A. Neviani, L. Vendrame, E. Zanoni, R.A. Hamm, R. J. Malik, F. Capasso, and S. Chandrasekhar, "Measurement of the electron ionization coefficient at low electric fields in InGaAs-based heterojunction bipolar transistors," *Applied Physics Letters*, vol. 66, no. 9, pp. 1095 – 1097, Feb. 1995.

16. Andrea Neviani, Gaudenzio Meneghesso, Enrico Zanoni, Madjid Hafizi, and Claudio Canali, "Positive Temperature Dependence of the Electron Impact Ionization Coefficient in $In_{0.53}Ga_{0.47}As$/InP HBT's," *IEEE Electron Device Letters*, vol. 18, no. 12, pp. 619 – 621, Dec. 1997.

17. Roger J. Malik, Naresh Chand, Julien Nagle, Robert W. Ryan, Kambiz Alavi, and Alfred Y. Cho, "Temperature Dependence of Common-Emitter I-V and Collector Breakdown Voltage Characteristics in AlGaAs/GaAs and AlInAs/GaInAs HBT's Grown by MBE," *IEEE Electron Device Letters*, vol. 13, no. 11, pp. 557 – 559, Nov. 1992.

18. J. Bude and K. Hess, "Thresholds of impact ionization in semiconductors," *Journal of Applied Physics*, vol. 72, no. 8, pp. 3554 – 3561, Oct. 1992.

19. C.R. Crowell and S. M. Sze, "Temperature Dependence of Avalanche Multiplication in Semiconductors," *Applied Physics Letters*, vol. 9, no. 6, pp. 242 – 244, Sept. 1966.

20. Kenko Taguchi, Toshitaka Torikai, Yoshimasa Sugimoto, Kikuo Makita, and Hisahiro Ishihara, "Temperature dependence of impact ionization coefficients in InP," *Journal of Applied Physics*, vol. 59, no. 2, pp. 476 – 481, Jan. 1986.

21. Michael Shur, *Physics of Semiconductor Devices,* Toronto: Prentice Hall, 1990, p. 190.

22. S.M. Sze, p. 99.

23. G.E. Stillman and C.M. Wolfe, "Avalanche Photodiodes" in *Semiconductors and Semimetals Volume 12: Infrared Detectors II*, ed. R.K. Willardson and Albert C. Beer, San Francisco: Academic Press, 1977, p. 326.

24. William Shockley, "Problems related to p-n junctions in silicon," *Solid State Electronics*, vol. 2, no. 1, pp. 35 – 67, 1961.

25. G.A. Baraff, "Distribution Functions and Ionization Rates for Hot Electrons in Semiconductors," *Physical Review*, vol. 128, no. 6, pp. 2507 – 2517, Dec. 1962.

26. G.E. Stillman and C.M. Wolfe, p. 329.

27. W.P. Dumke, "Theory of Avalanche Breakdown in InSb and InAs," *Physical Review*, vol. 167, no. 3, pp. 783 – 789, Mar. 1968.

28. Gary E. Bulman, Virginia M. Robbins, and Gregory E. Stillman, "The Determination of Impact Ionization Coefficients in (100) Gallium Arsenide Using Avalanche Noise and Photocurrent Multiplication Measurements," *IEEE Transactions on Electron Devices*, vol. 32, no. 11, pp. 2454 – 2466, Nov. 1985.

29. D. Buttari, A. Chini, G. Meneghesso, E. Zanoni, D. Sawdai, D. Pavlidis, and S.S.H. Hsu, "Measurements of the InGaAs Hole Impact Ionization Coefficient in InAlAs/InGaAs pnp HBTs," *IEEE Electron Device Letters*, vol. 22, no. 5, pp. 197 – 199, May 2001.

30. Claudio Canali, Federico Capasso, Roger Malik, Andrea Neviani, Paolo Pavan, Carlo Tedesco, and Enrico Zanoni, "Measurement of the Electron Ionization Coefficient at Low Electric Fields in GaAs-Based Heterojunction Bipolar Transistors," *IEEE Electron Device Letters*, vol. 15, no. 9, pp. 354 – 356, Sept. 1994.

31. N. Shamir and D. Ritter, "Lower Limit of Method for the Extraction of Ionization Coefficients from the Electrical Characteristics of Heterojunction Bipolar Transistors," *IEEE Transactions on Electron Devices*, vol. 47, no. 2, pp. 488 – 490, Feb. 2000.

32. Guofo Niu, John D. Cressler, Shiming Zhang, Usha Gogineni, and David C. Ahlgren, "Measurement of Collector-Base Junction Avalanche Multiplication Effects in Advanced UHV/CVD SiGe HBT's," *IEEE Transactions on Electron Devices*, vol. 46, no. 5, pp. 1007 – 1015, May 1999.

33. N. Shamir and D. Ritter, "Low Electric Field Hole Impact Ionization Coefficients in GaInAs and GaInAsP," *IEEE Electron Devices Letters*, vol. 21, no. 11, pp. 509 – 511, Nov. 2000.

34. N. Matine, M.W. Dvorak, C.R. Bolognesi, X. Xu, J. Hu, S.P. Watkins, and M.L.W. Thewalt, "Nearly ideal InP/GaAsSb/InP double heterojunction bipolar transistors with ballistically launched collector electrons." *Electronics Letters*, vol. 34, no. 17, pp. 1700-1702, 1998.

35. Yoshikazu Takeda, "Material Physics of InP-Based Compound Semiconductors" in *InP-Based Materials and Devices*, ed. Osamu Wada and Hideki Hasegawa, Toronto: John Wiley and Sons, 1999, p. 98.

36. http://www.ioffe.rssi.ru/SVA/NSM/Semicond/InP/thermal.html, December 18, 2004.

37. D. Ritter, R. A. Hamm, A. Feygenson, and M. B. Panish, "Anomalous electric field and temperature dependence of collector multiplication in InP/$Ga_{0.47}In_{0.53}As$ heterojunction bipolar transistors," *Applied Physics Letters*, vol. 60, no. 25, pp. 3150 – 3151, June 1992.

38. S.M. Sze, pp. 87 – 89.

39. S.M. Sze, p. 150.

40. John L. Moll, *Physics of Semiconductors,* Toronto: McGraw-Hill, 1964, p. 240 – 241.

41. Masanori Ito, Takao Kaned, Kazuo Nakajima, Yoshikazu Toyama, and Hiroaki Ando, "Tunneling Currents in $In_{0.53}Ga_{0.47}As$ Homojunction Diodes and Design of InGaAs/InP Hetero-structure Avalanche Photodiodes," *Solid State Electronics*, vol. 24, pp. 421 – 424, 1981.

42. D. Schmidt and D. Trommer, "Conservation of low dark current of InGaAs photodiodes after $NH_3F$/HF etch with a BCB passivation layer," IEEE Proceedings, p. 302 – 305, 2000.

43. Kent W. Carey, Shih-Yuan Wang, James S.C. Chang and K. Nauka, "Leakage Current in GaInAs/InP Photodiodes Grown by OMVPE," *Journal of Crystal Growth*, vol. 98, pp. 90 – 97, 1989.